TURUN
YLIOPISTO
UNIVERSITY
OF TURKU

FUSION GENES IN HIGH-GRADE SEROUS OVARIAN CANCER

Heidi Rausio

TURUN YLIOPISTON JULKAISUJA – ANNALES UNIVERSITATIS TURKUENSIS
SARJA – SER. D OSA – TOM. 1757 | MEDICA – ODONTOLOGICA | TURKU 2023

TURUN
YLIOPISTO
UNIVERSITY
OF TURKU

FUSION GENES IN HIGH-GRADE SEROUS OVARIAN CANCER

Heidi Rausio

TURUN YLIOPISTON JULKAISUJA – ANNALES UNIVERSITATIS TURKUENSIS
SARJA – SER. D OSA – TOM. 1757 | MEDICA – ODONTOLOGICA | TURKU 2023

University of Turku

Faculty of Medicine
Institute of Biomedicine
Pathology
Drug Research Doctoral Program (DRDP)

Supervised by

Docent, Kaisa Huhtinen
Institute of Biomedicine
University of Turku
Turku, Finland
Faculty of Medicine
University of Helsinki
Helsinki, Finland

Professor, Olli Carpén
Department of Pathology
University of Helsinki
Helsinki, Finland

Reviewed by

Docent, Leena Latonen
Institute of Biomedicine
University of Eastern Finland
Kuopio, Finland

Ph.D. Caroline Heckman
Institute for Molecular Medicine Finland
Helsinki Institute of Life Science
University of Helsinki
Helsinki, Finland

Opponent

Professor, Arto Mannermaa
Institute of Clinical Medicine
University of Eastern Finland
Biobank of Eastern Finland
Kuopio, Finland

ISBN 978-951-29-9521-9 (PRINT)
ISBN 978-951-29-9522-6 (PDF)
ISSN 0355-9483 (Print)
ISSN 2343-3213 (Online)
Painosalama, Turku, Finland 2023

UNIVERSITY OF TURKU
Faculty of Medicine
Institute of Biomedicine
Pathology
HEIDI RAUSIO: Fusion Genes in High-Grade Serous Ovarian Cancer
Doctoral Dissertation, 119 pp.
Drug Research Doctoral Programme
October 2023

ABSTRACT

High-grade serous ovarian cancer (HGSC) is the most common and lethal subtype of ovarian cancer. Debulking surgery is the primary treatment, supplemented by platinum and taxane combination chemotherapy. The response to treatment is generally good, but most patients eventually develop drug resistance, leading to disease progression and death. Nevertheless, the treatment strategy has remained relatively unchanged, and overall survival has hardly improved over the last 20 years.

The primary events in early HGSC development are the inactivation of the tumor suppressor p53, and the homologous recombination pathway, which results in a severely damaged genome and allows the development of individual cancer cell clones. Genomic rearrangements, including gene fusions may evolve, when two separate genes join to form a new gene product. Genes can also fuse at the RNA level due to splicing. The functional changes in fusion proteins and chimeric RNAs can cause cancer initiation, tumor progression, and drug resistance.

HGSC is a genetically unstable disease in which fusions are very common. Poor treatment outcomes can be associated with the emergence of treatment-resistant subclones. Deep sequencing has significantly increased the knowledge of the molecular characteristics of HGSC. Understanding the genomic and non-genomic abnormalities of HGSC tumors will help design personalized therapeutic approaches and discover novel mechanisms of drug resistance. However, at present, the role of gene fusions in HGSC is poorly studied.

This Ph.D. thesis aimed to identify new potential drug targets for ovarian cancer patients. Using computational modeling, we identified 228 novel fusion genes from 107 cancer samples of 36 HGSC patients. We demonstrated by laboratory experiments the presence of the most biologically interesting fusions in cancer cells. Furthermore, we investigated the PIK3R1-CCDC178 fusion protein and its role as a tumor-promoting alteration and impact on drug response. The fusion induced HGSC cell migration and resistance to platinum and trametinib treatment through ERK1/2 activation but the fusion-expressing cells remained sensitive to the combination of the treatments. Therapy resistance was associated with rod and ring-like cellular structure formation.

KEYWORDS: HGSC, p53, BRCA, fusion gene, rods and rings

TURUN YLIOPISTO
Lääketieteen tiedekunta
Biolääketieteen laitos
Patologia
HEIDI RAUSIO: Fuusiogeenit huonosti erilaistuneessa seroosissa munasarjasyövässä
Väitöskirja, 119 s.
Lääketutkimuksen tohtoriohjelma
Lokakuu 2023

TIIVISTELMÄ

Huonosti erilaistunut seroosi munasarjasyöpä (HGSC) on yleisin ja tappavin munasarjasyövän muoto. Perushoitomuoto on leikkaus, jota täydennetään platinan ja taksaanin yhdistelmähoidolla. Hoitovaste on usein hyvä, mutta suurimmalle osalle potilaista kehittyy lääkeresistenssi, mikä johtaa syövän etenemiseen ja kuolemaan. Hoitostrategia on pysynyt melko muuttumattomana eikä potilaiden kokonaiselossaoloajassa ole tapahtunut juurikaan edistystä viimeisten 20 vuoden aikana.

HGSC:n alkuvaiheessa p53-kasvunrajoiteproteiinin sekä homologisen rekombinaatiokorjausreitin toimimattomuus johtavat vaikeasti vioittuneeseen genomiin ja mahdollistavat yksilöllisten syöpäsolukloonien kehittymisen. Geenifuusiot voivat syntyä genomin uudelleenjärjestäytymisen seurauksena, jolloin kaksi erillistä geeniä muodostavat uuden geenituotteen. Geenit voivat fuusioitua myös RNA-tasolla silmukoitumisen seurauksena. Fuusioproteiinien ja -RNA:iden toiminnalliset muutokset voivat edesauttaa syövän syntymistä, etenemistä sekä lääkeresistenssin kehittymistä.

HGSC on geneettisesti hyvin epävakaa tauti, jossa fuusiot ovat erittäin yleisiä. Huono hoitotulos voidaan yhdistää hoitoresistenttien alakloonien syntymiseen. Syväsekvensointi on lisännyt merkittävästi tietoa HGSC:n molekulaarisista ominaisuuksista. Kasvainten genomisten ja ei-genomisten poikkeavuuksien ymmärtäminen auttaa yksilöllisten terapeuttisten ratkaisujen suunnittelussa ja uusien lääkeresistenssimekanismien löytämisessä. Toistaiseksi geenifuusioiden merkitystä HGSC:ssä on tutkittu melko vähän.

Väitöskirjatutkimukseni tarkoituksena oli löytää uusia potentiaalisia syöpälääkekohteita munasarjasyöpäpotilaille. Tunnistimme 228 uutta fuusiogeeniä 36:n HGSC-potilaan 107:sta syöpänäytteestä tietokonemallinnusta hyödyntäen. Osoitimme laboratoriokokein biologisesti mielenkiintoisimpien fuusioiden olemassaolon syöpäsoluissa. Tutkimme tarkemmin PIK3R1-CCDC178 fuusioproteiinin biologiaa ylituottosoluissa. Fuusio aikaansai ERK1/2 viestireitin aktivaation ja indusoi HGSC-solujen migraatiota ja resistenssin platina- ja trametinibihoidolle. Solut olivat kuitenkin herkkiä yhdistelmähoidolle. Lääkeresistenssi liittyi sauvamaisten ja rengasmaisten solunsisäisten filamenttirakenteiden muodostumiseen.

AVAINSANAT: HGSC, p53, BRCA, fuusiogeeni

Table of Contents

Abbreviations

ABL1	Abelson murine leukemia viral oncogene homolog 1
AKT	AKT Serine/Threonine Kinase
ALK	ALK Receptor Tyrosine Kinase
ATM	Ataxia-telangiectasia mutated
ATR	ATM- and Rad3-Related
AXL	AXL Receptor Tyrosine Kinase
BCR	Break-point cluster region
BMI-1	BMI1 Proto-Oncogene, Polycomb Ring Finger
BRCA	Breast cancer gene
CCDC178	Coiled-Coil Domain Containing 178
CDK	Cyclin Dependent Kinase
cDNA	Complementry DNA
CIN85	SH3 domain-containing kinase-binding protein 1
cis-SAGe	*Cis*-splicing between adjacent genes
CML	Chronic myelogenous leukemia
CTD	C-terminal regulatory domain
CTLA-4	Cytotoxic T-Lymphocyte Associated Protein 4
CTPS1	CTP synthase 1
CXCR4	C-X-C Motif Chemokine Receptor 4
DBD	DNA binding domain
DNA	Deoxyribonucleic acid
DON	6-Diazo-5-oxo-L-norleucine
EMSY	EMSY Transcriptional Repressor, BRCA2 Interacting
EMT	Epithelial-mesenchymal transition
EOC	Epithelial Ovarian Cancer
ERG	ETS Transcription Factor ERG
ERK1/2	Extracellular Signal-Regulated Kinase 1/2
FGFR	Fibroblast Growth Factor Receptor
FIGO	International Federation of Gynecology and Obstetrics
FISH	Fluorescence *in situ* hybridization
FTE	Fallopian tube epithelium

FTSEC	Fallopian tube secretory epithelial cell
GFP	Green fluorescent protein
GRIDSS	Genomic Rearrangement IDntification Software Suite
HEK293	Human embryonic kidney cell line
HGSC	High grade serous carcinoma
HR	Homologous recombination
HRD	Homologous recombination deficiency
HRR	Homologous recombination repair
IDS	Interval debulking surgery
IGV	Integrative Genomics Viewer
IMPDH2	Inosine monophosphate dehydrogenase 2
JAK	Janus Kinase
KRAS	KRAS Proto-Oncogene, GTPase
lncRNA	Long non-coding RNAs
mdm2	Mouse double minute 2 protein
MEK1/2	Mitogen-Activated Protein Kinase Kinase 1/2
MPA	Mycophenolic acid
mTOR	Mechanistic Target of Rapamycin Kinase
NACT	Neoadjuvant chemotherapy
ncRNA	Non-coding RNAs
NGS	Next-generation sequencing
NH3	Ammonia
NMD	Nonsense-mediated decay
NO	Nitric oxide
NTRK	Neurotrophic Receptor Tyrosine Kinase
OD	Oligomerization domain
OSE	Ovarian surface epithelium
OVCAR-8	Ovarian serous adenocarcinoma cell line
PALB2	Partner and localizer of BRCA2
PARP	Poly (ADP-ribose) polymerase
PBS	Phosphate-buffered saline
PCAWG	Pan-Cancer Analysis of Whole Genomes
PCR	Polymerase chain reaction
PD-1	Programmed cell death protein 1
PDGFB	Platelet Derived Growth Factor Subunit B
PDS	Primary debulking surgery
PI3K	Phosphoinositide 3-kinase
PIK3R1	Phosphoinositide-3-Kinase Regulatory Subunit 1
PRD	Proline-rich domain
PTEN	Phosphatase And Tensin Homolog

RAD51	RAD51 Recombinase
RET	Ret Proto-Oncogene
RNA	Ribonucleic acid
RNA-ISH	RNA *in situ* hybridization
RNA-Seq	RNA sequencing
ROS1	ROS Proto-Oncogene 1, Receptor Tyrosine Kinase
rRNA	Ribosomal RNA
RRs	Rods and rings
RT-PCR	Reverse transcriptase polymerase chain
RT-qPCR	Reverse-transcription quantitative polymerase chain
SAS	Sense–antisense
SBS	Sequencing by synthesis
STIC	Serous tubal intraepithelial carcinomas
SV	Structural variation
TAD	Transcriptional activation domains
TCGA	The Cancer Genome Atlas
TP53	Tumor Protein P53
UTR	Untranslated region
WEE1	WEE1 G2 Checkpoint Kinase
VEGF	Vascular endothelial growth factor
WGS	Whole genome sequencing
WHO	World Health Organization
WT-1	WT1 Transcription Factor

List of Original Publications

This dissertation is based on the following original publications, which are referred to in the text by their Roman numerals:

I Cervera, A*, **Rausio, H***, Kähkönen, T, Andersson N, Partel, G, Rantanen, V, Paciello, G, Ficarra, E, Hynninen, J, Hietanen, S, Carpén, O, Lehtonen, R, Hautaniemi, S, Huhtinen, K FUNGI: Fusion Gene Integration Toolset. *Bioinformatics*, 2021;19:3353–3355.

II **Rausio, H**✉, Cervera, A, Dahlström-Heuser, V, West, G, Oikkonen, J, Pianfetti, E, Lovino, M, Ficarra, E, Taimen, P, Hynninen, J, Lehtonen, R, Hautaniemi, S, Carpén, O, Huhtinen, K. PIK3R1 fusion induces platinum resistance in high-grade serous ovarian cancer by an unexpected mechanism. *Manuscript.*

* equal contribution, ✉ corresponding author

1 Introduction

Ovarian cancer is the seventh most common cancer in women worldwide, with over 314 000 cases diagnosed and 207 000 women dying annually (Sung et al., 2021). The corresponding numbers in Finland are approximately 560 diagnoses and 360 deaths per year (*Finnish Cancer Registry*, 2020). High-grade serous ovarian cancer (HGSC) is the most common and deadliest subtype of ovarian cancers. The primary loss of the tumor suppressor p53 and the inactivation of the homologous recombination (HR) pathway initiate chromosomal instability, which, together with genomic rearrangements, forms the structural basis for fusion genes (Bowtell, 2010; Lu et al., 2021). The response of HGSC tumors to DNA damage and copy-number changes underlies the ability of these tumors to manage genotoxic stress (Patch et al., 2015). A highly aberrant genome is a defining feature of HGSC (Bowtell, 2010).

The standard treatment for HGSC is debulking surgery followed by chemotherapy (Benedet et al., 2000). Treatment strategy has mostly stayed the same over the last decades. PARP inhibitors have demonstrated significant benefits exclusively for patients with HR deficiency (HRD) (Evans & Matulonis, 2017; Färkkilä et al., 2021). In addition, ovarian cancer is still a major clinical issue, with little progress in overall survival over the previous 20 years (Nesic et al., 2018). The poor outcome can be traced to the emergence of treatment-resistant subclones (Bashashati et al., 2013). Instead of depending on a handful of driver mutations, thousands of genes connected with many chromosomal aberrations may contribute to developing treatment resistance (Bowtell, 2010). To date, deep sequencing has significantly increased the knowledge of molecular characteristics in HGSC. Understanding the individual evolutionary trajectories and diverse genomic abnormalities prior to therapy aids the design of personalized therapeutic solutions and the investigation of drug resistance mechanisms (Bashashati et al., 2013).

Our study focused on identifying novel potential drug targets for ovarian cancer patients. We developed a computational pipeline to detect and prioritize fusion genes from RNA sequencing (RNA-Seq) data of HGSC patient tumors. The discovered fusions were experimentally confirmed to establish their presence in tumor cells and to demonstrate that the pipeline is functional. Fusion genes targeting the PI3K-AKT-mTOR pathway were selected for further *in vitro* experiments. We transfected

ovarian cancer cells with the fusion constructs. PIK3R1-CCDC178 induced changes in cell morphology and behavior. Therefore, we concentrated on this fusion to study its molecular effects on migration, proliferation, signaling cascades, and response to targeted pathway inhibitors and conventional cisplatin therapy.

2 Review of the Literature

2.1 High-grade serous ovarian cancer (HGSC)

2.1.1 Anatomy and histology of adnexa

The female reproductive organs include the ovaries, Fallopian tubes, uterus, vagina, and vulva (Figure 1) (Rosner et al., 2022). Adnexa refers to the Fallopian tubes and ovaries found on both sides of the uterus (Guile & Mathai, 2023). Fallopian tubes are hollow organs originating from the uterine horns and are anatomically divided into isthmus, ampulla, and infundibulum. Histologically, the Fallopian tubes comprise three primary layers: the mesosalpinx, which forms the serous membrane; the myosalpinx, which encompasses the muscular layer; and the endosalpinx, which constitutes the mucosal layer (Vang et al., 2017; Winuthayanon & Li, 2018). The mucosal layer includes secretory, ciliated and, Peg cells. In the distal part of the infundibulum, the mucosal epithelium folds give rise to branching structures known as fimbriae, which surround the ovaries (Rigby et al., 2022).

The ovarian cortex comprises the external epithelial layer, also known as germinal epithelium, and contains numerous ovarian follicles. The inner part of the ovary, medulla, is composed of loose connective tissue and a neurovascular network (Williams & Erickson, 2012). The peritoneum (broad ligament) covers the ovaries and the Fallopian tubes, linking these organs to the pelvic sidewalls (Craig et al., 2023).

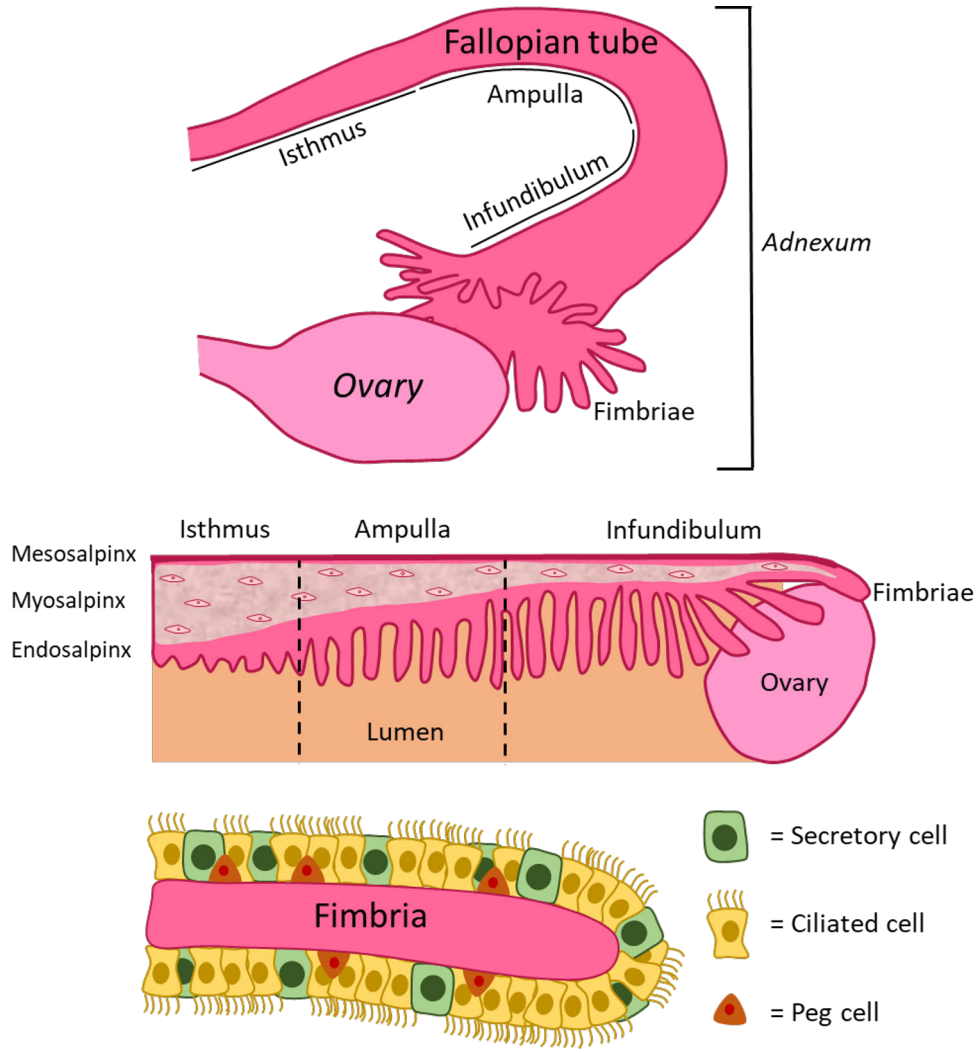

Figure 1. Anatomy of adnexum and cell types of mucosal fimbriae. The adnexum consists of a Fallopian tube and ovary. The sagittal cross section of the adnexum depicts the layers of the Fallopian tube, which, from the outermost to the luminal side, includes the mesosalpinx, myosalpinx, and endosalpinx. The endosalpinx is the luminal mucosal layer, which forms the fimbriae. Secretory, ciliated, and Peg cells form the outer surface of the fimbriae. Modified from (NCI, 2017; Ng & Barker, 2015).

2.1.2 Classification of epithelial ovarian cancer

Based on the World Health Organization (WHO) histopathologic classification of ovarian tumors in 2014, epithelial ovarian cancer (EOC) is classified into several distinct morphological and molecular subtypes. These include endometrioid, clear cell, seromucinous, low-grade serous, mucinous carcinomas, and Brenner tumors,

high-grade serous carcinomas, carcinosarcomas, and undifferentiated carcinomas (Kurman & Shih, 2016; Moriya, 2018; Mutch & Prat, 2014). HGSC is the most aggressive and lethal subtype of ovarian cancer, accounting for more than 70% of all EOCs (Kurman & Shih, 2016). Early-stage disease is typically asymptomatic, and there are currently no reliable screening methods to detect initial-stage cancer (*Finnish Cancer Registry*, 2020). Therefore, 80% of HGSCs are diagnosed at an advanced stage (*Finnish Cancer Registry*, 2020), International Federation of Gynecology and Obstetrics (FIGO) stages III or IV. FIGO stage III tumors involve one or both ovaries with peritoneal metastases outside the pelvis and/or positive regional lymph nodes. FIGO stage IV tumors are defined as distant metastasis; cancer cells are spread beyond the abdominal cavity (Benedet et al., 2000; Mutch & Prat, 2014).

2.1.3 Clinical characteristics and treatment of HGSC

HGSC occurs most commonly in postmenopausal women between 50 to 70 years of age (Benedet et al., 2000; Kim et al., 2018). Early-stage HGSC often exhibits no symptoms or presents with vague ones, resulting in delayed diagnosis (Benedet et al., 2000; *Finnish Cancer Registry*, 2020). While initial treatment responses are usually positive, most patients eventually relapse and develop drug resistance, resulting in disease progression and death (Nero et al., 2021). Despite these challenges, the treatment strategy has remained largely unchanged over the past few decades (Nero et al., 2021; Vaughan et al., 2011).

The selection of the primary therapeutic interventions is contingent upon the extent of cancer dissemination. If the cancer is operable, the first-line treatment consists of primary debulking surgery (PDS) followed by platinum-taxane chemotherapy. If surgical resection is not feasible, neoadjuvant chemotherapy (NACT) is employed to reduce cancer load before proceeding with interval debulking surgery (IDS) (Figure 7) (Nero et al., 2021). The amount of residual disease after surgery is the most crucial prognostic factor, addressing the importance of maximal tumor debulking (Kehoe et al., 2015; Polterauer et al., 2012).

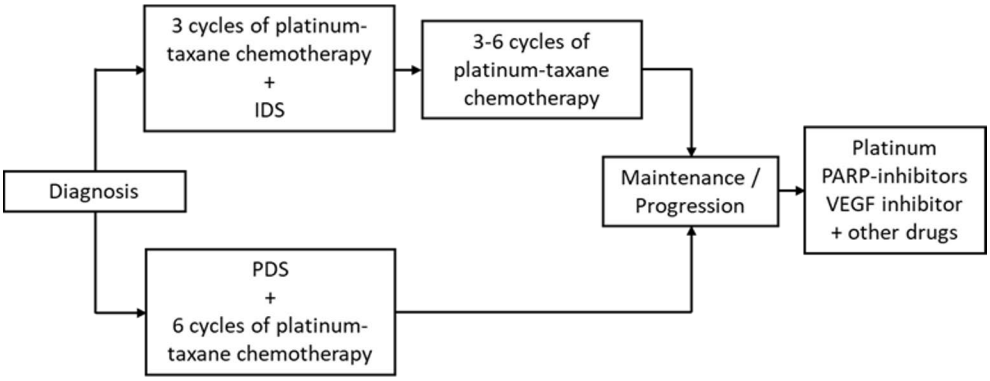

Figure 7. Treatment strategy for HGSC. Modified from (Nero et al., 2021).

2.1.3.1 Conventional platinum-taxane therapy

The platinum analogs, cisplatin (cis-diamminedichloroplatinum(II)) and carboplatin (cis-cyclobutanedicarboxylatodiammineplatinum(II)), are among the most widely used chemotherapeutic agents in numerous malignancies, including HGSC (Ho et al., 2016). Cisplatin was the first platinum-based drug approved for clinical use in 1978 (Kelland, 2007). Cisplatin replaced the existing drugs used for the treatment of ovarian cancer at that time and soon became the primary therapy (Markman, 2003) until carboplatin was approved in 1989 (Ghosh, 2019). Carboplatin was introduced with comparable effectiveness to cisplatin in treating ovarian cancer but with remarkedly reduced toxicity (Gurney et al., 1990) and therefore began to replace the cisplatin regimen (Markman, 2003).

Cisplatin contains a central platinum ion (Pt) with two chlorides (Cl) and two ammonia (NH3) ligands (Ghosh, 2019). The chloride concentration in the bloodstream is relatively high; therefore, cisplatin remains unchanged and neutral (Petrović & Todorović, 2016). However, plasma proteins (*e.g.*, albumin) can bind strongly to cisplatin, deactivating 65–95% of the drug within 24 hours of administration (Alderden et al., 2006). Cisplatin enters cells via passive diffusion across the plasma membrane. The mechanism of action begins inside the cell, where the chloride concentration is much lower (Petrović & Todorović, 2016). Platinum-chloride bonds are hydrolyzed in the cytosol, and the resulting species are good electrophiles that can bind to a variety of nucleophiles in the cell, including nitrogen donor atoms (guanine, G, and adenine, A) of nucleic acids (Dasari & Bernard Tchounwou, 2014). Most DNA-cisplatin adducts are formed by intrastrand 1,2-d(GpG) cross-links, which means that cisplatin binds to the reactive nitrogen atoms (N7) of two adjacent guanine bases within the same DNA strand. The other two intrastrand cross-links are 1,3-d(GpG) and 1,2-d(GpA). 1,2-intrastrand adducts are considered to induce cytotoxicity more effectively than 1,3-intrastrand adducts.

Adducts can also be formed between the two DNA strands by 1,3(GpXpG) interstrand binding. The adduct formation of cisplatin leads to DNA damage and apoptosis of the cell (Ghosh, 2019). The spectrum of platinum sensitivity ranges from initial resistance (observed in 15% of HGSC patients) to complete remission (approximately 85% of HGSC patients) (Cooke & Brenton, 2011; Nero et al., 2021). Nonetheless, 75% of the patients experience a relapse. Females with HR deficiency exhibit a more favorable response to platinum-based therapy compared to those who are HR proficient (Cooke & Brenton, 2011; Feng et al., 2023; Stewart et al., 2022). Identifying novel drug targets for the disease could be particularly advantageous for HGSC patients who respond poorly or not at all to platinum treatment.

Taxanes, a new class of drugs, were developed in the late 1980s and early 1990s (Lisio et al., 2019). Paclitaxel is a taxane prototype that targets microtubules. Microtubules are responsible for the development of the mitotic spindle during cell division. Furthermore, they are necessary for cell shape, motility, and cytoplasmic movement inside the cell. Paclitaxel stabilizes microtubules causing their dysfunctionality and thereby inducing cell death by disrupting the normal microtubule dynamics required for cell division (Lastair et al., 1995). A pivotal clinical trial indicated the efficacy of cisplatin-paclitaxel combination therapy; it significantly improved response rates, progression-free survival, and overall survival compared to the standard therapy at the time, cisplatin-cyclophosphamide (McGuire et al., 1996). Later, similar carboplatin-paclitaxel combination therapy trials also confirmed better tolerability of this combination (Andreas du Bois et al., 2003; Parmar et al., 2002). The combination of carboplatin and paclitaxel has been the foundation of chemotherapeutic treatment for HGSC for over 20 years (Benedet et al., 2000; A. Du Bois et al., 1999; McGuire et al., 1996).

Other conventional chemotherapy compounds include pegylated doxorubicin, topotecan, gemcitabine, etoposide, and vinorelbine. These drugs can be used as primary treatment, maintenance, or for relapsed disease (Lisio et al., 2019).

2.1.3.2 Complementary therapies

Most patients initially respond well to platinum-taxane combination therapy. However, the disease frequently recurs, at which point there are limited treatment options (Kurman & Shih, 2016). PARP inhibitors and bevacizumab are adjuvant treatments only approved in the 2010s as part of HGSC therapy (Table 1) (Lisio et al., 2019). They are used as maintenance drugs and for patients with progressive disease in addition to platinum-based treatment. Patients can also benefit from experimental drugs (Nero et al., 2021).

Poly (ADP-ribose) polymerase (PARP) is an enzyme critical in base excision repair, a repair mechanism for DNA single-strand breaks. PARP inhibition generates

an abundance of single-strand breaks, which may contribute to double-strand breaks during replication. The double-strand breaks are restored by homologous recombination repair (Helleday et al., 2008). For patients carrying *BRCA1/2* mutations or other homologous recombination deficiencies, the inhibition of PARP induces a synthetic lethal interaction. The accumulation of double-strand breaks and insufficient repair mechanisms can lead to chromosomal instability, cell cycle arrest, and subsequent apoptosis (Farmer et al., 2005). Olaparib, niraparib, and rucaparib are PARP inhibitors and are currently FDA-approved for recurrent ovarian cancer after showing consistent improvement in progression-free survival (Coleman et al., 2017; Mirza et al., 2016; Pujade-Lauraine et al., 2017). However, their efficacy is generally restricted to tumors with homologous recombination deficiency (Evans & Matulonis, 2017).

Bevacizumab is a humanized monoclonal antibody that targets vascular endothelial growth factor A (VEGF-A). When VEGF binds to its particular receptors, angiogenesis is initiated. Bevacizumab prevents binding between VEGF and the receptor by binding to the VEGF, thereby restraining angiogenesis. Anti-VEGF treatment can improve progression-free survival, but its effect on overall survival has been questioned (Schmid & Oehler, 2015).

Treating HGSC is complex, and clinicians strive to provide patients with individualized therapy by understanding the tumor profile that will respond to the available medicines at that precise moment of the disease (Nero et al., 2021). Unfortunately, despite the remarkable research over the past decades, it has been difficult to advance beyond platinum-based therapy, which is still the standard of care (Vaughan et al., 2011).

Table 1. Timeline of approved treatments in HGSC. Modified from (Lisio et al., 2019).

Before 1970	1970s	1980s	1990s	2000s	2010s
Alkylating agents - Cyclophosamide ***Anthracycline*** - Doxorubicin ***Antimetabolites*** - 5-fluorouracil	***Platinum*** - Cisplatin	***Platinum*** - Carboplatin	***Taxanes*** - Paclitaxel		***PARP inhibitors*** - Olaparib - Rucaparib - Niraparib ***Antiangiogenic therapy*** - Bevacizumab

2.1.4 Genetics of HGSC

Previously, it was thought that HGSC originates in the ovarian surface epithelium (OSE) or cortical inclusion cysts (Vang et al., 2013). However, according to current knowledge, the main origin of HGSC is "p53 signed" secretory epithelial cells of the Fallopian tube fimbriae (Figure 2), which form the precursor lesion, serous tubal intraepithelial carcinoma (STIC) (Kindelberger et al., 2007; Piek et al., 2001; Vang et al., 2017). HGSC has also been proven to arise from the intraluminal Fallopian tube epithelium (FTE) with identical immunohistochemical profile and *TP53* mutational status as fimbrial STICs and abdominal metastasis (Bijron et al., 2013; Jazaeri et al., 2011). The p53 signature depicts the loss of functional p53 due to *TP53* mutations, which is the primary event in HGSC initiation and progression. In addition, the dysfunction of the BRCA tumor suppressor proteins, leads to a deficiency in homologous recombination repair (HRR) of DNA double-strand breaks, which, in turn, initiates chromosomal instability and results in copy number changes (Bowtell, 2010). These events drive the molecular subtype specification; tumors are categorized as immunoreactive, proliferative, differentiated, and mesenchymal subtypes based on their gene expression features (Bowtell, 2010; Kurman & Shih, 2016). Histologically HGSC tumors are classified as usual type and SET variant (solid, pseudo endometrioid, transitional). SET tumors have *BRCA1* mutations and have a higher number of tumor-infiltrating lymphocytes than usual HGSC (Soslow et al., 2012).

When STICs, either originating from Fallopian tube secretory epithelial cells (FTSECs) of the fimbriae or the intraluminal Fallopian tube secretory epithelial cells, gain invasive features, they become HGSC and metastasize to the ovary and abdominopelvic cavity, including mesentery, omentum, lymph nodes and grow in the ascites fluid (Karst & Drapkin, 2010; Kurman & Shih, 2016; Vang et al., 2013). Furthermore, the cancerous cells have the potential to infiltrate the underlying tubal mucosa (Shih et al., 2021; Singh et al., 2017). HGSC is clinically classified into high-grade serous ovarian cancer (HGSOC), high-grade tubal carcinoma or high-grade peritoneal carcinoma, depending on assumed site of origin. However, they are one disease with similar origin and characteristics (Kim et al., 2018). Unfortunately, because HGSC is usually diagnosed at an advanced stage, the tumors have spread extensive throughout the peritoneal cavity and beyond and are not easy to cure. Furthermore, individual genetic variations present challenges to develop targeted treatments for these heterogeneous tumors. In addition, clonal lineages are unique for each patient (Kannan et al., 2014).

Fusion genes are common genetic aberrations in HGSC (Cervera et al., 2021; McPherson et al., 2011) and are a consequence of failed repair and splicing mechanisms (Dorney et al., 2023; Weckselblatt & Rudd, 2015). Novel chimeric RNAs and fusion proteins can perform a variety of new roles in tumor cells,

including gain- or loss-of-function and regulation of transcription and translation (Chwalenia et al., 2017). These changes may promote disease progression and chemoresistance (Schram et al., 2017). Therefore, discovery of specific molecular signatures between primary and relapsed tumors is essential for understanding the involvement of fusion genes in tumorigenesis and treatment resistance of HGSC.

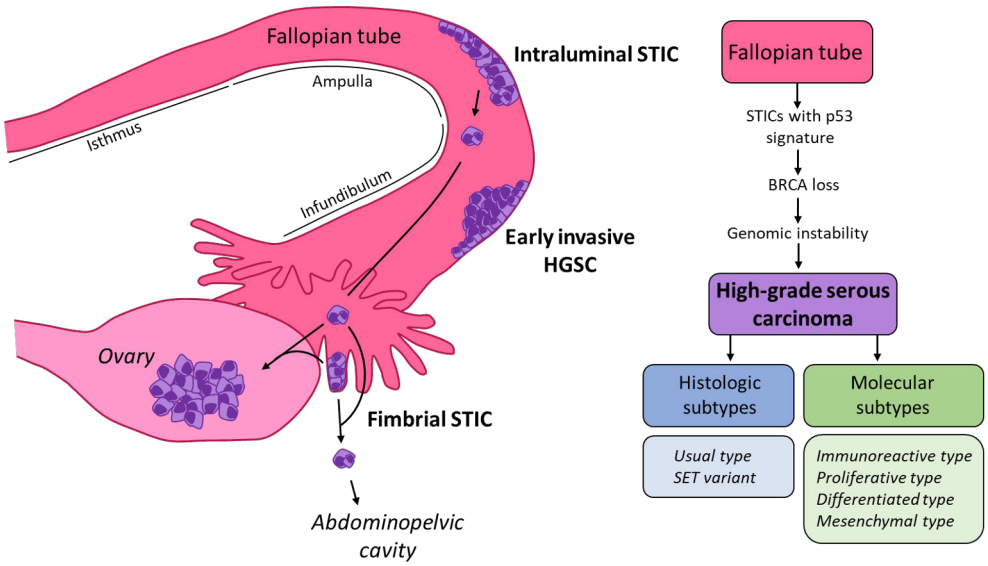

Figure 2. Origin and subtypes of HGSC. HGSC originates from serous tubal intraepithelial carcinomas (STICs). When the *TP53* mutated FTSECs gain invasive features, they become HGSC and metastasize to the ovary and abdominopelvic cavity or invade into the tubal mucosa. Histologically, HGSCs are divided into the usual type and SET variant. Modified from (Kurman & Shih, 2016; NCI, 2017).

2.1.4.1 Molecular features: *TP53*

TP53 is a tumor suppressor gene that encodes the 53 kDa protein p53 on chromosome 17p13.1. The full-length isoform of p53 is composed of 11 exons and includes 393 amino acids. p53 also has 23 different protein-coding isoforms (*TP53 Gene*, 2023) encoded by the *TP53* gene and produced via varying mechanisms, including alternative promoter usage, splicing, and translation start site (Bourdon, 2007). The p53 protein has five functional domains; two N-terminal transcriptional activation domains (TAD), a proline-rich domain (PRD), a DNA binding domain (DBD), an oligomerization domain (OD), and a c-terminal regulatory domain (CTD) (Figure 3) (Sullivan et al., 2017). p53 is foundational in regulating and progressing the cell cycle, apoptosis, DNA damage repair, senescence, and metabolism (Amelio & Melino, 2020). In a normal cell, wild-type p53 has a short half-life and is retained

at low protein levels (Maki & Howley, 1997) by the mouse double minute 2 protein (mdm2), which promotes rapid p53 degradation (Haupt et al., 1997; Kubbutat et al., 1997) In response to a variety of stressors, such as ultraviolet and ionizing radiation-induced DNA damage, hypoxia, abnormal proto-oncogene activation, mitogenic signaling, mitotic spindle damage, or nitric oxide (NO) production, p53 is stabilized, activated, and accumulated in the cell (Maki & Howley, 1997; Maltzman & Czyzyk, 1984). p53 performs the majority of its functions in the nucleus by acting as a sequence-specific DNA binding transcription factor that regulates the expression of numerous genes. For example, during DNA damage, active p53 is translocated to the nucleus, where it binds to DNA and promotes anti-tumorigenic effects by increasing the transcription of various critical genes. p53 also has cytoplasmic activities, such as inducing apoptosis via an intrinsic mitochondrial-mediated pathway (Aubrey et al., 2017).

Somatic *TP53* mutations are the most common and initial genetic change in HGSC. *TP53* is altered in nearly 100% of HGSC tumors (D. Bell et al., 2011), while only around 3% were recently reported to express wild-type p53 (Chui et al., 2020; Na et al., 2017). Furthermore, p53 is downregulated in most wild-type p53 HGSC tumors (64%, 9/14), *e.g.*, inactivated by mdm2 due to its amplification (Chui et al., 2020). According to The Cancer Genome Atlas (TCGA), the most frequent types of *TP53* variations in HGSC are missense (60–70%), followed by nonsense (10–25%) (D. Bell et al., 2011; Na et al., 2017), frameshift (15%), splice site (11%) and in-frame mutations (3%) (D. Bell et al., 2011). Missense mutations predominantly emerge in the DBD, resulting in the loss of wild-type p53 (Figure 3) (Brachova et al., 2013). However, these missense hotspot mutations result in the gain of p53 oncogenic function. Functional mutations (R248 and R273) disrupt direct p53 DNA binding, affecting its ability to transactivate promoters of its target genes. Structural mutations (R175, G245) result in p53 that is structurally unstable and partially unfolded, impairing its action (Brachova et al., 2013; Freed-Pastor & Prives, 2012). Nonsense mutations can result in a complete lack of p53 expression in HGSC (Brachova et al., 2013).

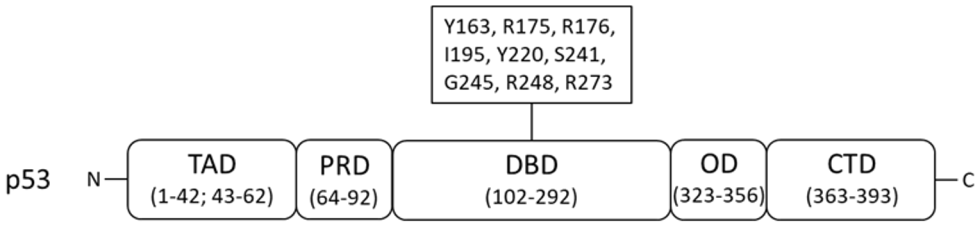

Figure 3. Protein domains of p53 protein and the nine most common hotspot mutations of *TP53* gene target DBD in HGSC based on the TCGA data. Modified from (Saleh & Perets, 2021).

The role and cause of *TP53* mutations as HGSC initiators in STICs are unknown (Saleh & Perets, 2021). Because mutated p53 is expressed in nearly all HGSC tumors (D. Bell et al., 2011) and mutations occur at an early stage of HGSC pathogenesis, it is thought that p53 acts as a driver gene in HGSC and that its dysfunction is required to initiate the disease's genomic instability (Bowtell, 2010). It is supposed that malignant transformation also acquires enhanced proliferation, nuclear pleomorphism, and loss of epithelial polarity to become invasive HGSC (Karst & Drapkin, 2010), and *TP53* mutation alone cannot transform the Fallopian tube epithelium and induce HGSC genesis. However, it has been demonstrated that mutant p53 has different effects depending on the cell type: mutant p53 promotes epithelial-mesenchymal transition (EMT) and migration in FTE but not in the ovarian epithelium (Quartuccio et al., 2015). In addition, various types of cells can engage in interactions. For instance, growth factors expressed in the ovaries can trigger the survival, migration, and attachment of FTSECs that harbor gain-of-function mutations of TP53 (R273H, R248, and R175) (Kang et al., 2020). Even if mutated p53 is a diagnostic marker for HGSC and plays a role in HGSC initiation and progression, a more profound knowledge of the mutant p53 mode of action is required (Brachova et al., 2013).

2.1.4.2 Molecular features: *BRCA1/2*

Approximately half of all HGSCs exhibit HR defects upon initial diagnosis (D. Bell et al., 2011). The genes associated with breast cancer, *BRCA1* located on chromosome 17q21 and *BRCA2* on chromosome 13q12.3, are classified as tumor suppressor genes. These genes encode pivotal proteins in maintaining genomic stability by mending double-strand DNA breaks (Friedman et al., 1994; Wooster et al., 1994). Cells are constantly exposed to factors, such as by-products of cellular metabolism, oxidative stress or chemical exposure, and spontaneous DNA mutation events, which can damage DNA (De Bont & van Larebeke, 2004). Nevertheless, cells possess an evolutionarily conserved mechanism called homologous recombination DNA repair, which enables them to endure genomic flaws.

The repair process involving BRCA1 and BRCA2 is triggered upon detecting a double-strand DNA break within a cell. First, ATM and ATR kinases recognize the double-strand break and come into play by phosphorylating downstream targets, including BRCA1. In collaboration with other proteins, BRCA1 acts as a scaffold to orchestrate the assembly of repair proteins BARD1 and BRIP1 (C. S. Walsh, 2015). An MRN complex (including Mre11, RAD50 and NBS1) resects DNA in the 5′ to 3′ direction producing single-stranded DNA (ssDNA) tails (T. Liu & Huang, 2016). The ssDNA molecules are coated with replication protein A (RPA). To substitute RPA with RAD51 on ssDNA, the recruitment of BRCA2 is facilitated by PALB2 and leads to the loading of RAD51 onto the RPA-coated DNA, assisted by RAD51B,

RAD51C, and RAD51D (Bhat & Cortez, 2018; Krejci et al., 2012; C. S. Walsh, 2015). Subsequently, this complex facilitates the creation of RAD51 filaments, initiating strand invasion when the RAD51-ssDNA filaments infiltrate the other parental double-strand DNA molecule. This homologous DNA allows for accurate and error-free synthesis and repair of DNA (C. S. Walsh, 2015).

HR defects can arise due to either inherited or somatic mutations in *BRCA1* and *BRCA2* genes. Additionally, such defects can stem from mutations in other genes involved in HR, including *ATM*, *ATR*, *EMSY*, *CHEK2*, *PALB2*, *RAD51*, and *PTEN*, although these occurrences are less frequent (D. Bell et al., 2011; Garsed et al., 2022; Pennington et al., 2014). Approximately 8–12% of HGSC patients have pathogenic germline *BRCA1* mutations, while 5–7% have *BRCA2* mutations (D. Bell et al., 2011; T. Walsh et al., 2011). Somatic mutations affect around 3% of *BRCA1* and *BRCA2* patients. HR deficiency can also arise due to epigenetic inactivation through promoter hypermethylation. Notably, 11% of *BRCA1* and 3% of *RAD51C* genes experience hypermethylation, resulting in mutation accumulation and the progression of cancer (D. Bell et al., 2011).

Females who inherit pathogenic variants in one of these genes are more likely to develop breast and ovarian cancer. They are also at a higher risk of getting cancer at a younger age than women who do not have such a variant. The cumulative risk of ovarian cancer is 44% for BRCA1 carriers and 15% for BRCA2 carriers until age 80 (Bell et al., 2011a). *PALB2* (partner and localizer of BRCA2) is a more recently identified susceptibility gene for breast and ovarian cancer, and mutant *PALB2* has been linked to an elevated risk of HGSC, especially in the Finnish population (Chui et al., 2020; Erkko et al., 2007; Kuusisto et al., 2011).

Pathogenic *BRCA* variants vary greatly within different populations (Figure 4) (Abul-Husn et al., 2019; Nurmi et al., 2019). BRCA defects result in genomic instability, which promotes sustained proliferative signaling, resistance to cell death, evasion of growth suppressors, replicative immortality, avoiding immune destruction, angiogenesis, and invasive and metastatic capabilities (Bowtell, 2010; Hanahan, 2022).

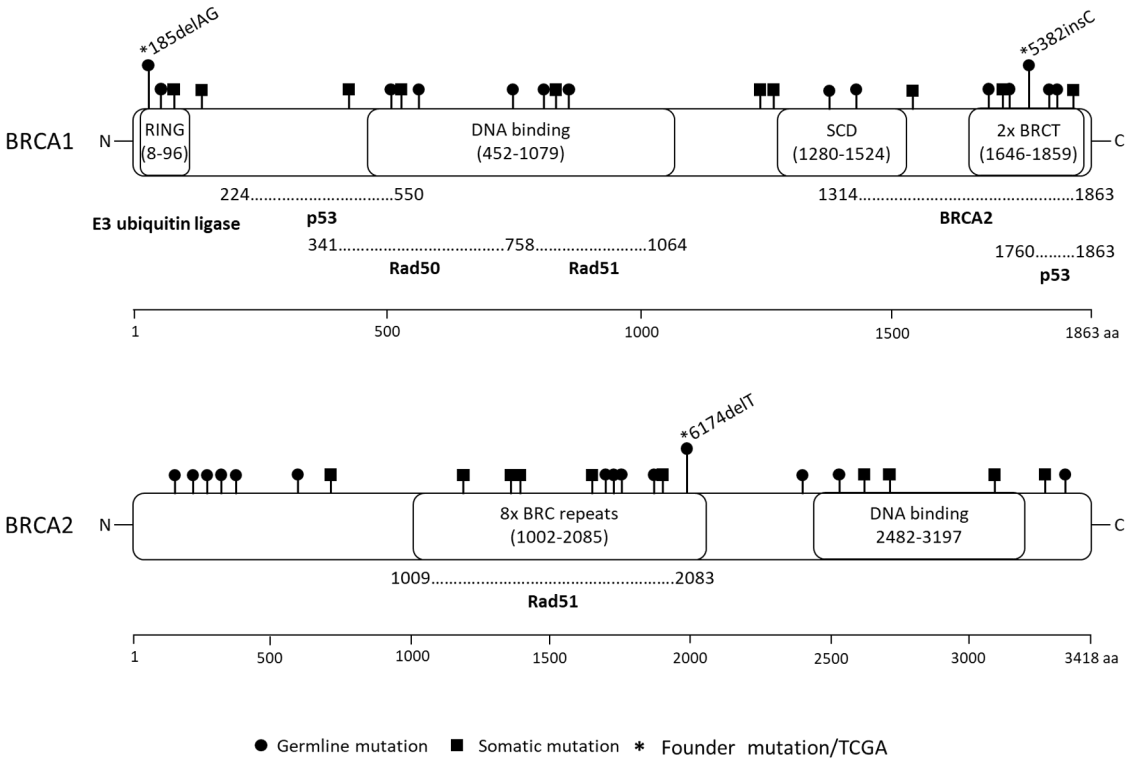

Figure 4. Protein domains and founder mutations of BRCA1 and BRCA2. BRCA1 has 1863 amino acids and multiple key functional domains interacting with various proteins. BRCA2 consists of 3418 amino acids but contains only two known functional domains. BRCA1 is also required for cell-cycle progression, ubiquitylation, transcription, and chromatin remodeling, while BRCA2 functions are poorly known (Narod & Foulkes, 2004; Nesic et al., 2018). Germline and somatic mutations of *BRCA1/2* vary between populations. Founder mutations marked with *. Modified from (D. Bell et al., 2011).

2.1.4.3 Signaling pathway alterations in HGSC

In HGSC, many signaling pathways are deregulated. Approximately 45% of HGSC patients have altered PI3K-AKT-mTOR/RAS-MEK-ERK signaling cascades (Bell et al., 2011a). The reason for the activation of these signaling pathways is unknown (Chesnokov et al., 2021; P. Liu et al., 2009; Rinne et al., 2021). In the past, the prevailing notion was that the PI3K-AKT-mTOR and RAS-MEK-ERK pathways functioned as distinct linear signaling pathways, each activated by separate stimuli. However, contemporary understanding reveals that these pathways collaborate with one another (Figure 5) (Cuesta et al., 2021; Cully et al., 2006; Mendoza et al., 2011).

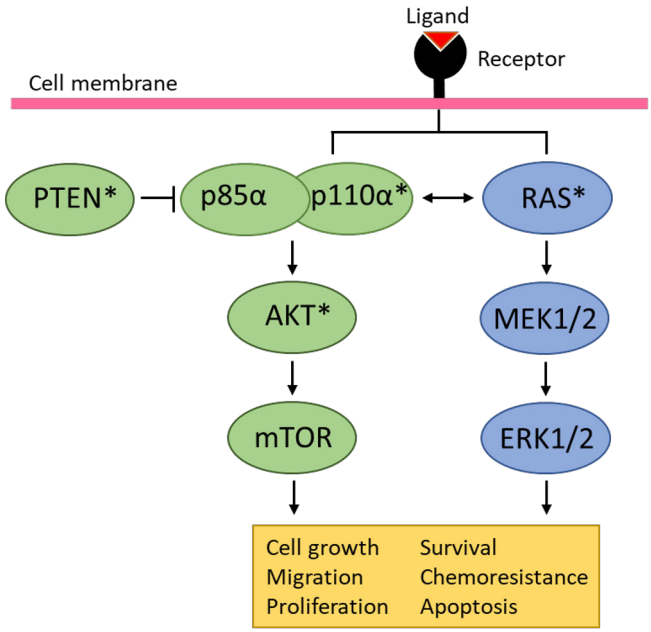

Figure 5. Illustration of PI3K-AKT-mTOR and RAS-MEK1/2-ERK1/2 pathways. Pathway-activating protein alterations are marked with *. Modified from (Downward, 2008).

The dysregulation of the PI3K-AKT-mTOR pathway plays a significant role in promoting cell proliferation, migration, and resistance to chemotherapy in HGSC (Rinne et al., 2021). *PIK3R1* located on chromosome 5 encodes the p85α protein and serves as a regulatory subunit of PI3 kinase (P. Liu et al., 2009; Rinne et al., 2021). The p85α protein comprises SH3, BH, and three SH2 protein domains (Figure 6). Within the regulation of the PI3K-AKT-mTOR pathway, the SH2 binding domains play a crucial role in stabilizing the catalytic subunit of PI3K, p110α, encoded by the *PIK3CA* gene. These SH2 domains are also necessary for the phosphorylation induced by ligands on receptor tyrosine kinases. Following this phosphorylation, the inhibitory effect of p85α on p110α is released, ultimately resulting in the activation of the PI3K-AKT-mTOR signaling cascade. The PTEN phosphatase can counteract the pathway to which p85α binds through its SH3 and BH domains (Daphne W Bell, 2012; P. Liu et al., 2009; Rathinaswamy & Burke, 2020).

PIK3R1 is rarely mutated in HGSC (Bell et al., 2011b), and the pathway-activating alterations of the PI3K-AKT-mTOR pathway typically involve *PTEN* (7% deleted) and *PIK3CA* (18% amplified) (Bell et al., 2011b; Bowtell, 2010; Bowtell et al., 2015; Masoodi et al., 2020). However, it is often mutated in many other malignancies (X. Li et al., 2021). *PIK3R1* mutations affect cellular signaling, including the ERK/MAPK cascade, cellular phenotypes, and therapeutic responses (L. Chen et al., 2018; Cheung et al., 2011, 2014; X. Li et al., 2021; Y. Liu et al.,

2022). In addition, it has been demonstrated that a truncating p85α mutation enhances the invasion of ovarian endometrioid cancer cells by activating ERK1/2 (Cheung et al., 2014).

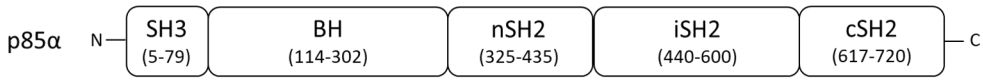

Figure 6. Protein domains of p85α. SH3, Src homology 3 domain; BH, breakpoint cluster region homology-domain; n/i/cSH2, N-terminal/Inter/C-terminal Src homology 2 domains. Modified from (Daphne Bell, 2012).

The role of the RAS-MEK1/2-ERK1/2 pathway can vary between functioning as an oncogene or tumor suppressor, contingent upon factors such as signal intensity, the context or tissue in which the signal has erroneously triggered, or the tissue-specific tumor microenvironment (Burotto et al., 2014). Many proteins within the RAS-MEK1/2-ERK1/2 pathway are commonly altered in HGSC (Chesnokov et al., 2021). For example, based on TCGA data, *KRAS* amplification has been demonstrated in 11% of HGSC cases, resulting in the activation of the RAS-MEK1/2-ERK1/2 pathway (D. Bell et al., 2011; Burotto et al., 2014). Including all possible alterations, 53% of HGSC cases demonstrate a *KRAS* alteration. The interaction between PI3K-AKT-mTOR and RAS-MEK1/2-ERK1/2 signaling pathways may enable even more complex regulation of signaling pathways in cancer cells. For instance, the crosstalk could represent a potential mechanism for resistance, sustaining tumor growth (Hendrikse et al., 2023). Kinase inhibitors as monotherapy have yielded disappointing results, whereas treatments combining kinase inhibitors targeting signaling pathways or combining them with chemotherapy have shown more promising outcomes. However, these approaches are not anticipated to result in a universally applicable breakthrough therapy due to the heterogeneity of the disease. Nonetheless, they may benefit certain HGSC patients (Skorda et al., 2022).

2.2 Fusion genes

Gene fusions result from either genomic or nongenomic rearrangements. (Mukherjee et al., 2023). Genomic rearrangements are a type of structural variation (SV) that is normal and beneficial to human health and adaptability (Weckselblatt & Rudd, 2015). However, chromosomal aberrations are a significant class of somatic alterations in cancer that can play critical roles inter alia in the early stages of tumorigenesis (Mertens et al., 2015; Mitelman et al., 2007). The first cancer-associated chromosomal rearrangement was discovered in chronic myelogenous leukemia (CML), resulting from the neoplastic transformation of hematopoietic stem

cells (Nowell & Hungerford, 1960; Rowley, 1973). The genetic abnormality of CML is a translocation (9;22), which generates a gene fusion consisting of the break-point cluster region (*BCR*) gene fused to the second exon of the Abelson murine leukemia viral oncogene homolog 1 (*ABL1*) (Heisterkamp· et al., 1983; Shtivelman et al., 1985). The *BCR-ABL* fusion is necessary for the development, maintainance, and progression of CML. However, disease progression from chronic to aggressive blast phase necessitates additional genetic and epigenetic abnormalities. Patients with chronic-phase CML have been successfully treated with imatinib, an ABL1 tyrosine-kinase inhibitor (Ren, 2005).

The first gene fusion in a solid tumor was found in a benign salivary gland tumor (Mark et al., 1980). Today fusion genes have been discovered in a variety of solid tumors, including glioblastoma, melanoma, prostate, breast, lung, colorectal, head and neck, and ovarian cancers. Moreover, several cancers can potentially be treated with fusion-targeted therapy (Table 2). Because many gene fusions are tumor-specific, they can also be used as biomarkers to identify cancer types, detect early-stage cancer, evaluate drug response, and predict disease progression (Latysheva & Babu, 2016). The discovery and elucidation of fusion genes in diverse cancer types may lead to more effective therapeutics for cancer patients in the future (Parker & Zhang, 2013).

Table 2. Examples of fusion genes in different cancers with approved or potential targeted therapies (Pederzoli et al., 2020; Schram et al., 2017).

Cancer	Fusion	Targeted therapy
Chronic myelogenous leukemia	BCR-ABL1	Dasatinib, imatinib, nilotinib, ponatinib
Non-small cell lung cancer (NSCLC)	ALK fusions; EML4-ALK	Alectinib, brigatinib, ceritinib, crizotinib
Glioblastoma	FGFR fusions; FGFR3-TACC3	Erdafitinib, infigratinib, pemigatinib, ponatinib
NSCLC	ROS1 fusions	Crizotinib, ceritinib, cabozantinib
Sarcoma	COL1A1–PDGFB	Imatinib
NSCLC	RET fusions	Vandetanib, lenvatinib, sorafenib, apatinib
Papillary thyroid cancer	NTRK fusions	Larotrectinib, entrectinib
Prostate cancer	TMPRSS2-ERG	Not fusion-targeting approaches; peptidomimetics, PARP inhibitors

2.2.1 Genomic and nongenomic rearrangements

Genomic rearrangements are abnormalities in chromosome structure (Tuna et al., 2019). Fusions caused by genomic rearrangements are classified as either direct (produced by a single structural rearrangement event) or composite events (caused by many structural rearrangement events) (Dorney et al., 2023). In addition, composite fusions are subclassified as bridging and two-hop fusions (Calabrese et al., 2020; Nattestad et al., 2018). In the bridged fusions, a third chromosomal location connects two genes. However, this bridge is frequently lost in the final mRNA transcript (Calabrese et al., 2020). In the two-hop fusions, the third genomic region remains part of the mature mRNA (Namba et al., 2021).

Genomic rearrangements can occur through six known mechanisms; translocation, insertion, inversion, tandem duplication, deletion and chromothripsis (Figure 8). Translocations and insertions are large-scale aberrations between distant genetic regions (Tuna et al., 2019). 1) An interchromosomal translocation, also known as a reciprocal translocation, is the exchange of regions between two nonhomologous chromosomes. These rearrangements can occur between any two chromosomes (Shtivelman et al., 1985; Tuna et al., 2019). 2) Insertions, which are the other type of translocations, are caused by an erroneous transfer of DNA fragments from one region to another within the same chromosome (intrachromosomal) or from one chromosome to another (interchromosomal). 3) An inversion arises when a chromosome breaks or rearranges within a single chromosome. Inversions are classified into two types: the reversal of DNA regions can emerge with (pericentric) or without (paracentric) a relationship to the centromere. 4) Chromosome deletion is an alteration in which a chromosome fragment is lost during DNA replication. 5) In tandem duplication, extra copies of a genomic region are formed, resulting in different copy numbers of genes. If the duplicated sections are adjacent to the original, the process is called tandem duplication; if different locations on the chromosome separate them, the process is called displaced duplication (Tuna et al., 2019). 6) Chromothripsis occurs when a single chromosome, chromosome region, or a few chromosomes are fragmented, and the DNA segments are incorrectly rejoined. Chromothripsis has the potential to generate a massive number of fusion genes in a single event (Holland & Cleveland, 2012; Tuna et al., 2019).

Genomic rearrangements can be classified as balanced or unbalanced. Balanced translocations do not result in copy number alterations or phenotypes unless key genes are disrupted at breakpoints (Weckselblatt & Rudd, 2015). Interchromosomal translocations, intrachromosomal insertions, and para- and pericentral inversions are balanced genomic rearrangements. Deletions, interchromosomal (nonreciprocal) insertions, duplications, and chromothripsis result in unbalanced chromosomes; they either miss or have repeated DNA regions (Mertens et al., 2015; Tuna et al., 2019;

Weckselblatt & Rudd, 2015). Tumor cells have a high level of genomic instability, and fusions can occur as a result of intricate mechanisms involving several genetic rearrangements (Taniue & Akimitsu, 2021).

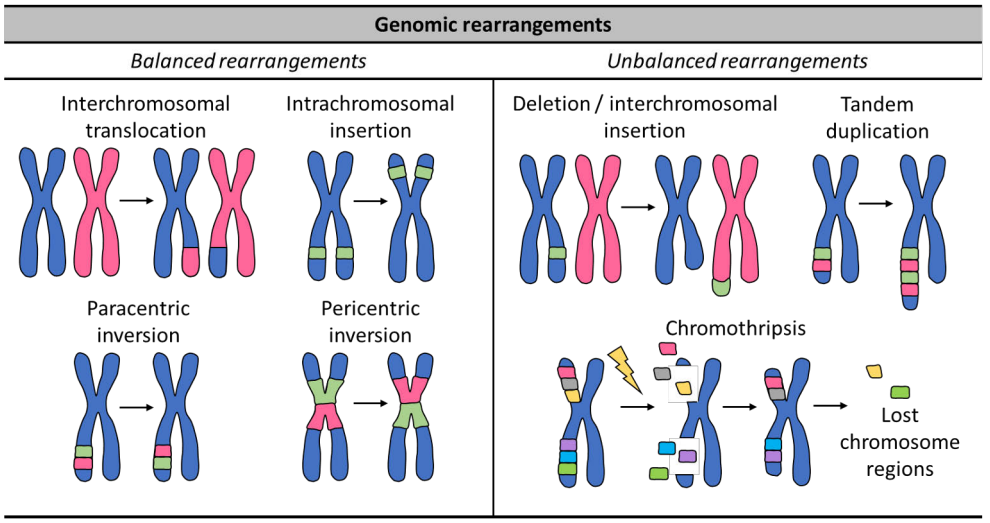

Figure 8. The six types of genomic rearrangements. Modified from (Pederzoli et al., 2020).

According to the extensive cancer genome study, Pan-Cancer Analysis of Whole Genomes (PCAWG), at least 18% of the fusions are nongenomic rearrangements (Calabrese et al., 2020). These aberrations occur at the RNA level due to *cis*-splicing between adjacent genes (*cis*-SAGe) and *trans*-splicing (Dorney et al., 2023). The specifics of these splicing mechanisms are unknown (Chwalenia et al., 2017). Fusion RNAs formed by splicing processes and transcriptional read-through have substantially closer breakpoints than those generated by genomic rearrangements (Calabrese et al., 2020). When the splicing machinery does not recognize the gene borders, adjacent genes can be spliced together into a single chimeric RNA through *cis*-SAGe (Figure 9) (Sibley et al., 2016). The recurrent *cis*-spliced fusion RNAs have been observed in many cancer types with cancer-promoting abilities (Wu et al., 2020; Zhang et al., 2012).

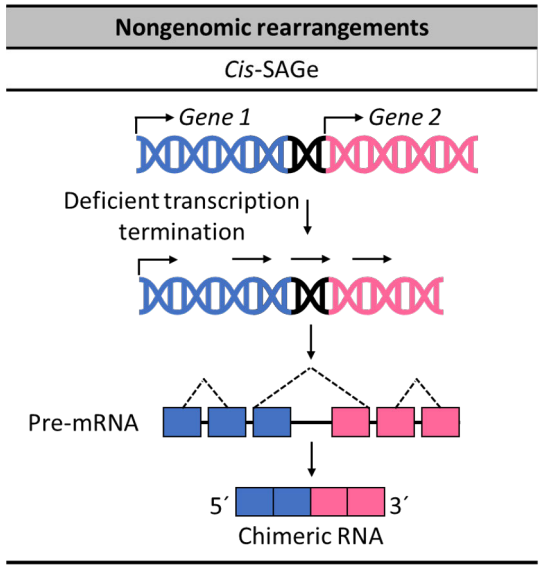

Figure 9. *Cis*-splicing between adjacent genes. Modified from (Mukherjee et al., 2023).

Trans-splicing is classified as intergenic or intragenic (Figure 10) (Dorney et al., 2023). During intergenic *trans*-splicing, two distinct pre-mRNA molecules produced from different genes are spliced (intron removal) and fused to form chimeric mRNAs (Jia et al., 2016; H. Li et al., 2008).There are three types of intragenic *trans*-splicing: intragenic exon repetition, exon shuffling, and sense–antisense (SAS) chimeras within the same gene transcripts (Chwalenia et al., 2017). SAS fusions occur when bidirectional transcripts from the same gene fuse (Wang et al., 2021). The unique RNAs produced by *cis*- and *trans*-splicing increase the complexity of the proteome while also providing new regulatory mechanisms for gene activity (Lei et al., 2016). Several cancers have been linked to abnormal splicing, typically caused by mutations in *cis*- and *trans*-splicing regulatory regions and altered splicing factor expression (Coltri et al., 2019).

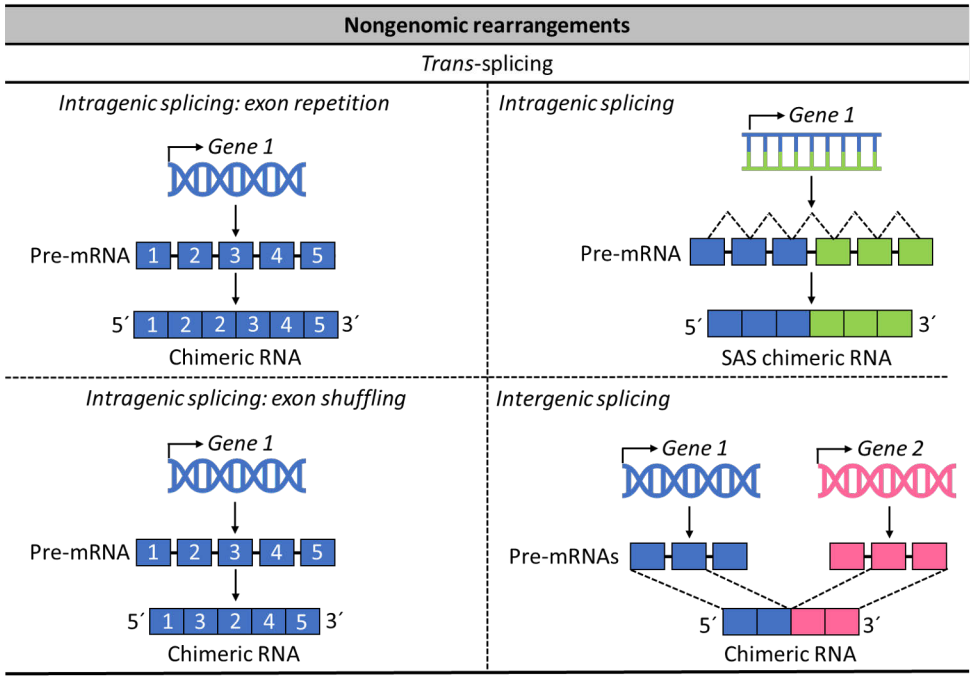

Figure 10. Four *trans*-splicing mechanisms. Modified from (Chwalenia et al., 2017).

2.2.2 Biological functions and clinical relevance of fusion genes and RNAs

Both genomic and nongenomic rearrangements can provide functional chimeric proteins and RNAs (Latysheva & Babu, 2016). Many gene fusions happen randomly due to genomic instability or defective splicing machinery (Vogelstein et al., 2013). The functions of fusion genes and RNAs vary depending on where the junction is located (Chwalenia et al., 2017). Fusion RNAs containing the fusion junction within the protein-coding region tend to be out-of-frame, and such fusions are unlikely to be functional. Out-of-frame fusions can also result in a premature stop codon when the whole transcript is targeted for degradation by nonsense-mediated decay (NMD). However, as long non-coding RNAs, out-of-frame fusions can also perform regulatory activities (Chwalenia et al., 2017). If the changes occur within untranslated regions (UTRs), the parental gene expression is likely to be deregulated at either the transcriptional or translational level (Chwalenia et al., 2017; Latysheva & Babu, 2016): the 5′ UTR is in charge of translational regulation, and the 3′ UTR is a known target location for several regulatory micro-RNAs that help to regulate mRNA stability and protein translation. The transcript can be translated into a novel chimeric protein if the open reading frame is retained during chimeric RNA synthesis (Chwalenia et al., 2017).

The functional changes in fusion proteins and chimeric RNAs can cause cancer initiation, tumor progression, and drug resistance (Schram et al., 2017). Previously, most of the human genome's nonprotein-coding section was considered "junk DNA." However, the development of high-throughput sequencing technologies has revealed the existence of different non-coding RNAs (ncRNA). Especially, long non-coding RNAs (lncRNA) have been associated with diverse biological processes and tumorigenesis (Anastasiadou et al., 2017). LncRNAs can influence cell proliferation and apoptosis, genetic instability, DNA damage repair, metabolic reprogramming, EMT and metastasis, host immunological responses, tumor angiogenesis, cancer stemness, and therapeutic resistance (Nadhan et al., 2022). Gene fusions frequently have an oncogenic effect by altering the regulation of other genes or proteins (*e.g.*, by fusing a strong promoter to a proto-oncogene) and causing either gain- or loss-of-function of one of the implicated genes *(e.g.*, by rendering constitutive activation of a tyrosine kinase and truncating a tumor suppressor gene) (Latysheva & Babu, 2016). Gene fusions aid in the identification of molecular cancer subgroups, the stratification of patients, the monitoring of residual disease after treatment, and the prediction of relapse (Latysheva & Babu, 2016). Currently, chimeric RNAs are commonly identified through RNA-Seq techniques. These unique RNA structures are found not only in normal physiological processes but also in cancers, where they can play a significant role in oncogenesis and cancer heterogeneity (Figure 11) (Chwalenia et al., 2017).

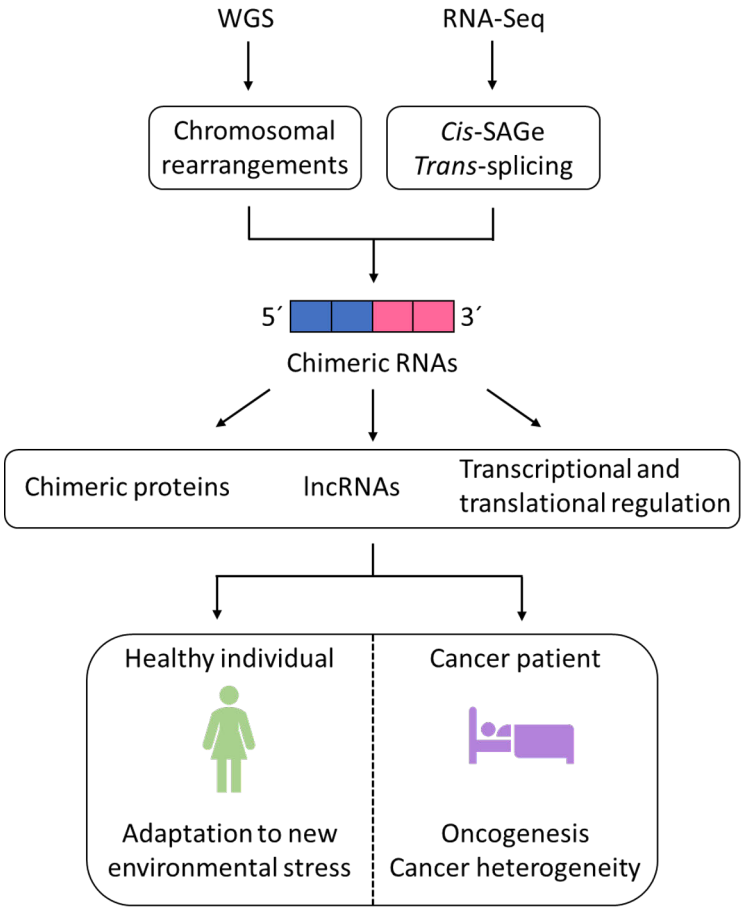

Figure 11. The functional impact of genomic and nongenomic rearrangements in healthy individuals and cancer patients. Modified from (Chwalenia et al., 2017; Mukherjee et al., 2023).

2.2.3 Detection methods of gene fusions

Detection methods for gene fusions have advanced significantly during the past several decades. Chromosomal rearrangements can be detected by chromosome banding technique, fluorescence *in situ* hybridization (FISH), Southern blotting, comparative genome hybridization, polymerase chain reaction (PCR), and whole genome sequencing (Caetano-Anollés, 2013; Huang & Chen, 2017; Shakoori, 2017; Southern, 2006; van Belzen et al., 2021; Weiss et al., 1999). The first discovered fusion gene, *BCR-ABL*, was detected by chromosome banding technique (Rowley, 1973). When cells are in metaphase, this approach allows each chromosome and chromosome region to be recognized based on its distinct band pattern (Huang & Chen, 2017). FISH can simultaneously visualize several chromosome structures in

different colors, considerably improving the portrayal of breakpoints in nondividing cells and metaphase chromosomes with structural rearrangements (Shakoori, 2017). The PCR method provides for quantitative genotyping and identification of single nucleotide polymorphisms and genetic changes even when only a tiny proportion of the sample carries the mutation (Deepak et al., 2007). Standard fusion detection methods currently used in the clinic include FISH, immunohistochemistry, and next-generation sequencing (Schram et al., 2017).

Fusion RNAs that are generated by splicing cannot be detected by the DNA-based assays. Technologies used to detect these fusion RNAs are reverse transcription polymerase chain reaction (RT-PCR), Northern blotting, and RNA *in situ* hybridization (RNA-ISH) and RNA sequencing (Jalali et al., 2017; Lovatt & Eberwine, 2013; van Belzen et al., 2021).

2.2.3.1 Next-generation sequencing

Deep-sequencing technologies have provided a completely new technique to identify fusions at the DNA or RNA levels in a single experiment (Mertens et al., 2015). The Illumina sequencer uses the sequencing by synthesis (SBS) method, and the workflow of this approach consists of four main steps: sample preparation, cluster generation, SBS, and data analysis. The first step is sample preparation, including DNA and/or RNA (reverse transcribed into cDNA for sequencing) extraction from the cells. For library preparation, the DNA is fragmented, and specific adapters are added to both ends to create sequencing libraries (Goodwin et al., 2016).

Clustering is a process that generates clusters by bridge amplification of the fragments. The complementary sequences of the adapters allow the DNA fragments to attach to the flow cell. The flow cell is a glass slide with lanes covered with two types of oligos. A polymerase forms a double strand by adding nucleotides to the template. The DNA is denatured, and the original strand is washed away, leaving the complementary strand attached to the oligo. This single strand folds and engages with another oligo in the flow cell, generating a bridge structure. Similarly, a polymerase duplicates the template in the flow cell, starting a fresh cycle of DNA denaturation and washing away, and a new template folding on a new oligo: clustering results in millions of copies of ssDNA after several amplification cycles (Goodwin et al., 2016).

The next step in the NGS workflow is sequencing. Natural complementarity allows chemically modified nucleotides to attach to the DNA template strand. Each nucleotide has a fluorescent tag and a reversible terminator that prevents the following base from being integrated. Following the insertion of each nucleotide, the clusters are excited by a light source, which emits a distinctive fluorescent signal. This process is called SBS. The reads are washed away after reading the forward

DNA strand, and the procedure is repeated for the reverse strand. This method is called paired-end sequencing (Goodwin et al., 2016).

Data analysis is the last step. After sequencing, the software identifies nucleotides in a process called base calling. Quality control and cleaning procedures are used to process the data. Then the sequencing reads are aligned with the reference genome, providing information about the specific origin of each base pair in the genome. By variant calling, genetic variation and individuals' genotypes are identified from the mapped reads at different locations in the genome (Meyerson et al., 2010; Zhao et al., 2020). Finally, data can be interpreted.

There are multiple sofwares, algorithms (*e.g.* deFuse, ChimeraScan, and FusionHunter) and visualization tools to identify fusion genes from sequence data (Carrara et al., 2013; Latysheva & Babu, 2016). Thousands of chimeric RNAs and gene fusions have now been published in multiple databases including Mitelman, ChimerDB, FusionCancer, and ChiTaRs (Latysheva & Babu, 2016).

2.3 Fusion genes in HGSC

The first genomic rearrangements in ovarian cancer were already described in 1979 by the banding technique (Atkin & Baker, 1987; Bello & Rey, 1990; Kusyk et al., 1982; Van Der Riet-Fo et al., 1979). However, it was not until the 2010s that the vast leap of identifying novel fusion genes in HGSC was taken. Many fusion genes have been discovered in HGSC using deep sequencing technologies. Even while fusion genes are frequent in HGSC, only a few have been verified to be involved in the biological processes of tumor progression and treatment resistance.

In 2011, McPherson *et al.* discovered the first fusion genes in ovarian carcinomas, showing that fusion events are frequent in ovarian cancers. They developed a computational method, deFuse, to discover fusions in tumor RNA-Seq data. Forty ovarian tumor samples were studied, out of which five were HGSC. RT-PCR confirmed the results, and they demonstrated 11 novel fusion genes in HGSC tumor samples (Table 3) (McPherson et al., 2011). The same year, Salzman *et al.* described a recurrent fusion gene, *ESRRA-C11orf20*, in HGSC. *ESRRA* is a crucial regulator of gene expression, and *C11orf20* is an essentially uncharacterized gene adjacent to the *ESRRA*. *ESRRA-C11orf20* was found by deep paired-end mRNA sequencing, followed by deep sequencing of the corresponding genomic region. 67 cases were studied, and fusion was found in 15% of the tumors (Salzman et al., 2011).

CDKN2D-WDFY2 is the first fusion gene whose biological effects have been studied. Transfection of the cloned fusion construct resulted in the loss of wild-type CDKN2D and WDFY2 protein expression, as well as the gain of a short WDFY2 protein isoform that was apparently controlled by the *CDKN2D* promoter. In addition,

truncated WDFY2 protein expression in transfected cells affected PI3K/AKT pathway protein expression. These findings indicated that CDKN2D-WDFY2 fusion could be an essential molecular biomarker for understanding and characterizing sublineages among heterogeneous HGSC tumors (Kannan et al., 2014). Soon, Kannan *et al.* published other fusions with functional characteristics. The mRNA-Seq data from TCGA uncovered a novel cancer-enriched chimeric RNA, *MUC1-TRIM46-KRTCAP2*. In a cohort of 59 patients with HGSC, a collective of six isoforms involving *MUC1-TRIM46-KRTCAP2* were identified, connected by distinct annotated splice sites within these genes. When the *MUC1-TRIM46-KRTCAP2* isoform cDNA was transfected into mammalian cells, it led to the production of mutant MUC1 fusion proteins. These proteins lacked glycosylation and were localized in the cytoplasmic membrane, mirroring the characteristics of tumor-associated MUC1. Notably, MUC1 is highly expressed in 90% of HGSC cases and is recognized as both a clinical biomarker and therapeutic target. Hence, the newly discovered chimeric *MUC1-TRIM46-KRTCAP2* isoforms could potentially offer improved variations of MUC1 with similar clinical utility (Kannan, Kordestani, et al., 2015).

The third fusion gene discovered by Kannan *et al.* was a fusion between *BCAM*, a membrane adhesion molecule, and *AKT2*, a pivotal kinase in the PI3K signaling pathway. This fusion was present in 7% of the 60 patients. They also indicated that *BCAM-AKT2* was translated into an in-frame fusion protein in the patient's tumor. The activity of endogenous AKT2 is tightly regulated by external stimuli. Interestingly, BCAM-AKT2 escaped the regulation from external stimuli. The *BCAM-AKT2* fusion gene, created through chromosomal translocation using the CRISPR/Cas9 method, induced morphological transformation in both OVCAR-8 and HEK-293T cell lines, indicating that *BCAM-AKT2* was oncogenic. *BCAM-AKT2* was the first fusion gene discovered in HGSC that translated an abnormal but functioning kinase fusion protein with carcinogenic characteristics (Kannan, Coarfa, et al., 2015).

Multiple fusions without known functions or direct clinical relevance in HGSC have been reported. *DPP9* gene fusions might promote tumorigenesis (Smebye et al., 2017), the *ROS1* fusion gene and protein have been detected in HGSC patients with so far no significant clinicopathology (Aydin et al., 2018), the *AGK-BRAF* fusion was mentioned without indicated relevance in HGSC (Chui et al., 2021), *SPON1-TRIM29* promotes tumor growth and chemoresistance in an ovarian cancer cell line (Nagasawa et al., 2022), *MAN2A1-FER* was found in ovarian cancer and could increase proliferation and invasiveness, however, the exact histologic classification of the ovarian cancer was not stated (Z. H. Chen et al., 2017), and *MTCH2-AGBL2* and *NF1-RAB11FIP4* fusions were specified in the supplementary data in a study which aimed to use tumor genomics to create prediction models, which would predict an optimal or complete cytoreduction before debulking surgery (Cardillo et al., 2022).

Few studies have revealed that fusions can have clinical implications. *ESR1-CCDC170* was investigated by Yang *et al.* who showed that the presence of this fusion was related to short-term survival. In 2019, Christie *et al.* reported 15 different transcriptional fusion partners involving *ABCB1* in HGSC tumors. *ABCB1* encodes multidrug resistance protein (MDR1) implicated in chemotherapeutic drug efflux. The number of cycles of MDR1-substrate treatment administered was highly related to fusion positivity. MDR1 inhibition boosted paclitaxel sensitivity more than 50-fold in a fusion positive ovarian cancer cell line. This suggested that convergent evolution of *ABCB1* fusions is common in chemotherapy-resistant recurrent ovarian cancer (Christie et al., 2019).

The findings from these above-mentioned 17 studies on fusion genes in HGSC reveal that certain fusion events can be prominent in individual research. However, the specific fusions vary across investigations and are not consistently recurring. Among these studies, four fusions, *JUND-LSM4, MTCH2-AGBL2, AC004475.1-PRPF6*, and *NF1-RAB11FIP4*, were identified in two publications (Table 3). When focusing solely on the genes involved in the fusions, *RAD51B* was detected in 4 out of the 17 papers, and *MTCH2, MACF1, NF1, LRRFIP1*, and *INO80C* were found in 3 out of the 17 publications. In total, 68 genes were identified in at least two of the research papers, indicating some level of consistency in their detection across multiple studies.

Table 3. Fusion genes in HGSC. Collected from publications between 2011-2022.

Fusions in HGSC	Function/relevance	Reference
CAPNS1-WDR62, LETM1-USP15, RAB6A-USP43, ELL-CYLN2, FRYL-SH2D1A, GTF2I-PGPEP1, PRR12-FLT3LG, FLNB-VPS8, LMF1-UMOD, SLC37A1-ABCG1, STK3-NPAL2	The first fusions detected in HGSC	McPherson et al., 2011
ESRRA-C11orf20	May play a role in pathogenesis	Salzman et al., 2011
CDKN2D-WDFY2, TMEM66-MSRB3, FAM19A3-LPP, RFX2-CCDC94, NR2F6-MAST3, WDFY2-S1PR5	*CDKN2D-WDFY2*: alterations in PI3K-AKT pathway protein expression	Kannan et al., 2014
BCAM-AKT2	AKT2 kinase activation	Kannan et al., 2015
MUC1-TRIM46-KRTCAP2	*MUC1-TRIM46-KRTCAP2* isoforms resembled tumor-associated MUC1 features in transfected cells. May have clinical utility.	Kannan et al., 2015

Fusions in HGSC	**Function/relevance**	**Reference**
STPG1-BRCA2, CCDC122-BRCA2, BRCA2-BRCA2, NF1-NF1, none-NF1, NF1-none, VPS54-NF1, NF1-RAB11FIP4, EVI2B|NF1-NF1, RNF135-NF1, LRRC37B-NF1, RNF135-RNF135, none-RAB11FIP4, LPAR6|RB1-CHRNA3, RB1-none, RB1-RB1, none-RB1, ATR-RB1, RB1-LPAR6|RB1, RB1-FRMD6, FRMD6-RB1, RB1-CAB39L, LPAR6|RB1-none, PTEN-PTEN, PTEN-none, none-PTEN, PTEN-RNLS, none-LIPA, none-RAD51B, RAD51B-none, PIGH-RAD51B, RAD51B-RAD51B, ACOXL-BCL2L11, none-FOXO1, SNX3-FOXO3, none-FOXO3, ABCB1-SLC25A40, ABCB1-PRAF2, none-ABCB1, ABCA4-ABCB1, RUNDC3B-CFTR, CTTNBP2-RUNDC3B	Homologous recombination repair: loss of *PTEN* and *RAD51B*, potentially involved in mechanisms of chemotherapy resistance; loss of *FOXO1/3* and *BCL2L11* and promoter rearrangement of *ABCB1*	Patch et al., 2015
DPP9-PPP6R3, DPP9-PLIN3, EEF2-ARAP1, MTCH2-ZNF554, NADSYN1-NUDT19, ZNF44-CCDC84, FCF1-LYNX1, VRK1-TDP1, DDA1-FAM129C, B4GALT5-SLC34A2, TDRD9-ASPG, TMEM123-MMP27, VRK1-TDP1, PDE4D-CCNB1, COL9A1-DGCR5, RBM43-NRG4, ZBTB46-WFDC13, TAP2-HLA-DOB, TAP2-HLA-DOB, GALNT8-KCNA6, PPP2R2B-SKP1, KIAA1409-COX8C, MGEA5-KCNIP2, TM2D1-TRMT5, CDHR3-MVP, TC2N-CATSPERB, TAP2-HLA-DOB, POU5F1-LAMA3, CLU-BCAM, UCHL3-LMO7, PKHD1L1-EBAG9, GNE-COG7, FGFR2-FAM24B, CHRM3-SCRN3, CHRM3-WDR72, PLXNB1-PRKAR2A, FBRS-TIAL1, MAML3-INPP4B, CDC42BPB-SPEG, DSTYK-SLC22A4	*DPP9-PPP6R3 and DPP9-PLIN3*: potentially tumorigenic	Smebye et al., 2017
ROS1 fusion	NA	Aydin et al., 2018
ESR1-CCDC170, DLEU1-DLEU7, KMT2E-LHFPL3, LOC101928103-ABAC12 + 124 other fusion genes	*ESR1-CCDC170*: Poor prognosis	Yang et al., 2018
SLC25A40-ABCB1, MATR3-ABCB1, PRRC2C-ABCB1, ARPC1B-ABCB1, CNOT4-ABCB1, GTF2I-ABCB1, KMT2E-ABCB1, PHTF2-ABCB1, WRN-ABCB1, CALU-ABCB1, ITGB8-ABCB1, NAP1L1-ABCB1, CLOCK-ABCB1, ATP5J2-ABCB1, CUX1-ABCB1, MTERF-ABCB1, TMEM243-ABCB1	*SLC25A40-ABCB1*: Drug resistance	Christie et al., 2019
OGT–MUC16, NCL–MUC16, MUC16–NCL, WWOX–MALAT1, THAP11–ATXN3, SMG1–MALAT1, MALAT1–VPS13B, XIST-EBF1, VPS13B-MALAT1, STAG3-C19MC, MALAT1-USP9X, MALAT1-MACF1, MALAT1-ETV6, FOXP1-MALAT1	Potential biomarker; *MALAT1-FOXP1* favorable prognosis	Eismann et al., 2020

Fusions in HGSC	Function/relevance	Reference
Z68871.1-LINC00630, ZBTB8OS-AC090627.1, ARL17A-KANSL1, TOGARAM1-FANCM, UBE2F-LRRFIP1, AC007952.4-RN7SL2, AP3D1-ARHGDIA, ARHGAP1-CKAP5, DOT1L-GCGR, FAM20C-AC093627.4, INPP5B-PLEKHO1, MTCH2-AGBL2, FAM98B-FRMD5, LUC7L-AXIN1, MAGED2-ZFAT, NFE2L1-PNPO, TMCC1-CD96, NRIP1-AJ009632.2, PACS1-HAUS3, PGM2L1-POLD3, SMARCA4-ZNF700, AUTS2-INO80C, JMJD1C-CCNYL1, PARP4-BAGE2, PRSS42P-PRSS50, PSPC1-ZMYM5, SRGAP3-AC068631.1, ZNF609-SNX1, AC004475.1-PRPF6, BTBD10-TEAD1, NFKBIB-TEAD1, UBA2-RAD51B, CC2D1A-CPNE8, CHTOP-PCAT1, FBXO34-SORCS3, GRIN2A-C16orf72, PCAT1-C1orf210, PIK3R3-ANKFN1, RB1CC1-LINC02091, TRMT1-CPA4, AF235103.3-ZNF250, LINC02408-CAND1, MECOM-AC116337.3, TRAPPC3-MAP7D1	*ZBTB8OS-AC090627.1, ARL17A-KANSL1*: Poor survival. Any of the fusion transcripts were not significantly associated with chemo-response	Newtson et al., 2021
AGK-BRAF	NA	Chui et al., 2021
A total of 228 fusions	PI3K-AKT-mTOR pathway associated fusions	Cervera et al, 2021
A total of 597 fusions were discovered, out of which 104 listed	Creation and validation of models to predict response to primary treatment	Gonzalex et al., 2021
SPON1-TRIM29	Promotes cell and tumor growth and enhances chemoresistance in stably expressing fusion A2780 cells	Nagasawa et al., 2022
MTCH2-AGBL2, NF1-RAB11FIP4	NA	Cardillo et al., 2022

2.3.1 Future prospects: fusions as drug targets

The ambitious goal of precision medicine in cancer treatment is the development of therapies that only target cancer cells. Fusion genes and RNAs are often shown to be both tissue and cancer-specific, making them appealing targets (Mukherjee et al., 2023). In addition, fusions are usually present at subclonal levels within tumors and frequently are the founding genetic aberrations that drive cancer development (Brien et al., 2019).

Many of the ongoing clinical trials in HGSC are combination studies; platinum, taxane, or PARP inhibitor with a novel complementary drug. These complementary drugs are mainly PI3K-AKT-mTOR pathway inhibitors and immunotherapies,

already approved with another indication (Table 4). Fusions vary significantly between patients, which implies that developing medications targeting fusion proteins in HGSC is unrealistic. On the other hand, a unique fusion can be an oncogenic driver for any single patient, thus enabling her to potentially benefit from the existing targeted therapy.

Numerous cancer omics studies increase the understanding of tumor hallmarks at the molecular level and also supply large amounts of data for therapeutic repurposing by utilizing advanced bioinformatics (B. Chen et al., 2020; Fernandez-Banet et al., 2015). Computer processing can incorporate drug action mechanisms, phenotypes, and molecular biological features of cancer to find novel drug-disease associations (Mottini et al., 2021; Nowak-Sliwinska et al., 2019). The drug repurposing approach may also provide novel treatment options for HGSC patients from existing drugs.

Table 4. Drugs in recently completed or active clinical trials with HGSC indication. The target depicts the target of the complementary drug.

NCT Number	Drug	Target
NCT04729387	Alpelisib	PI3K inhibitor
NCT01283035	MK2206	AKT inhibitor
NCT02208375	Capivasertib; Vistusertib	AKT inhibitor; mTOR inhibitor
NCT03648489	TAK228	mTORC1/2 inhibitor
NCT04729608	Batiraxcept	AXL inhibitor
NCT02713386	Ruxolitinib Phosphate	JAK inhibitor
NCT01116648	Cediranib Maleate	VEGFR inhibitor
NCT02659241	Adavosertib	WEE1 inhibitor
NCT03096054	LY3143921 hydrate	CDK inhibitor
NCT03206645	Unesbulin	BMI-1 inhibitor
NCT05188781	Pembrolizumab; Anlotinib	PD-1; RTK inhibitor
NCT03311334	DSP-7888; Nivolumab	WT-1-derived immunomodulator; PD-1 inhibitor
NCT02179970	Plerixafor	CXCR4 inhibitor
NCT02839707	Atezolizumab	PD-1 inhibitor
NCT02834013	Ipilimumab	CTLA-4 inhibitor

3 Aims

The aim of this thesis was to identify and characterize novel fusion genes in HGSC, with special emphasis on their potential as novel drug targets. The specific aims for the studies were as follows:

1) to identify and validate fusion genes and corresponding fusion proteins in human HGSC tissue specimens with a combination of analysis tools developed for this purpose (Study I)

2) to study the functional role and regulation of fusion genes in fusion overexpressing HGSC cells (Study II)

3) to evaluate the response of fusion-expressing HGSC cells to conventional platinum therapy and PI3K/RAS pathway inhibitors (Study II)

4 Materials and Methods

4.1 Patient material, RNA extraction, sequencing and fusion gene detection (I)

Patients treated at the Department of Obstetrics and Gynecology, Turku University Hospital, were included in the study and approved by the Ethics Committee of the Hospital District of Southwest Finland. The study, known as the Mupet study (ETMK:53/180/2009) and Mupet phase 2 / HERCULES (ETMK: 145/1801/2015), obtained informed consent from all participating patients. Treatment options included either primary surgery followed by six cycles of platinum-taxane chemotherapy or three cycles of neoadjuvant chemotherapy (NACT) followed by interval debulking surgery and three to six chemotherapy cycles.

During the surgical procedures, tumor specimens were collected for both morphological diagnosis and research purposes. Multiple fresh frozen tissue, serum, and plasma samples, along with detailed clinical descriptions, were collected at various stages of treatment and follow-up until disease progression occurred. Additionally, benign ovarian tumor tissues (fibroma, mucinous, and serous cystadenoma) were collected from four patients (EOC1016, EOC758, EOC421, and EOC263).

RNA and DNA were extracted from patient tumor tissue samples and bening tissues using AllPrep DNA/RNA Mini Kit (Qiagen) according to the manufacturer's instructions for deep sequencing. For library preparation ribosomal RNA was removed by an rRNA removal kit, and rRNA-free residue was cleaned by ethanol precipitation. After segmentation, the rRNA-depleted RNA was reverse-transcribed into cDNA using random hexamer primers. The ends were repaired before amplifying and purifying the fragmented cDNA, and adapters were ligated. RNA and DNA were deep sequenced on Illumina platforms. Library preparation and deep sequencing were performed at Beijing Genomics Institute (BGI) Health Hong Kong Company Limited.We developed a fusion gene identification toolset, FUNGI, to detect fusion genes from the RNA sequencing data. FUNGI supports six fusion detection algorithms with prioritization and visualization modules and is described in more detail in the results section. FUNGI was applied to an ovarian cancer dataset of 107 tumor samples from 36 HGSC patients (Table 5). FUNGI and its

documentation are available at Bitbucket (*Bitbucket*, 2021) as stand-alone or from Anduril (*Anduril*, 2021). Genomic verification of the fusion genes was done using Genomic Rearrangement IDntification Software Suite (GRIDSS).

Table 5. Patient characteristics. Modified from Study I.

		N	%
Number of patients		36	
Age at diagnosis	Median (range)	68,0	(39–83)
Histology	High grade serous	38	100,0 %
Stage (FIGO 2014)	II	1	2,6 %
	III	26	68,4 %
	IV	11	28,9 %
Treatment line	PDS	14	36,8 %
	NACT	24	63,2 %
Residual disease	No macroscopic disease	14	36,8 %
	1-10 mm	14	36,8 %
	>10 mm	7	18,4 %
	Not specified	3	7,9 %
Platinum free interval	< 6 months	13	34,2 %
	> 6 months	18	47,4 %
	No progression	7	18,4 %
Time to death	< 24 months	10	26,3 %
	> 24 months	14	36,8 %
	Alive, followup time > 34 months	14	36,8 %
Primary therapy outcome	Complete response	21	55,3 %
	Partial response	7	18,4 %
	Progressive disease	9	23,7 %
	Died during chemotherapy	1	2,6 %

4.2 cDNA preparation, RT-PCR and agarose gel electrophoresis (I and II)

RNA was reverse transcribed into cDNA using a SensiFAST cDNA Synthesis Kit (Bioline) according to the manufacturer´s instructions using a Veriti 96-Well Thermal Cycler-PCR machine (Thermo Fisher Scientific). Fusion-specific cDNA primers were designed using the Primer3 program for the prioritized fusion genes found by FUNGI (Table 6). Fusion sites were amplified using DreamTag Green PCR Master Mix (Thermo Fisher Scientific) and the amplified products separated by agarose gel electrophoresis. DNA fragments were visualized under UV light and

extracted using Macherey-Nagel NucleoSpin Gel and PCR Clean-up Kit according to the manufacturer´s instructions, and Sanger sequenced. Fusion breakpoints were verified by FinchTV 1.4.0.

Table 6. Fusion-specific primers. Modified from Study I.

Fusion	Forward primer sequence	Reverse primer sequence
AKT2-PBX4	ATGTCCTGCTGCCCTGAG	GCTTGGCCCTGTAGTCAGAG
AKT2-ZNF546	CCACTGGCCGCTACTACG	TGACTAACGCATCCCATCTG
CDH2-INO80C	ATCCGACGAATGGATGAAAG	CCCTTTCAGAAGCGAGGATT
MLLT10-FYB	GCTTGCTATGGCATTGTTCA	TTTCCAGCACCATCAGAGTG
PIK3R1-CCDC178	ATGAAACCACAGGGGAAAGG	GAAGATTCCTCCTGCACAGC
PTK2-AGO2	TCGTCGTCTGCCTTCGCTTC	TAACTCTCCTCGGGCACTTCT
PTPN11-CFAP54	TGAAATACGACGTTGGTGGA	TGCAACCATTAGCCAGATCA
RFX1-SLC1A6	CCCGTCACCCAAGAGAGAT	GGTGTACATGCCCAGCTGAC
SBF1-MAPK11	ACGTACCGGGTCATCTTCAC	GACAGCTTCTTCACCGCCAC
TPM3-C1orf189	GCTGAAAGGGACAGAGGATG	TGGCATACGGGTTTCTTCTC
XPO1-USP34	CATTGTTTCCCAGCATTCCT	AGCACTTGAACTTGGGCAAT

4.3 RT-qPCR (I and II)

Expression of the selected fusion genes or wild-type genes from patient tumor tissues was quantified in triplicate cDNA samples using CybrGreen RT-qPCR. Relative fusion mRNA expression was calculated using the $2^{-\Delta\Delta CT}$ method by comparing genes of interest to *GAPDH* and the fusion-negative control sample. The primers listed in Table 6 were also used in RT-qPCR analysis.

The expression was calculated with the following formula:

1. Normalization to the housekeeping gene, *GAPDH*

   $\Delta Cq_{(\text{Fusion sample})} = Cq_{(\text{Target, Fusion sample})} - Cq_{(\textit{GAPDH}, \text{Fusion sample})}$

   $\Delta Cq_{(\text{Fusion-negative sample})} = Cq_{(\text{Target, Fusion-negative sample})} - Cq_{(\textit{GAPDH}, \text{Fusion-negative sample})}$

2. Normalization of $\Delta Cq_{(\text{Fusion sample})}$ to $\Delta Cq_{(\text{Fusion-negative sample})}$

   $\Delta\Delta Cq = \Delta Cq_{(\text{Fusion sample})} - \Delta Cq_{(\text{Fusion-negative sample})}$

3. Calculation of the expression ratio

   $2^{-\Delta\Delta CT}$ = normalized expression ratio

To investigate the expression of genes associated with epithelial-mesenchymal transition (EMT), the study set was the same as for the fusion expression analysis. The same formula ($2^{-\Delta\Delta CT}$ method) was applied to calculate the expression ratio. The data was first normalized to *GAPDH* and then to the control cell gene expression, allowing for a reliable comparison of gene expression levels. Primers used in this assay are listed in the Table 7.

Table 7. EMT primers (II).

Gene	Forward primer sequence	Reverse primer sequence
CDH1	CCCGGGACAACGTTTATTAC	GCTGGCTCAAGTCAAAGTCC
CDH2	CTCCATGTGCCGGATAGC	CGATTTCACCAGAAGCCTCTAC
FOXC2	GGGGACCTGAACCACCTC	AACATCTCCCGCACGTTG
SLUG	TGGTTGCTTCAAGGACACAT	GTTGCAGTGAGGGCAAGAA
SNAIL	GCTGCAGGACTCTAATCCAGA	ATCTCCGGAGGTGGGATG
TWIST	GGGCCGGAGACCTAGATG	TTTCCAAGAAAATCTTTGGCATA
VIM	AAAGTGTGGCTGCCAAGAAC	AGCCTCAGAGAGGTCAGCAA
ZEB1	TGTTACCAGGGAGGAGCAGT	GCTTCATCTGCCTGAGCTTC
ZEB2	AAGCCAGGGACAGATCAGC	CCACACTCTGTGCATTTGAACT
GAPDH	CATCCTGGGCTACACTGAGC	GTCAAAGGTGGAGGAGTGGG

4.4 RNA *in situ* hybridization (I)

Based on the manufacturer's instructions, fusion gene expression, and localization were visualized by the BaseScope assay (Advanced Cell Diagnostics). Customized BaseScope probes were used for *AKT2-PBX4* (#719661), *AKT2-ZNF546* (#719671), and *PIK3R1-CCDC178* (#719681) fusions, and in addition, BaseScope Positive Control Probe *Hs-PPIB-1ZZ* (#701041) and Negative Control Probe DapB-1ZZ (#701021). Formalin-fixed paraffin-embedded tissue sections were deparaffinized, treated with target retrieval reagents at 98°C for 15 min, and digested with protease IV for 15 min at 40°C in the hybridization oven. The slides were next hybridized with the BaseScope probes for 2h at 40°C, followed by serial amplification steps at 40°C in the hybridization oven or at room temperature as instructed, and finally incubated with the FastRed substrate at room temperature to visualize the hybridization signals. The stained slides were digitalized using a 3DHISTECH Pannoramic 250 FLASH II digital slide scanner at the Genome Biology Unit supported by HiLIFE and the Faculty of Medicine, University of Helsinki, and Biocenter Finland.

4.5 Cell culture (II)

The high-grade ovarian serous adenocarcinoma cells OVCAR-8 (National Cancer Institute Frederick Cancer DCTD Tumor and Cell line repository) and the human embryonic kidney cells HEK293 (American Type Culture Collection, Manassas, VA) were cultured in RPMI-1640 media (Gibco, Thermo Fisher Scientific) supplemented with 10% fetal bovine serum (FBS, Biowest), 2% ultraglutamine (Lonza) and 1% penicillin-streptomycin (Gibco, Thermo Fisher Scientific). Cells were maintained at 37°C in a humidified 5% CO2 atmosphere.

4.6 Plasmids (II)

The PIK3R1-CCDC178_pcDNA3.1(+)-CeGFP (GeneScript Biotech) plasmid contained the *PIK3R1-CCDC178* fusion gene optimized for fusion protein production and enhanced green fluorescent protein (eGFP). The insert was removed from the PIK3R1-CCDC178_pcDNA3.1(+)-CeGFP plasmid by using NheI, BamHI, and XbaI restriction enzymes and ligated according to sticky-end ligation protocol (Thermo Fischer Scientific) to create a control plasmid. The PIK3R1-CCDC178_pcDNA3.1(+)-CeGFP and pcDNA3.1(+)-CeGFP plasmids were transformed into competent *E. coli* using heat shock. Bacteria were grown on Luria broth (LB) agar plates (Fisher BioReagents) containing 5% ampicillin (Fisher BioReagents) and incubated overnight at 37°C. Isolated colonies were grown in LB broth (Fisher BioReagents) overnight at 37°C and selected with 5% ampicillin. For DNA extraction, a Nucleospin Plasmid QuickPure kit was utilized following the manufacturer's protocol. Plasmid purity was assessed by gel electrophoresis and Sanger sequencing. Specifically, the fusion insert was extracted using NotI and BamH1 restriction enzymes, while PCR amplification was carried out using the T7 promoter primer.

4.7 Transfections (II)

PIK3R1-CCDC178_pcDNA3.1(+)-CeGFP and pcDNA3.1(+)-CeGFP plasmid DNA were transfected into OVCAR-8 cells using Lipofectamine 2000 (Invitrogen). HEK293 cells were transfected using FuGene reagent (Promega) according to manufacturer´s protocol and selected using 150–300 µg/ml geneticin (Invitrogen). Cells were sorted by FACS by GFP intensity to create stably expressing cell lines. Cell lines were cultured in RPMI-1640 media supplemented with 10% fetal bovine serum, 2% ultraglutamine, 1% penicillin-streptomycin and 50 µg/ml geneticin. All *in vitro* experiments were performed with stably expressing GFP-control vector cell lines and PIK3R1-CCDC178-GFP fusion cell lines in Geneticin-free media. Cells

were regularly tested for mycoplasma using a MycoALert PLUS mycoplasma detection kit (Lonza).

4.8 Colony assay (II)

Two thousand cells were seeded on 12-well plates. After five days, cells were washed with PBS and incubated with different treatments for 72h. Cells were washed with PBS, stained with crystal violet dye for 10 mins and washed with tap water three times. The stain was extracted with 1% SDS for 30 min in a shaker at 80 rpm. Absorbance was measured at 600 nm wavelength using Victor2 1420 Multilabel Counter.

4.9 IC50 and cell viability (II)

To determine IC50 and cell viability, a colorimetric method, the CellTiter 96 AQ_{ueous} One Solution Cell Proliferation Assay (MTS) (Promega) was used. First, 1000 cells were plated on 96-well plates and incubated overnight. The cells were then treated with cisplatin and PI3K and RAS pathway inhibitors at increasing concentrations (0, 1, 10, and 100 µM) for 72 hours. Cells were incubated with 20 µl of CellTiter 96 AQ_{ueous} One Solution for 1,5 hours, and absorbance was measured at 490 nm wavelength. IC50 values were calculated using a sigmoidal fitting curve in Origin 2016.

For cell viability assays, 10 000 cells were seeded and incubated overnight. The cells were treated with 5 µM cisplatin, 3 µM trametinib, and their combination for five days. As mentioned above, absorption was measured at 490 nm every 24 hours using CellTiter 96 AQ_{ueous} One Solution.

4.10 Cell migration assay (II)

Thirty thousand cells per well were seeded to obtain confluent density on 96-well IncuCyte ImageLock plates (Essen Bioscience) and incubated overnight. Cell monolayers were scratched using the IncuCyte 96-well WoundMaker Tool (Essen Bioscience), washed once with PBS, and replaced with fresh media. The cells were scanned every second hour for 72 hours in the IncuCyte ZOOM imaging device to investigate cell migration over the initially scratched wound.

4.11 Western blot (I and II)

Tumor tissues were lysed with RIPA buffer supplemented with protease and phosphatase inhibitors (Pierce, Thermo Scientific) and processed with the Ultra-

Turrax homogenizer. The samples were sonicated and centrifuged for 20 min 10,000G at +4°. Control-GFP and PIK3R1-CCDC178-GFP expressing OVCAR-8 and HEK293 cells were lysed with M-PER mammalian protein extraction reagent (Thermo Scientific) supplemented with lysis buffer protease and phosphatase inhibitor (Pierce, Thermo Scientific). The samples were incubated for 2 hours at 4°C, centrifuged at 17 000 rcf for 30 min at 4°C, and supernatants collected. Western blotting was performed using 4–20 % sodium dodecyl-sulfate polyacrylamide gel electrophoresis (SDS-PAGE) gels, and 20–50 µg protein was separated at 200V for 45 min. Proteins were transferred to 0.2 µm nitrocellulose membranes (Bio-Rad Laboratories, Inc.) by Trans-Blot Turbo Transfer System (Bio-Rad Laboratories, Inc.), which were blocked with 5% milk for 1h. Membranes were incubated overnight with the primary antibodies (Table 8) at 4°C, washed three times for five minutes with TBST, incubated for 1 h with the secondary antibody, and washed three times in TBST. Blots were detected using ECL blotting substrate (Pierce ECL Western Blotting Substrate, Thermo Scientific) and/or SuperSignal West Femto Maximum Sensitivity Substrate, Thermo Scientific).

Table 8. Antibodies with applications.

Antibodies	Application	Company	Catalog number	Dilution	Original publication
AKT1	WB	Cell Signaling	2938	1:1000	II
AKT2	WB	Cell Signaling	3063	1:1000	II
AKT2	WB	Novus Biologicals	H00000208M06	1:1000	I
anti-mouse Alexa Fluor 488	IF	Life Technologies	A11059	1:400	II
anti-mouse Alexa Fluor 555	IF	Life Technologies	A21427	1:400	I, II
anti-mouse Alexa Fluor 647	IF	Invitrogen	A21236	1:400	II
anti-rabbit Alexa Fluor 488	IF	Invitrogen	A11001	1:400	I, II
CDH2	WB	Abcam	66025	1:2000	I
CIN85	IF, WB	Santa Cruz Biotechnology	sc-166862	IF; 1:50, WB; 1:1000	II
CTPS1	IF	Atlas antibodies	HPA051322	1:200	II
GAPDH	WB	ThermoFisher	MA5-31457	1:5000	II
GAPDH 488	WB	Proteintech	CL488-60004	1:5000	II
GFP	IF	Santa Cruz Biotechnology	sc-9996	1:200–1:500	II
GFP	IF	Novus Biologicals	NB600-308	1:200–1:500	II

Antibodies	Application	Company	Catalog number	Dilution	Original publication
HRP-conjugated rabbit anti-mouse	WB	Dako Denmark A/S	P0161	1:5000	I, II
HRP-conjugated swine anti-rabbit	WB	Dako Denmark A/S	P0217	1:5000	I, II
IMPDH2	IF	Atlas antibodies	HPA001400	1:500	II
MAPK11	WB	Novus Biologicals	NBP1-47513	1:500	I
mTOR	WB	Cell Signaling	2983T	1:1000	II
p44/42 MAPK (ERK1/2)	WB	Cell Signaling	4695	1:1000	II
pan-AKT	WB	Cell Signaling	4691	1:1000	II
PBX4	WB	Novus Biologicals	H00080714-M01	1:500	I
Phospho-AKT1	WB	Cell Signaling	9018	1:1000	II
Phospho-AKT2	WB	Cell Signaling	8599	1:1000	II
Phospho-c-Raf	WB	Cell Signaling	9427	1:1000	II
Phospho-MEK1/2	WB	Cell Signaling	9154	1:1000	II
Phospho-mTOR	WB	Cell Signaling	5536T	1:1000	II
Phospho-p44/42 MAPK (ERK1/2)	WB	Cell Signaling	4370	1:1000	II
Phospho-pan-AKT	WB	Cell Signaling	4060	1:1000	II
Phospho-PI3 Kinase p85	WB	Abcam	ab182651	1:1000	II
PI3 Kinase p85	WB	Invitrogen	PA5-32550	1:1000	I, II
p-PTEN	WB	Cell Signaling	9549	1:1000	II
RFX1	WB	Novus Biologicals	NBP2-20142	1:500	I
SBF1	WB	Novus Biologicals	NBP1-98522	1:300	I
XPO1	WB	Novus Biologicals	NB100-56493SS	1:250	I
α-tubulin		Sigma-Aldrich	T5168	1:1000	I
β-tubulin	WB	Proteintech	CL488-66240	1:5000	II

4.12 Immunofluorescence stainings (II)

Coverslips were coated with Geltrex and cells seeded at the desired density then incubated overnight. Rod and ring structures (RRs) were induced with mycophenolic acid (MPA) for 4 hours and with 6-Diazo-5-oxo-L-norleucine (DON) for 24 hours. Cells were fixed with 4% paraformaldehyde (PFA) for 10 min and washed with PBS. Cells were permeabilized and blocked with 0.5% Triton and 5% bovine serum albumin in PBS for 30 min at room temperature. Cells were incubated with primary antibodies (Table 8) overnight at 4°C. Coverslips were washed with PBS, and secondary antibody incubation was performed at room temperature for 1.5 hours. ProLong Diamond Antifade Mountant with DAPI (Thermo Fisher Scientific) was used for mounting. Fluorescence images were taken using the Invitrogen EVOS M5000 Imaging System (Thermo Fisher Scientific) and confocal images by 3i Spinning Disc. Representative middle Z-stack sections were used from the confocal images.

4.13 Correlative light-electron microscopy (CLEM) (II)

Cells were plated on 35 mm petri dishes with gridded glass bottoms (MatTek). Cells were treated with 5 μM cisplatin for 96 hours. The medium was removed and cells were fixed for 10 min with 4% PFA in 0.2 M HEPES buffer (pH 7.4), which was prewarmed to 37°C. PFA was removed and 0.2 M HEPES was added. After the initiative fixation phase contrast and fluorescence images were taken using Invitrogen EVOS M5000 Imaging System (Thermo Fisher Scientific) to trace later the structures on electron microscope images. Next, the prefixed cells were further fixed with 2% glutaraldehyde in 0.2 M HEPES (pH 7.4) for two hours at room temperature. Cells were stored in 0.2 M HEPES at 4°C overnight.

Sample preparation was performed from this step on by the Cell Imaging and Cytometry Core, Turku Bioscience Centre, with the support of Biocenter Finland. Cells were then washed with 0.2 M HEPES twice and postfixed with 1% osmium tetroxide containing 1.5% potassium ferrocyanide for one hour. Next, cells were washed with 0.2 M HEPES twice for 5 min. Dehydration was performed with 70%, 95%, and 100% ethanol at +4°C for one minute in each concentration and finally with 100% ethanol for 30 min at room temperature. The cells were then incubated in a mixture of Epon resin and 100% ethanol for 30 min and finally in 100% Epon for 2 hours. Beem capsules filled with Epon were set upside down on top of the samples, guided by the grid markings in the glass bottom of the dish. After 36 hours of incubation at +60°C, capsules were removed from the dishes, and the blocks were trimmed to expose the cells of interest for thin sectioning. Sections were cut using a

diamond knife and collected on Pioloform-coated one-slot grids. Imaging was performed using a JEM-1400Plus transmission electron microscope.

4.14 Immunoprecipitation (II)

Control and PIK3R1 fusion cells were cultured in T75 flasks. When the cells reached 90% confluence, they were detached using trypsin and centrifuged at 1000 rpm for 5 minutes. Cell pellets were lysed with Lysis buffer (Chromotek) containing proteinase and phosphatase inhibitors (Thermo Scientific). The lysates were incubated on ice for 30 minutes with periodic mixing. After incubation, cell debris was removed by centrifugation at 17 000G for 10 minutes at 4°C. A 50 µl aliquot of the supernatant was saved as the input fraction.

For immunoprecipitation of the GFP-tagged fusion protein complex, GFP-Trap Dynabeads (Chromotek) were used. The samples were prepared by using 5x volumes of bead slurry (125 µl) and cell pellets (5x T75) per sample. The equilibrated beads were rotated with the diluted lysate for 1.5 hours at 4°C. Subsequently, the beads were separated using a magnet and washed twice with Wash buffer (Chromotek). Proteins were eluted with 2x Laemmli buffer following the manufacturer's protocol. Elution was achieved by adding 50 µl of Acidic Elution Buffer (Chromotek) to the sample, followed by constant up-and-down pipetting for 60 seconds at room temperature. The eluate was then neutralized by adding 5 µl of Neutralization Buffer (Chromotek).

Next, the samples were run on SDS-gels at 200V for 45 minutes. The gels were stained overnight with PageBlue Protein Staining Solution (Thermo Fisher Scientific) and washed with Milli-Q water for 4 hours. Finally, the proteins were left on the beads for the LC-ESI-MS/MS analysis.

4.15 LC-ESI-MS/MS Analysis (II)

Mass spectrometry analyses were performed at the Turku Proteomics Facility supported by Biocenter Finland. The LC-ESI-MS/MS analyses were performed on a nanoflow HPLC system (Easy-nLC1000, Thermo Fisher Scientific) coupled to the Q Exactive HF mass spectrometer (Thermo Fisher Scientific) equipped with a nano-electrospray ionization source. Peptides were first loaded on a trapping column and subsequently separated inline on a 15 cm C18 column (75 µm x 15 cm, ReproSil-Pur 3 µm 120 Å C18-AQ, Dr. Maisch HPLC GmbH, Ammerbuch-Entringen, Germany). The mobile phase consisted of water with 0.1% formic acid (solvent A) or acetonitrile/water (80:20 (v/v)) with 0.1% formic acid (solvent B). A linear 20 min gradient from 6 to 39% of eluent B, followed by a wash stage with 100% of eluent B, was used to eluate peptides. MS data were acquired automatically by using

Thermo Xcalibur 4.1 software (Thermo Fisher Scientific). CCDC178 fusion peptides were manually added to the library due to a modified amino acid sequence. An information dependent-acquisition method consisted of an Orbitrap MS survey scan of mass range 350–1750 m/z followed by HCD fragmentation for the 10 most intense peptide ions.

5 Results

5.1 Fusion gene detection and validation (I)

In Study I, a computational pipeline called FUsioN Gene Integration toolset, FUNGI, was built for fusion gene detection and prioritization. Fusions found by FUNGI were experimentally further validated.

5.1.1 Computational pipeline

We employed six fusion calling algorithms: Arriba, ChimeraScan, EricScript, FusionCatcher, SOAPFuse, and STAR-Fusion, to detect fusion genes using RNA sequencing data (Figure 12). Subsequently, the identified fusions underwent annotation and scoring through FusionAnalyzer filters. To ensure accuracy, we used Ensembl and fusion calling project information for additional annotation of the fusions. The reported breakpoints of each identified fusion were carefully cross-referenced with the Ensembl database to verify their alignment with existing genes. This process allowed us to annotate the fusion genes with Ensembl IDs and eliminate pairings involving paralogs, homologs, and genes with unknown functions. Next, we compared the remaining fusions with existing fusion datasets to exclude any common artifacts or fusions previously reported in healthy individuals. To assess their oncogenic potential, both Pegasus and Oncofuse scoring methods were applied after filtration.

To visualize and validate the fusions further, FusionVisualizer was utilized to create a virtual reference for each fusion. This virtual reference was then reconstructed and mapped accordingly. To ensure quality and authenticity, all fusions were meticulously inspected using Integrative Genomics Viewer (IGV).

At the completion of this thorough analysis, a total of 218 261 fusions were initially detected from the RNA-Seq data through the FUNGI pipeline from 107 tumor samples from 36 HGSC patients. However, after rigorous filtration, 228 fusion gene pairs remained for further investigation and analysis. The observed range of uniquely expressed fusions among the samples spanned from 1.2% to 14.1%.

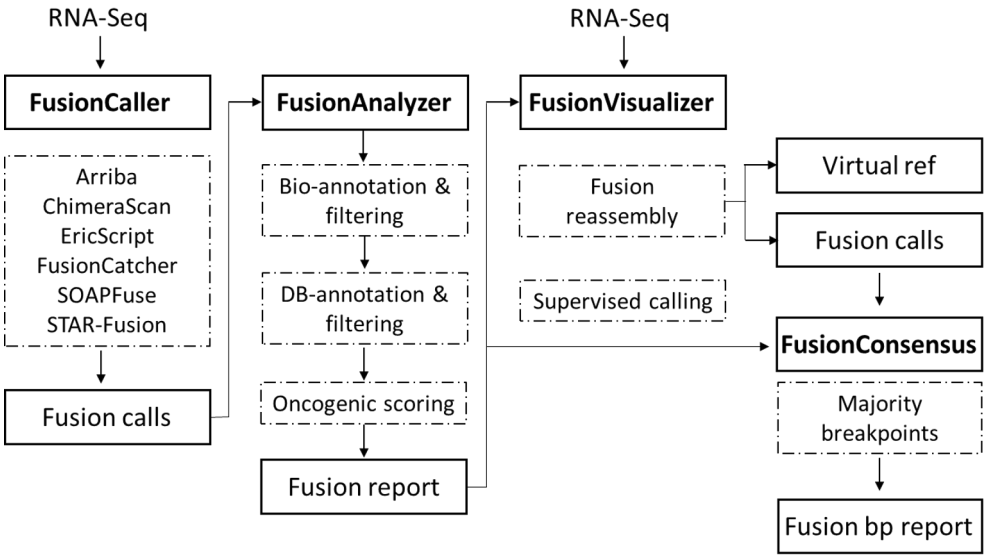

Figure 12. Schematic representation of the FUNGI. Modified from Study I.

5.1.2 Experimental validation confirms the computational pipeline's utility in detecting relevant fusion events

After identifying 228 fusions, a manual review of the literature was conducted. We focused on investigating the molecular functions and processes associated with the genes involved in these fusions, particularly in the context of HGSC. Moreover, we examined whether any of the gene partners were previously implicated in fusions linked to other cancers. To investigate the fusions at the DNA level, GRIDDS was utilized as the FUNGI was performed on RNA-Seq data.

Based on the biological significance, visualization score, and RNA-Seq/WGS (Whole Genome Sequencing) matching, the fusions were prioritized and ranked. Subsequently, the top 20 fusions were considered, and the first 11 from this list (Table 9) were selected for further experimental validation.

Table 9. List of the top 20 fusions based on their visualization score, which ranges from 0 to 3 (where 3 indicates the best visualization) at the RNA level. These fusions were identified through matching WGS and RNA-Seq data, and their biological relevance. NA denotes not available.

Fusion	Visualization Score	WGS/RNA-Seq matched	Validated	Biological Relevance Gene1	Biological Relevance Gene2
AKT2-PBX4	1	Yes	Yes	PI3K pathway	Transcription
AKT2-ZNF546	3	Yes	Yes	PI3K pathway	Transcription
CDH2-INO80C	3	NA	Yes	Cell adhesion	DNA damage and DNA repair, Transcription
MLLT10-FYB1	NA	Yes	Yes	Transcription	Adaptor protein
PIK3R1-CCDC178	1	Yes	Yes	PI3K pathway	NA
PTK2-AGO2	3	NA	Yes	Cell migration, adhesion *etc.*	RNA-mediated gene silencing, Transcription
PTPN11-CFAP54	NA	Yes	Yes	Protein phosphatase	Cilium biogenesis/degradation, Differentiation
RFX1-SLC1A6	3	Yes	Yes	Transcription	Amino-acid transport
SBF1-MAPK11	3	Yes	Yes	Adaptor protein	Stress response, Transcription
XPO1-USP34	3	Yes	Yes	mRNA and protein transport	Ubl conjugation pathway, Wnt signaling pathway
TPM3-C1orf189	1	Yes	NA	Actin-binding, TPM3-ROS1 fusion	NA
CHD9-CCND3	3	Yes	No	Transcription	Cell cycle, Transcription, KCNMB4-CCND3 fusion
NECTIN2-TANC2	3	Yes	No	Cell adhesion	NA
RAD52-FRMD3	1	Yes	No	DNA damage, DNA repair	Tumor suppressor, Membrane protein primarily found in ovaries
NEO1-AKAP13	3	Yes	No	Cell adhesion	p38 MAPK signaling
TPD52L1-RNF217	3	Yes	No	Cell proliferation and calcium signaling *etc.*	Ubl conjugation pathway
DIP2C-ADARB2	3	Yes	No	NA	mRNA processing
DPYSL3-JAKMIP2	3	Yes	No	Cytoskeleton remodelling	Component of the Golgi matrix
CHD9-TANGO6	3	Yes	No	Transcription	NA
SPECC1-MVP	1	Yes	No	SPECC1-PDGFRB fusion	mRNA and protein transport, Drug resistance in ovarian cancer

By RT-PCR and Sanger sequencing, we were successful in confirming 10 out of the 11 fusions in tumor tissues (Figure 13). None of these fusions were detected in benign tumors. This outcome served as compelling evidence of FUNGI's capability to identify and prioritize biologically significant fusion events within the data.

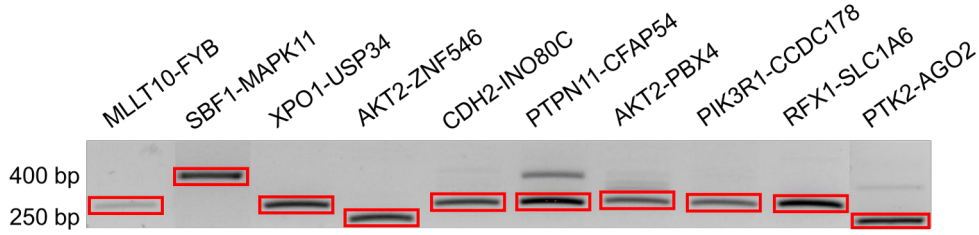

Figure 13. RT-PCR and Sanger sequencing of the ten biologically interesting fusion genes. Modified from Study I.

As a representative example for the experimental validation, we focused on the *AKT2-PBX4* fusion. Through RT-PCR analysis, we successfully confirmed the presence of *AKT2-PBX4* mRNA in the same two HGSC tumor samples (T) that were initially identified by the RNA-Seq data. The fusion was not detected in any of the benign (B) ovarian tumors, providing strong evidence of the pipeline's specificity (Figure 14). Furthermore, to ensure comprehensive validation, we utilized RT-qPCR and RNA *in situ* hybridization techniques. These additional tests confirmed the expression of the *AKT2-PBX4* fusion specifically in tumor tissues, while it was not observed in the fusion-negative benign tumor samples.

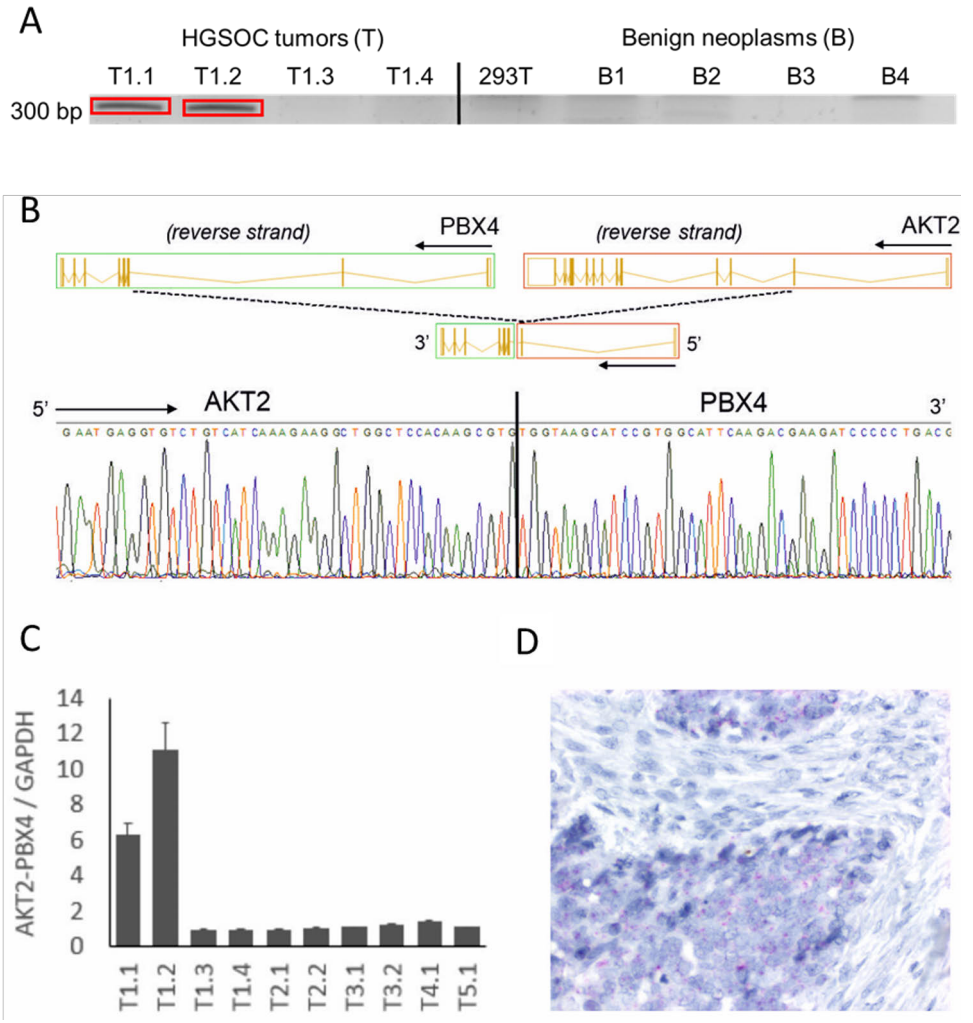

Figure 14. Experimental validation of the *AKT2-PBX4* fusion. A) RT-PCR and Sanger sequencing of the AKT2-PBX4 fusion. 293T is a fusion-negative HEK293T cell line. B) The FinchTV sequence tracing demonstrated the precise nucleotide breakpoint of the *AKT2-PBX4* fusion in cDNA, which resulted in the fusion of exons 1–2 of *AKT2* to exons 3–7 of *PBX4*. C) The expression of the *AKT2-PBX4* fusion was found in two of the four tumors (T1.1-T1.4) of the patient T1, as predicted by the pipeline. A total of ten individual tumors from five patients (T1-T5) were studied. D) RNA *in situ* hybridization for the *AKT-PBX4* fusion showed a red fusion signal in cancer cells but not in the surrounding stroma. Modified from Study I.

In addition, RT-qPCR validation for the *AKT2-ZNF546, CDH2-INO80C*, and *PIK3R1-CCDC178* fusions successfully confirmed their expression in the respective specific tissues (Figure 15). This validation also solidified the pipeline's significance in identifying relevant fusion events.

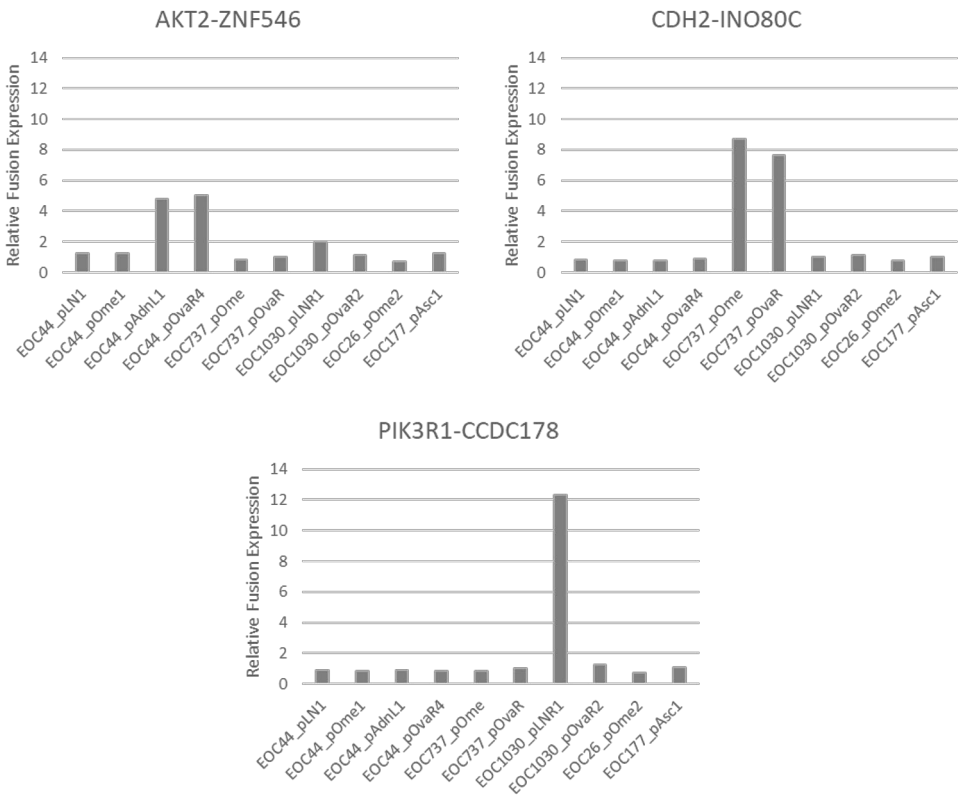

Figure 15. RT-qPCR confirmed *AKT2-ZNF546, CDH2-INO80C*, and *PIK3R1-CCDC178* fusions from the ten individual tumors from five patients.

5.2 Biological function of the PIK3R1-CCDC178 fusion (II)

The *PIK3R1-CCDC178* fusion was verified in Study I and was selected for further investigation in Study II to assess its functional characteristics. The *PIK3R1-CCDC178* fusion was particularly intriguing for biological studies due to its potential involvement in the PI3K-AKT-mTOR pathway. This pathway plays a crucial role in processes like proliferation, migration, and cisplatin resistance (P. Liu et al., 2009). The PIK3R1 fusion protein is composed of a truncated p85α with a modified c-terminal CCDC178 sequence. Consequently, we hypothesized that these structural alterations in p85α could lead to changes in PI3K-AKT-mTOR signaling. In the results, the *PIK3R1-CCDC178* fusion is referred to as "PIK3R1 fusion" because it lacks the CCDC178 protein. Study II aimed to investigate the functional role of the GFP-tagged PIK3R1 fusion in the OVCAR-8 HGSC cell line, where it was stably overexpressed.

5.2.1 PIK3R1 fusion induces cell motility

Initially, we investigated the impact of the PIK3R1 fusion protein on both cell growth and migration in OVCAR-8 cells. The results revealed a significant increase in motility among the PIK3R1 fusion cells during a wound healing assay, indicating an enhanced capacity for invasion and metastatic spread (Figure 16). Additionally, we observed that the PIK3R1 fusion cells exhibited unstructured growth patterns, whereas the control cells expressing the vector formed round and compact colonies.

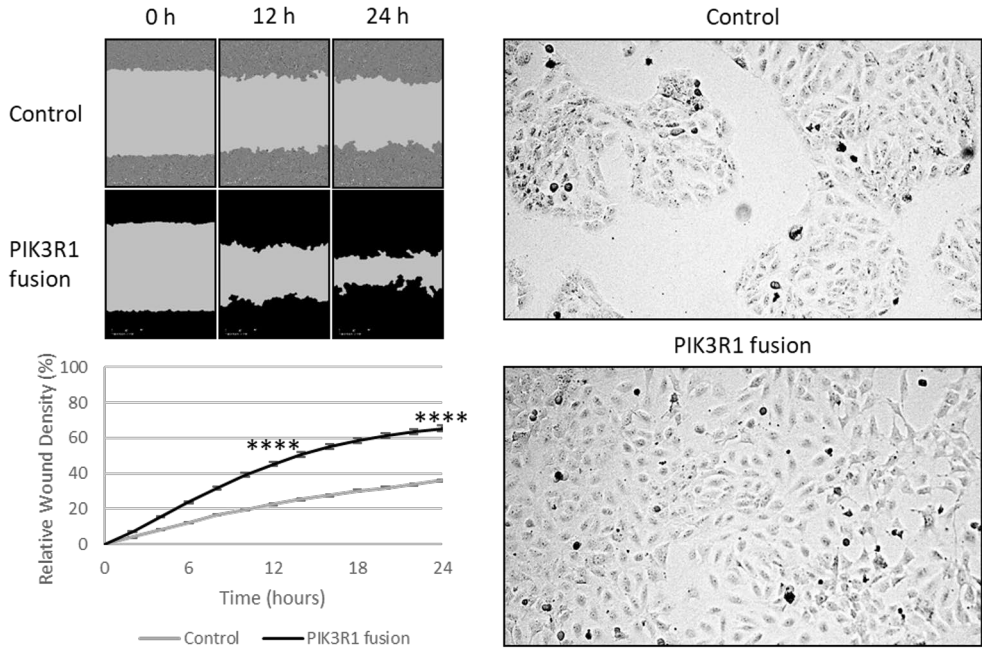

Figure 16. A wound healing assay assessed for migration of vector control and PIK3R1 fusion cells. Phase contrast microscopy of cell morphologies at 10x magnification. Statistical analysis by unpaired *t*-test; ****$p \leq 0.0001$. Error bars represent ±SEM. Modified from Study II.

In light of the unstructured morphology observed in the PIK3R1 fusion cells, we sought to explore the possibility of EMT underlying this phenomenon. We examined EMT biomarkers to determine if they could account for the loose cell-cell contact and increased migration observed. Surprisingly, the expression levels of these EMT biomarkers remained collectively unchanged (Figure 17), showing neither a decrease nor an increase, suggesting that alternative mechanisms may be responsible for the observed cellular behavior.

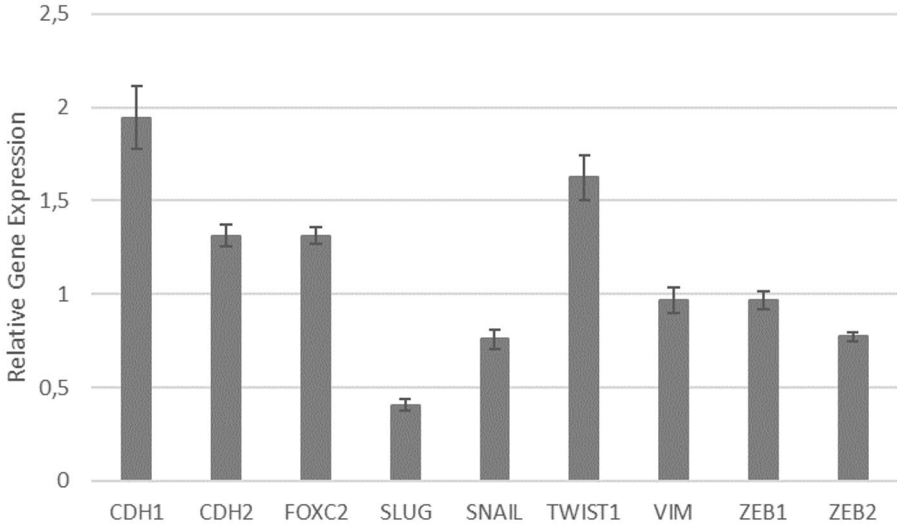

Figure 17. EMT biomarkers were assessed in PIK3R1 fusion cells. The data were normalized to *GAPDH* and with the expression of the target gene in control cells. Error bars represent ±SEM.

5.2.2 ERK1/2 is activated in the PIK3R1 fusion cells and the fusion cells express rod and ring-like structures

Our hypothesis was centered on the idea that the PIK3R1 fusion could enhance the activation of the PI3K-AKT-mTOR signaling cascade by either losing its inhibitory effect on the p110α subunit or experiencing a flawed interaction with PTEN phosphatase due to the absence of SH2 domains. However, when we conducted Western blot analyses, we made an unexpected discovery: the expression of the wild-type p85α was reduced in the fusion cells, while ERK1/2 showed a significant increase in activation levels (Figure 18). In addition, treatment with tipifarnib, an inhibitor targeting the upstream protein Ras, resulted in a mere 1.4-fold reduction in ERK1/2 phosphorylation within the fusion-expressing cells. In contrast, the vector control cells exhibited a more pronounced decrease of 5.2-fold. These outcomes implied that the activation of ERK1/2 by the PIK3R1 fusion occurs through a mechanism independent of Ras.

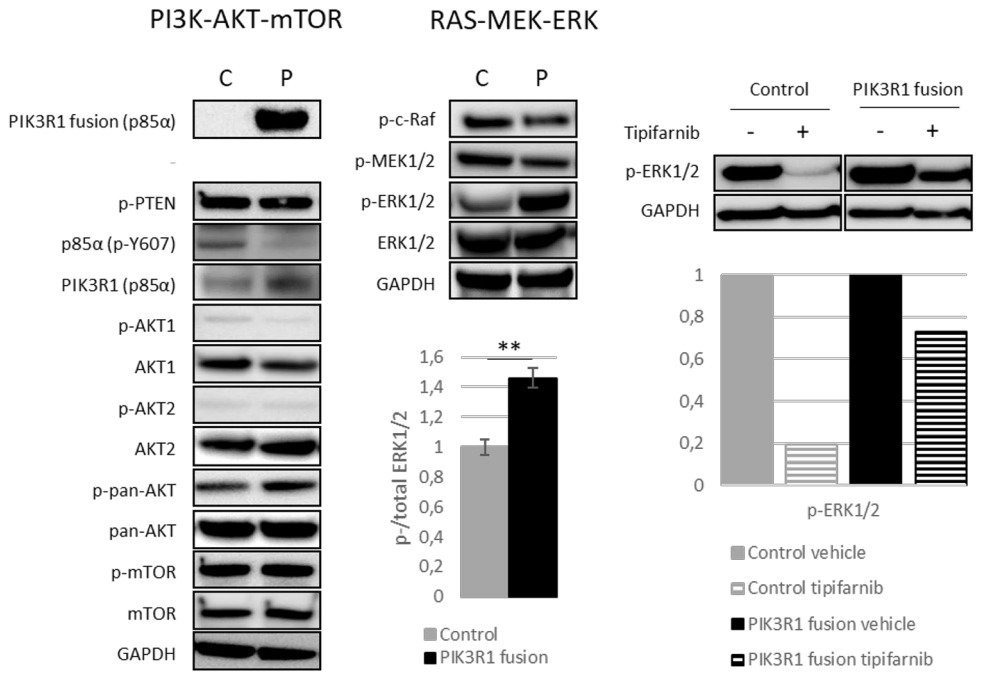

Figure 18. PI3K-AKT-mTOR and RAS-MEK-ERK pathway activation was studied by Western blot. ERK1/2 was activated in the PIK3R1 fusion cells. The fusion-expressing cells sustain elevated ERK1/2 phosphorylation even after exposure to a 10 µmol/L Ras inhibitor, tipifarnib, for a duration of 12 h. Statistical analysis by unpaired *t*-test; $^{**}p \leq 0.01$. Error bars represent ±SEM. Modified from Study II.

5.2.3 PIK3R1 fusion cells are resistant to cisplatin and trametinib and express rod and ring-like structures

Cell survival was assessed using a colony assay to investigate the impact of inhibitors targeting the PI3K-AKT-mTOR and RAS-MEK1/2-ERK1/2 pathways. Cisplatin, the conventional chemotherapy drug for HGSC, was also included in the study. Before conducting the experiments, we determined the appropriate concentrations of the drugs by calculating their IC50 values (Figure 19). The cells did not show a significant response to the inhibitors or cisplatin in this assay.

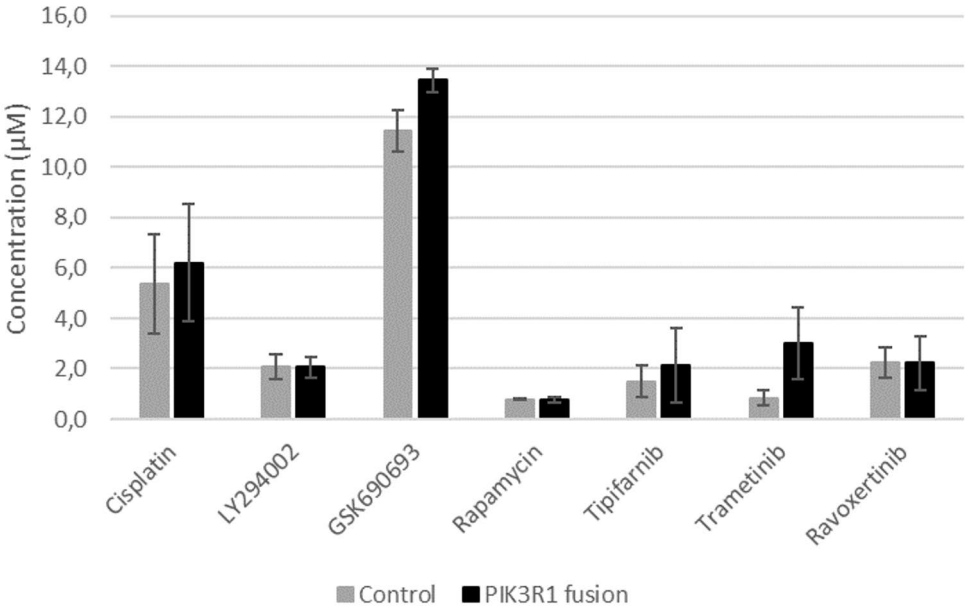

Figure 19. IC50 values of control and PIK3R1 fusion cells. Cells were treated with increasing concentrations of cisplatin. Cell viability was assessed by MTS assay at 72 h. IC50 values were obtained (from sigmoidal curves) by means of Origin 2016 software. The mean of three biological replicates is shown. Error bars represent ±SEM.

Nevertheless, during the colony assay studies, we observed that PIK3R1 fusion cells displayed increased resistance to cisplatin (Figure 20). Additionally, fusion cells showed resistance to trametinib, an inhibitor of MEK1/2, but not to inhibitors targeting PI3K or AKT. Notably, when examining GFP-tagged PIK3R1 fusion cells treated with cisplatin or trametinib using fluorescence microscopy, we noticed the formation of peculiar complexes within the cells. Furthermore, the level of treatment resistance appeared to be correlated with the number and size of these structures.

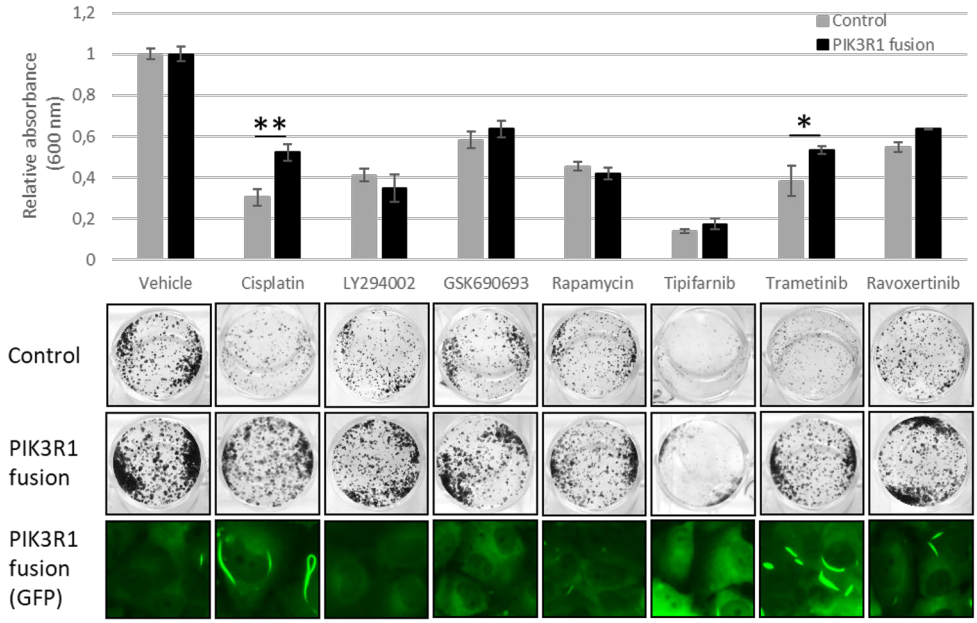

Figure 20. The reaction of cells to cisplatin and pathway inhibitors in a colony formation experiment. Cells were cultured for 8 days without therapy or for 3 days commencing on day 5 with cisplatin, LY294002 (PI3Ki), GSK690693 (pan-AKTi), rapamycin (mTORi), tipifarnib (Rasi), trametinib (MEKi), and ravoxertinib (ERKi). Data are normalized to the vehicle. The fluorescence images in the bottom row show the expression of protein complexes in PIK3R1 cells after various treatments. Statistical analysis by unpaired *t*-test; $*p \leq 0.05$, $**p \leq 0.01$. Error bars represent ±SEM. Modified from Study II.

The dynamic protein complexes in the PIK3R1 fusion-expressing cells resembled filamentous assemblies called rod and ring structures (RRs). These structures are cytoplasmic rod (10 µm in length) and ring (2–5 µm in diameter) -shaped complexes. Despite their intriguing nature, the exact function of RRs remains unclear (Calise & Chan, 2020). Inosine monophosphate dehydrogenase 2 (IMPDH2) and CTP synthase 1 (CTPS1) are the primary components of RRs, and their inhibition by mycophenolic acid (MPA) or 6-Diazo-5-oxo-L-norleucine (DON) results in filament production (Pareek et al., 2021; Siddiqui & Ceppi, 2020; Villa et al., 2019).

To investigate whether the structures formed in the PIK3R1 fusion-expressing cells were RRs, we induced their formation using MPA or DON. While these aggregated PIK3R1 fusion proteins were frequently found around the nuclei, resembling RRs, they did not colocalize with the typical RRs (Figure 21). Notably, the fusion protein aggregations were significantly thicker in diameter compared to the original RRs. Further examination through correlation light-electron microscopy

revealed a strong association of the rod and ring-like structures with filaments, possibly composed of actin or intermediate filaments.

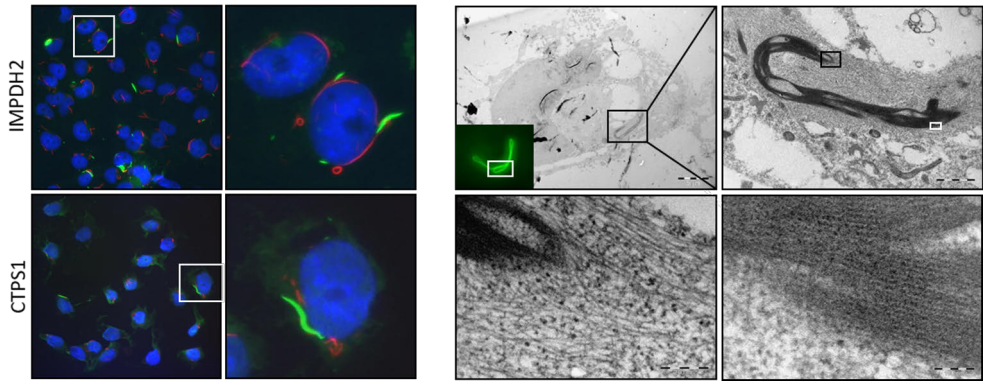

Figure 21. GFP-tagged PIK3R1-tagged fusion (green) did not colocalize with IMPDH2 (red) or CTPS1 (red) rod and rings (RRs) elicited by 1 μM MPA for 4 h and 100 μM DON for 24 h. Analysis of the PIK3R1 fusion protein complex using light and electron microscopy. PIK3R1 fusion cells were treated for 96 hours with 5 μM cisplatin to produce protein complexes. Fusion protein aggregates are evident near the nucleus but do not colocalize with cellular organelles. The tail of the protein aggregation and ribosomes in the cytoplasm (shown in the black box) and the filamentous structure of the PIK3R1 fusion protein complex (shown in the white box). The scale bars in the electron microscope images are 5 μm, 1 μm, 200 nm, and 100 nm, respectively. Modified from Study II.

5.2.4 PIK3R1 fusion protein colocalizes with CIN85

To explore the protein composition of the RR-like structures and their potential role in cisplatin resistance, we conducted immunoprecipitation on the GFP-tagged fusion protein. Mass spectrometry was utilized to analyze the material from two biological replicates of untreated vector control cells (n = 94) and PIK3R1 fusion-expressing cells (n = 163), as well as one replication each of cisplatin-induced vector control cells (n = 114) and cisplatin-induced PIK3R1 fusion-expressing cells (n = 119).

In the analysis, we identified a total of 234 unique proteins between the precipitates from the fusion-expressing and control cells. Out of these, 16 proteins were consistently present in all three replicates of the fusion-expressing cells, making them the most reliable candidates for further investigation (Table 10). Among these proteins, CIN85 and CD2AP stood out due to their significant number of unique peptides and high Mascot scores, which were also observed in the fusion peptides. These findings indicate the potential importance of CIN85 and CD2AP in the context of the RR-like structures and their potential role in conferring cisplatin resistance.

Table 10. GFP-tagged fusion protein immunoprecipitation and mass spectrometry analysis validated the 16 most abundant proteins in the fusion structures. Modified from Study II.

Protein name
SH3 domain-containing kinase-binding protein 1 (CIN85)
CD2-associated protein
Phosphatidylinositol 3-kinase regulatory subunit alpha (fusion)
Coiled-Coil Domain (fusion)
Heat shock cognate 71 kDa protein
CAD protein
Elongation factor 1-alpha 1
Heat shock 70 kDa protein 1B
Protein S100-A10
Heat shock protein beta-1
60S ribosomal protein L23
F-actin-capping protein subunit alpha-1
Tubulin beta chain
Keratin, type II cytoskeletal 7
ATPase family AAA domain-containing protein 3B
DnaJ homolog subfamily A member 3, mitochondrial

With the use ofconfocal microscopy, we confirmed the colocalization of the PIK3R1 fusion with CIN85 both under standard culture conditions and after cisplatin exposure (Figure 22A). Notably, the expression of CIN85 was observed to increase in both control cells and PIK3R1 fusion cells following cisplatin treatment as revealed by confocal microscopy (Figure 22B).

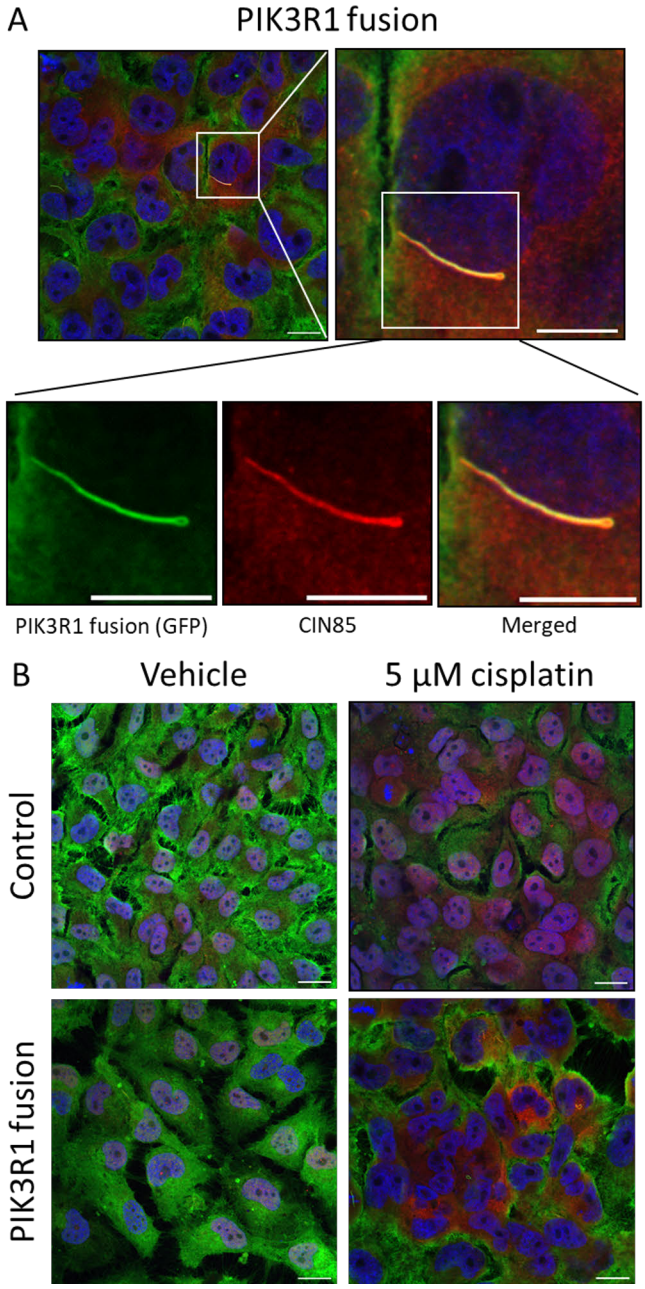

Figure 22. Confocal microscopy images of PIK3R1 fusion and CIN85 colocalization. A) CIN85 colocalized with the fusion-expressing structures. The scale bars in the top left-handed image indicate 20 µm, while the four other images have scale bars of 10 µm. B) Treatment with cisplatin resulted in increased CIN85 expression in both fusion and control cells. The images have scale bars representing 20 µm. The cells were either cultured under standard conditions or treated with cisplatin before fixation and labeling with GFP (PIK3R1, green), CIN85 (red), and DNA (DAPI, blue). Modified from Study II.

Upon examining the protein expression of CIN85, we noticed that the smaller 47 kDa isoform of CIN85 was significantly increased in the PIK3R1 fusion cells treated with either vehicle or cisplatin (Figure 23). However, the larger 85 kDa isoform of CIN85 did not show a significant increase under the same conditions.

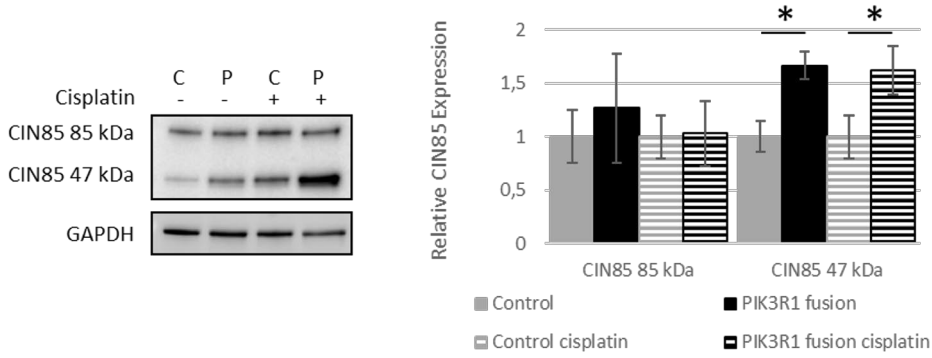

Figure 23. CIN85 47 kDa isoform expression was increased in the fusion expressing cells under normal culture conditions and after 3d cisplatin exposure (n = 3). Data are represented as mean ± SEM, statistical analysis by unpaired *t*-test; **p* ≤ 0.05. Modified from Study II.

5.2.5 PIK3R1 fusion induces resistance to cisplatin and trametinib associated with rod and ring-like structure formation

We investigated the relationship between CIN85 expression and ERK1/2 activation. The analysis yielded a noteworthy finding: there was a consistent increase in the expression of the CIN85 47 kDa isoform, and this upregulation corresponded with an increase in ERK1/2 phosphorylation (Figure 24).

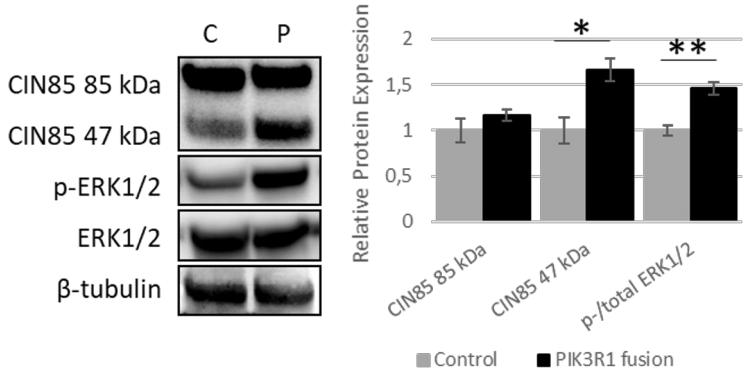

Figure 24. Western blot analysis of CIN85 and ERK1/2 expression from control and PIK3R1 fusion cells under normal culture conditions. Statistical analysis by unpaired *t*-test; **p* ≤ 0.05, ***p* ≤ 0.01. Error bars represent ±SEM. Modified from Study II.

In order to investigate the potential relationship between RR-like structure formation and cisplatin resistance, we carried out a parallel study examining cell viability (Figure 25). We exposed the cells to 5 μM cisplatin and 3 μM trametinib. The analysis confirmed that the PIK3R1 fusion cells maintained their ability to proliferate during the five-day cisplatin exposure, in contrast to the vector control cells, where 52% had died by day five. Additionally, the PIK3R1 fusion cells exhibited significant resistance to trametinib. However, it is worth noting that the PIK3R1 fusion cells became susceptible to the combined therapy of cisplatin and trametinib, suggesting a potential therapeutic option.

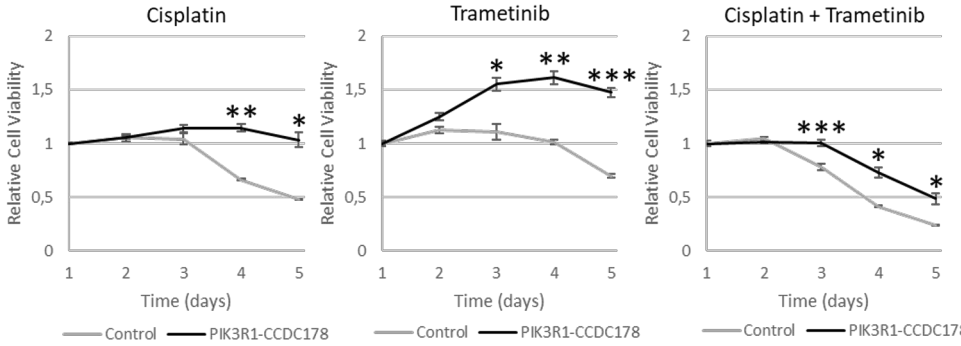

Figure 25. Under cisplatin and trametinib treatment, PI3KR1 fusion-expressing cells remained viable (MTS assay). The viability was normalized to the vehicle and 1-day cell viability. Statistical analysis by unpaired *t*-test; **p* ≤ 0.05, ***p* ≤ 0.01, ****p* ≤ 0.001. Error bars represent ±SEM.Modified from Study II.

Treatment resistance was found to be closely associated with a significant increase in the formation of RR-like structures (Figure 26). These structures, initially appearing as short formed within 48 hours after treatment, demonstrated growth in both length and thickness over time. In untreated PIK3R1 fusion cells, only 6.4% exhibited RR-like structures. After 48 and 72 hours of cisplatin treatment, 32% and 52% of PIK3R1 fusion cells exhibited RR-like structures, respectively. Similarly, after trametinib exposure, 34% and 54% of cells expressed RR-like structures at the same time points. Remarkably, when subjected to the combined treatment of cisplatin and trametinib, the corresponding percentages were 32% and 51%, respectively. This suggests a link between the induction of RR-like structures and the development of treatment resistance in the PIK3R1 fusion cells.

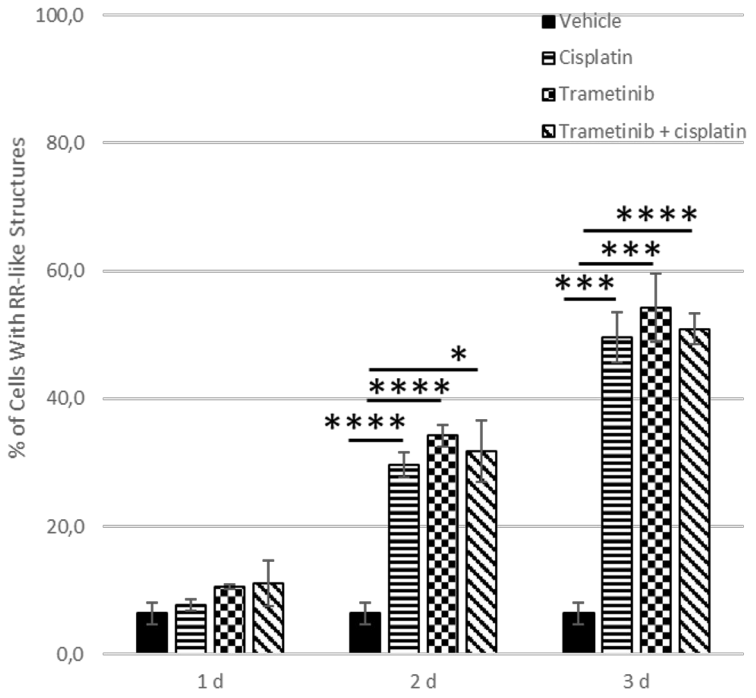

Figure 26. Cisplatin and trametinib developed RR-like structures in fusion-expressing cells in a three-day linear fashion (average SEM). At each time point, 63 to 269 cells were counted. Unpaired *t*-test; *$p \leq 0.05$, **$p \leq 0.01$, ***$p \leq 0.001$, ****$p \leq 0.0001$.

5.2.6 PIK3R1 fusion expression is enriched in the lymph node metastasis

Using RNA-Seq data, FUNGI detected the presence of the PIK3R1 fusion in two out of three HGSC tumors: a right ovarian tumor lesion (pOvaR2) and a metastasis of a right para-aortic lymph node (pLNR1). However, it was not identified in another right ovarian tumor lesion (pOvaR1) through the fusion detection algorithm in whole genome sequencing data. Nevertheless, manual evaluation revealed the existence of the fusion at the DNA level. The fusion was not initially detected due to a bridging process that possibly caused the fusion to be overlooked. Specifically, *PIK3R1* was found to be fused with *AC012123.8*, which then further fused to *CCDC178*.

Notably, despite the substantial differences in tumor purities, with pOvaR2 having 50% tumor purity and pLNR1 only 9%, a similar number of junction reads were identified in both RNA and DNA from both locations. This indicated that fusion-bearing cells were enriched in lymph node metastases.

To further validate the enrichment of the fusion in the lymph node, the relative fusion expression was assessed in patient samples using RT-qPCR (Figure 27). The

fusion expression was detectable only in the pLNR1, while it was undetectable in the primary tumor pOvaR2 and other fusion-negative tumors. These findings confirmed the enrichment of the fusion in the lymph node. Additionally, RNA *in situ* hybridization validated and localized the fusion signal in a subset of tumor cells in pOvaR2, providing further evidence to support the hypothesis that fusion-expressing cells had metastasized from the ovarian tumor pOvaR2 to the lymph node. The fusion's ability to enhance cancer cell motility also contributed to supporting this hypothesis.

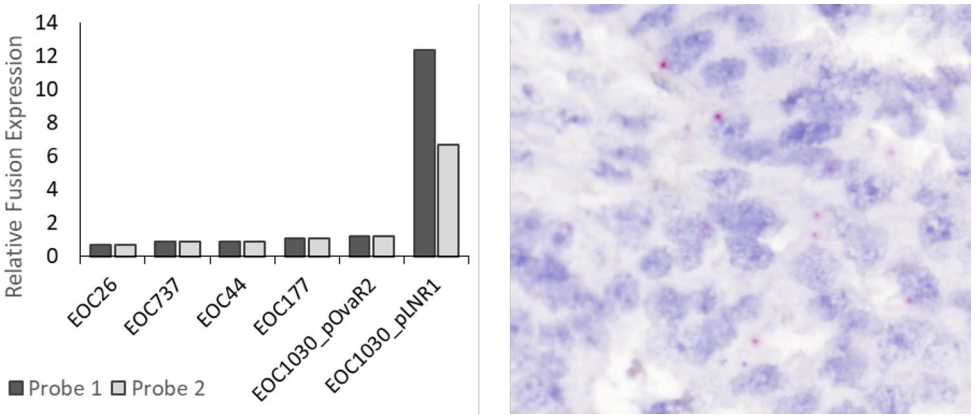

Figure 27. Fusion transcript expression was elevated in the patient's lymph node metastasis EOC1030_pLNR1, but was below the detection limit of RT-qPCR in EOC1030_pOvaR2 and fusion-negative tumors. RT-qPCR data were analyzed using the $2^{-\Delta\Delta Ct}$ method. The signal (red dots) was localized in the tumor cells of the sample pOvaR2 by RNA *in situ* hybridization. Modified from Study II.

In summary of Study II, the formation of rod and ring-like structures is closely linked to cell survival and treatment resistance (Figure 28). The presence of the PIK3R1 fusion enhances malignant traits such as cell migration by activating ERK1/2, either directly or indirectly. Additionally, there is a noticeable decrease in the expression of wild-type p85α. Furthermore, CIN85 has the potential to hinder the activity of the fusion protein by binding to its SH3 domain. Interestingly, under cisplatin treatment, the PIK3R1 fusion interacts with CIN85, resulting in the formation of filamentous RR-like structures. Moreover, this interaction is associated with the development of simultaneous chemoresistance, indicating the complex involvement of the PIK3R1 fusion and CIN85 in the response to cisplatin treatment.

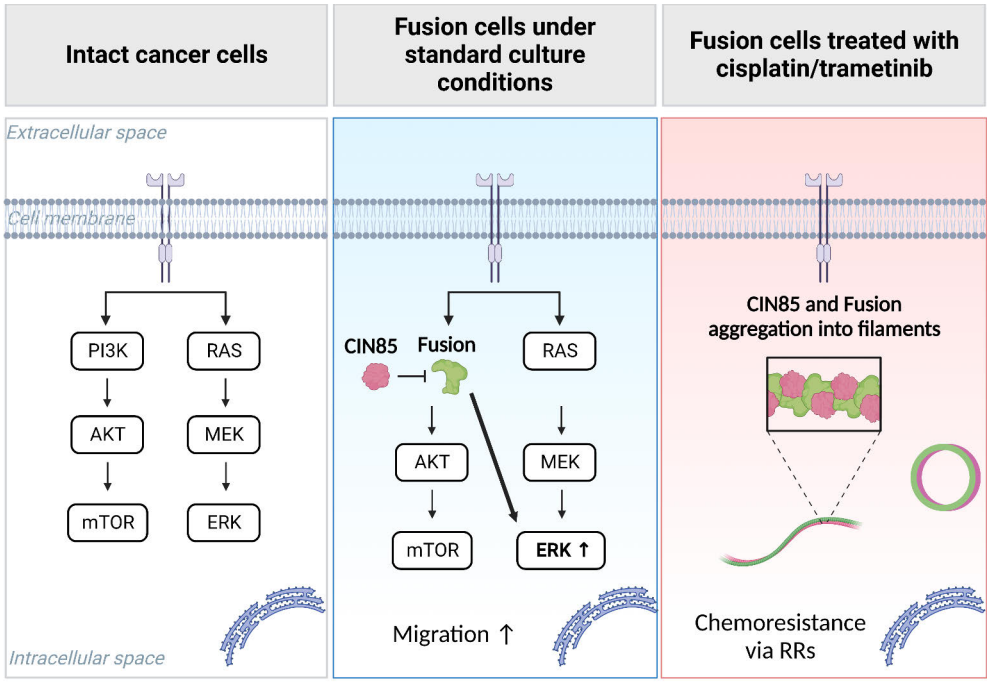

Figure 28. Graphical illustration of events leading to chemoresistance. Created with BioRender.com. Modified from Study II.

6 Discussion

Chromosomal instability is a defining characteristic of HGSC (Bowtell, 2010). The knowledge of fusion genes has remarkably increased since the first fusion genes in HGSC were revealed in 2011. Fusion gene detection has been revolutionized by the low-cost, high-throughput, massively parallel sequencing technology (Dorney et al., 2023; Schuster, 2007). Fusion genes are common in HGSC, but their role in HGSC pathogenesis, disease progression, and therapy resistance has yet to be understood. Recent studies have shown that unique gene fusions have oncogenic properties. However, the fusion genes identified vary among the patients in the studies, making it unlikely to discover a targeted drug that would benefit a larger patient group. Still, a single patient can benefit from an existing targeted drug. A deeper understanding of how fusion proteins interfere with cellular processes, how they are regulated, and what downstream targets they have will provide crucial insights into finding new therapies for HGSC. We approached this issue by developing a computational tool to detect novel fusion genes in HGSC. In addition, we studied the biological functions of the PIK3R1-CCDC178 fusion protein as cancer-promoting alteration.

6.1 Fusion gene detection and validation (I)

Bioinformatics approaches have facilitated the discovery of novel fusion gene or RNA candidates due to advances in sequencing technology and computational capability (Lou et al., 2013). The main issue is to continue enhancing the bioinformatic tools needed to handle the enormously massive data volumes generated by deep sequencing (Carrara et al., 2013). Refining fusion detection tools, candidate fusion prioritizing algorithms, and dedicated fusion databases would be prudent to reduce the likelihood of false positive and false negative calls (Pederzoli et al., 2020).

Multiple bioinformatics pipelines (*e.g.,* FusionHub and rnafusion) have been built to aid in the detection of chimeric transcripts (Ewels et al., 2020; Panigrahi et al., 2018). Each has its own set of characteristics, strengths, and weaknesses. The sensitivity and specificity of fusion RNA detection algorithms vary greatly. Algorithm-based fusion detection also provides both false positive and false negative findings. Arriba and STARFusion, for example, have excellent sensitivity, but

SOAPFuse offers better specificity for detecting fusion events (Haas et al., 2019). Nevertheless, the candidate fusions obtained by algorithms should be experimentally validated. Usually, experimental verification of potential fusions is confirmed using RT-PCR and Sanger sequencing, utilizing fusion-specific primers that cover the junction positions of the fusion RNAs. During the reverse transcription phase of cDNA production, template switching and the formation of hairpin loops might occur, resulting in spurious fusions (Houseley & Tollervey, 2010). Therefore, the fusions should be validated using non-RT-based assays, such as Northern blot analysis (Lovatt & Eberwine, 2013).

In the current work, the fusion detection pipeline, termed FUNGI, was developed and tested. One of FUNGI's strengths is integrating six algorithms to call fusions from the RNA-Seq data. When many algorithms identify the fusion event, it is more likely to be accurate. Fusions were confirmed at the genomic level using GRIDDS, which failed to find PIK3R1 fusion. However, the manual inspection of the fusion by GenomeSpy verified the fusion at the DNA level. At the genomic level, PIK3R1 fusion contains segments from *PIK3R1*, *AC012123.8*, and *CCDC178*. PIK3R1 fusion is likely a bridge fusion. In a bridge fusion, the middle region is removed by splicing from the mature mRNA (Calabrese et al., 2020), which is not seen in the fusion at the RNA level. This finding also addresses the importance of manual visualization of the fusions.

Fusions can be prioritized and visualized after being detected by FUNGI's combined algorithms. Prioritization is based on fusion annotation with the Ensembl database, verifying that each fusion aligns with existing genes and provides, *e.g.*, gene ontology terms. Fusions were compared to existing fusion datasets to filter out typical artifacts or fusions previously described in healthy people. However, many of these newly identified fusion candidates in the databases still need to be experimentally validated, and some may represent artifacts of the sequencing processes (Barresi et al., 2019) whereupon artifacts could potentially manifest subsequent to the exclusion procedure. Fusions are scored with numeric values after filtration by Pegasus and Oncofuse, which predict the oncogenic potential of the fusions. FUNGI is similar to FusionHub and rnafusion pipelines. However, FUNGI combines two steps that FusionHub and rnafusion do not: fusion calling and oncogenic scoring.

While sequencing technology is sensitive and can detect unusual events, it is also prone to errors (Lou et al., 2013). Errors can arise at any analysis stage, including library preparation and bioinformatic analysis of the sequences, due to flaws in the reference genome assembly or substantial sequence similarities across genes (Shiroguchi et al., 2012; Sleep et al., 2013). Therefore, the experimental analysis was in a significant role in confirming FUNGI's functionality and specificity. Multiple approaches validated the discovered and prioritized fusion genes. Firstly, fusions

were established with the standard RT-PCR method and Sanger sequencing. RNA *in situ* hybridization can be considered a non-RT-based assay because it directly reveals the fusions at the RNA level. In addition, the expression level of the selected fusion genes from the tumor tissues was confirmed by RT-qPCR. We also used Western blot analysis to ensure that the fusions were translated into proteins. To conclude, selected fusions were confirmed comprehensively at both RNA and protein levels.

Despite efficient sequencing technologies, recurring fusion genes have yet to be described in HGSC. Our findings also address that fusion genes are common in HGSC, but recurrent fusion events are rare. Thus, more physiologically and therapeutically significant genetic changes should be seen using large and qualified cohorts *e.g.* the DECIDER cohort and Australian Ovarian Cancer Study (*AOCS*, 2017; *Decider Project*, 2021). Future collaborations between computational and biological experts will be required to identify possible fusions associated with tumorigenesis and treatment resistance. In addition, genomic alteration data should be implemented for clinical use to provide better patient care (Pederzoli et al., 2020).

6.2 Biological function of the PIK3R1-CCDC178 fusion (II)

6.2.1 Pathogenesis and disease progression

Loss of p53 and the homologuous recombination repair pathway are the primary events in HGSC initiation (Bowtell, 2010). Subsequently, the malignant transformation acquires additional characteristics, such as the loss of epithelial polarity, facilitating invasion (Karst & Drapkin, 2010). The PIK3R1 fusion induced phenotypic changes both in OVCAR-8 and HEK293 cells: the cells grew in unstructured colonies and easily detached from the cell culture flasks after trypsin handling. In addition, fusion cells were significantly more motile than cells lacking the fusion.

In clinical samples, the presence of the PIK3R1 fusion was observed in both the primary ovarian tumor and the lymph node. The exact disease stage at which the PIK3R1 fusion occurred cannot be determined. If the fusion had developed after the initial events, it could have been linked to the pathogenesis of HGSC, providing a molecular mechanism for cancer cells to become invasive by disrupting cell-cell contact. Nevertheless, it is conceivable that the fusion event occurred during a more advanced phase of the disease. The disease diagnosis was established at FIGO stage III, and if the fusion was a potent oncogenic driver, one would anticipate a higher enrichment of the fusion in the samples at this stage. On the other hand, rather than showing widespread intra-abdominal spreading, metastases were primarily found in the abdominal lymph node. In this scenario, the fusion-bearing cells could have

disseminated from the ovarian tumor to the lymph node. Another possibility is that the fusion may have spread to the lymph node via the lymphatic route, which is a less common metastasis pathway, making the potential effect of the PIK3R1 fusion more plausible. However, it is essential to note that these are speculative hypotheses.

Gene fusions that may promote disease initiation in HGSC are HRR-associated loss-of-function fusions in *PTEN* and *RAD51B* (Patch et al., 2015). Loss of PTEN activity can impede DNA repair efficiency, leading to the accumulation of DNA lesions and genomic instability (Hou et al., 2017). The *ESRRA-C11orf20* fusion can also be mentioned in this connection because Salzman et al. hypothesized that this fusion might have a role in HGSC pathogenesis. In one tumor, the *ESRRA-C11orf20* fusion resulted in a genomic rearrangement, while in the second tumor, there was evidence of local copy number variation at the *C11orf20* and *ESRRA* locus. Unfortunately, the functional role of the *ESRRA-C11orf20* fusion remains to be established (Salzman et al., 2011). Nonetheless, two other groups have demonstrated that elevated expression of *ESRRA* is correlated with decreased overall survival, and the *ESRRA* locus is associated with increased susceptibility to ovarian cancer, which implies the potential importance of the *ESRRA-C11orf20* fusion (Permuth-Wey et al., 2011; Sun et al., 2005).

The *CDKN2D-WDFY2* fusion resulted in *CDKN2D* loss, which can impair both cell cycle control and DNA repair (Kannan et al., 2014). CDKN2D is a negative regulator in cell growth that controls the G1/S transition (Ortega et al., 2002). CDKN2D also plays an essential function in DNA repair since it is increased during genotoxic stress, and high levels are required for effective DNA repair (H. Liu et al., 2022). The inability to repair DNA damage caused by the absence of functioning CDKN2D could contribute to increased gene mutations and chromosomal recombinations in HGSC (Kannan et al., 2014). *CDKN2D-WDFY2* induced a loss of wild-type *CDKN2D* expression. Therefore, it may boost cell proliferation, one of the characteristics required for the malignant transition of HGSC to become invasive.

Fusion genes may have a role in the pathophysiology of HGSC. However, due to the late stage of diagnosis, studying initiative molecular changes in HGSC is challenging. Even though the fusions are not directly implicated in HGSC pathogenesis, they may enhance disease progression in the early stages.

6.2.2 OVCAR-8 and HEK293 cell lines

We studied the functional role of the PIK3R1 fusion on the overexpressing OVCAR-8 and HEK293 cell lines. Both OVCAR-8 and HEK293 are commercially available. The OVCAR-8 cell line originates from HGSC, whereas HEK293 cells are frequently employed in cell experiments due to their reliable growth and ease of transfection. OVCAR-8 cells express mutated *TP53*, *CTNNB1*, *ERBB2* and *KRAS*,

with the *TP53* mutation c.376-1G>A (p.Tyr126_Lys132del, c.376_396del21) being classified as pathogenic (*Cellosaurus OVCAR-8*, 2023).

All the experiments were primarily performed in OVCAR-8 cells, and the main results were subsequently validated in the non-cancerous HEK293 cells. However, in HEK293 cells, AKT may be constitutively activated, which was not ideal for our study on the PI3K-AKT-mTOR signaling pathway. Nevertheless, we confirmed the effect of the PIK3R1 fusion on ERK1/2 activation in both cell lines. Notably, ERK1/2 expression was not elevated in the control cells, indicating that the mutational status of OVCAR-8 cells did not impact the results, and the observed effects were specifically driven by the presence of the PIK3R1 fusion.

Ideally, studying the effects of a native fusion would involve using a patient-derived cell line, similar to how *SLC25A40-ABCB1* was studied on ascites-isolated cells. Findings obtained from cells with their original molecular alterations and intracellular environments are more reliable. However, extracting the desired tumor cells from the tumor bulk can be challenging, and the tumor purity may be low, leading to potential enrichment of other cell types like fibroblasts in the cell lines. Moreover, the fusion of interest should be highly expressed for effective study. Despite these challenges, we were able to obtain comparable results using the PIK3R1 fusion-overexpressing OVCAR-8 and HEK293 cell lines.

6.2.3 PI3K-AKT-mTOR and RAS-MEK-ERK signaling pathways

Roughly 45% of patients with HGSC exhibit modified PI3K/RAS signaling pathways (D. Bell et al., 2011). However, there is only a little evidence of the fusion gene involvement in the pathway activation in HGSC. CDKN2D-WDFY2 fusion has been described with potential PI3K-AKT-mTOR pathway association via WDFY2-AKT interaction (Kannan et al., 2014). Another AKT fusion is BCAM-AKT2, which was shown to be translated into an in-frame fusion protein in the patient's tumor. This fusion was constitutively phosphorylated, and activated as a functional kinase in the patient´s cells. In addition, in the gene-edited OVCAR8 and HEK-293T cells, BCAM-AKT2 induced focus formation suggesting that the fusion was oncogenic (Kannan, Coarfa, et al., 2015).

We hypothesized that PIK3R1 fusion promotes the PI3K-AKT-mTOR signaling cascade activation by losing the inhibitory effect on the p110α subunit or by a faulty interaction with PTEN phosphatase due to a lack of SH2 domains. Interestingly, our findings showed that in the PIK3R1 fusion expressing cells, the fusion targeted both PI3K-AKT-mTOR and RAS-MEK-ERK pathways. PIK3R1 fusion expression decreased wild-type p85α and increased the ERK1/2 activation. Otherwise, both signaling cascades remained intact. When we suppressed Ras protein with tipifarnib,

we only saw a 1.4-fold decrease in ERK1/2 phosphorylation in the fusion expressing cells, but a 5.2-fold decrease in the vector control cells. These findings suggest that PIK3R1 fusion had an alternative way to promote ERK1/2 activation. However, the mechanism remained unknown.

The RAS-MEK-ERK signaling pathway is also involved in regulating various cellular processes, including growth, proliferation, survival, and differentiation, and has recently been suggested to contribute to platinum resistance in ovarian cancer (Kielbik et al., 2018; Z. Li et al., 2019). In addition, a truncated p85α resulted from a mutated *PIK3R1* is associated with increased invasion via ERK1/2 activation. Theoretically, PIK3R1 fusion, which results in a shortened p85α, the activation of ERK could be influenced by this alteration in PIK3R1 fusion cells. Theoretically, the activation of ERK could be influenced by this alteration in PIK3R1 fusion cells since the PIK3R1 fusion results in a shortened p85α.

The response of ERK to cisplatin is intricate, as these proteins can, in many instances, either induce apoptosis, suppress it, or not play a role in this process. The ultimate outcome is influenced by the cell type, as well as the proliferation and differentiation status of tumor cells (Brozovic & Osmak, 2007). For example, Kielbiek et al., have shown that cisplatin induces ERK1/2 activation and thereby promotes progression of cells to move from the cell growth phase (G1) to DNA synthesis (S) (Kielbik et al., 2018). On the other hand, previous studies by Hayakawa and Mansouri have linked cisplatin-induced activation of ERK1/2 to either pro-survival or pro-apoptotic effects on ovarian cancer cell lines (Hayakawa et al., 1999; Mansouri et al., 2003).

Several targeted drugs for HGSC that are currently being investigated are associated with the PI3K-AKT-mTOR pathway. Our study results indicated no difference in the response of PI3K-AKT-mTOR pathway inhibitors between PIK3R1 fusion cells and control cells. However, PIK3R1 fusion cells showed resistance to trametinib and conventional cisplatin treatments individually. Interestingly, they exhibited sensitivity to the combined treatment of cisplatin and trametinib. A similar finding was reported by Li et al., who discovered that inhibiting ERK using selumetinib (MEK inhibitor) resensitized platinum-resistant ovarian cancer cells to cisplatin (Z. Li et al., 2019). If the PIK3R1 fusion is detected in relapsed tumor samples, it would be valuable to experimentally test the response of platinum and trametinib combination treatment to determine whether this treatment approach could be beneficial for the patient.

6.2.4 Treatment resistance via rods and rings

Cancer cells must remodel cellular metabolism to satisfy the demands of endless growth and proliferation. IMPDH2 and CTPS1 are enzymes involved in purine and

pyrimidine *de novo* nucleotide synthesis. IMPDH2 and CTPS1 are both known to create cytoplasmic structures called rods and rings (RRs). These assemblies take the form of rods, which are approximately 10 μm in length, and rings with a diameter of 2-5 μm. Despite their identification, the exact function of these structures is not fully understood (Calise & Chan, 2020).

The first report of RRs dates back to 2011, but they were originally discovered in 2005 from hepatitis C patients undergoing interferon-α and ribavirin combination therapy (Carcamo et al., 2011). Ribavirin inhibits IMPDH2 and interferes with RNA metabolism, which is necessary for viral replication (Covini et al., 2012). CTPS1 can be inhibited with a glutamine antagonist, 6-diazo-5-oxo-norleucine (DON). Inhibition of IMPDH2 and CTPS1 with the above-mentioned treatments result in RR assembly (Carcamo et al., 2011).

In RRs, IMPDH2 is the primary protein, and its structure has been studied extensively in recent years. Filament aggregation enables allosteric regulation, reducing sensitivity to feedback inhibition and ensuring the synthesis of guanine nucleotides for rapidly proliferating cells (Calise et al., 2016, 2018; Johnson & Kollman, 2020) Currently, it is known that several genes are associated with IMPDH2 filaments. Increased IMPDH2 expression has been observed in many cancers, but independent IMPDH2 assembly into filament structures has not been described in cancer cells (Calise & Chan, 2020; Shiyu et al., 2018).

The PIK3R1 fusion was associated with the induction of RR-like filament structures after cisplatin and trametinib exposure. Interestingly, these fusion structures did not colocalize with IMPDH2 or CTPS1 proteins. However, they were associated with CIN85, specifically the 47 kDa isoform of CIN85 containing an SH domain and proline-rich region. These corresponding domains were also present in the PIK3R1 fusion protein.

CIN85 could inhibit PIK3R1 fusion effects. Cells expressing the fusion consistently showed ERK1/2 activation, boosting the malignant phenotype. Additionally, under standard culture conditions, the fusion-expressing cells displayed proliferation similar to the control cells. However, when exposed to cisplatin, which is known to induce ERK1/2 activation, the effect might have been too much for the cells, considering the fusion itself already promoted ERK1/2 activation. As a result, fusion cells may have started expressing CIN85 to inhibit the fusion and its effects. The presence of the smaller CIN85 isoform enabled the cells to respond faster to environmental changes, such as cisplatin treatment. During cisplatin treatment, fusion cells neither proliferated nor underwent cell death, but instead, they entered a cell cycle arrest-like state.

When ERK is activated in the cells, they would be expected to be sensitive to MEK inhibition (Cheung et al., 2014). Surprisingly, PIK3R1 fusion cells displayed significant resistance to trametinib, even though it reduced the expression of

ERK1/2, and these cells retained their proliferative ability. Upon trametinib treatment, fusion cells expressed RR-like structures, which were shorter and thinner compared to the structures induced by cisplatin. However, PIK3R1 fusion cells showed sensitivity to the combined treatment of cisplatin and trametinib, consistent with previous research. Our observations of the RR-like structures were confirmed in fusion overexpressing cell lines. Currently, there is no antibody to confirm the RR-like structure formation in the patient´s tissue sample.

We did not investigate the potential activation of the PI3K-AKT-mTOR signaling pathway when cells were treated with trametinib. It remains uncertain whether this pathway could be activated, leading to cell proliferation and resistance to trametinib through crosstalk between the PI3K-AKT-mTOR and RAS-MEK-ERK pathways.

RR-like structures could potentially serve as an advanced survival mechanism: their presence may be linked to the activation of survival pathways within cancer cells, enabling them to evade cell death induced by treatments. The precise mechanisms through which RR-like structures contribute to resistance in PIK3R1 fusion cells require further investigation.

7 Conclusions and future perspectives

This thesis concentrated on fusion gene detection and studying the functional role of the PIK3R1 fusion. Based on this thesis:

Fusion gene detection and validation (I)

1) Algorithm based fusion detection is a relevant method to discover and prioritize biologically appealing fusion events
2) Fusion genes are common in HGSC
3) Recurrent fusion events are rare in HGSC

Biological function of the PIK3R1-CCDC178 fusion (II)

4) *In vitro* analyses are needed to understand the functional role of novel fusion genes
5) The functional role of a gene fusion cannot be predicted based only on the fusion gene structure
6) Fusion genes can reveal susceptibility genes/regions and vulnerabilities of HGSC tumors providing novel therapeutic targets
7) Multidisciplinary research is required to understand the functions of fusion genes in HGSC progression and treatment resistance

Acknowledgements

The research detailed in this doctoral thesis was conducted at the Faculty of Medicine, Institute of Biomedicine, University of Turku.

I want to express my heartfelt gratitude to my supervisors, Professor Olli Carpén and Docent Kaisa Huhtinen, for providing me with this valuable opportunity. Kaisa, I want to convey my sincere gratitude for your consistent support and guidance throughout this journey. In particular, I would like to mention your contribution to promoting the experimental part of the first subproject and helping to receive the much-needed grants. Olli, I appreciate all your support and contribution during these years. Your feedback and unwavering encouragement propelled me to see this journey through.

My profound gratitude goes to Docent Vanina Dahlström-Heuser for imparting a wide array of cell culture and laboratory techniques and inspiring me with your constant stream of innovative ideas. I acknowledge Tiia Kähkönen, Milla Hollmén, Sofia Hakala, and Randa Mahran for contributing to the wet lab work. Regrettably, there were many occasions where our hard work resulted in disappointment. Nevertheless, I genuinely value your efforts and output. I also thank the Carpén/Huhtinen lab members, particularly Pia Roering, Peppi Alho, and Ph.D. Tarja Lamminen, for your support during the highs and lows of this endeavor.

During this project, I have been privileged to be part of the HERCULES/ DECIDER consortium. I want to thank Professor Sampsa Hautaniemi, Docent Rainer Lehtonen, Ph.D. Jaana Oikkonen and Ph.D. Taru Muranen from the University of Helsinki, and Ph.D. Alejandra Cervera from the National Institute of Genomic Medicine, Mexico, for their contribution and collaboration. Docent Johanna Hynninen from the Turku University Hospital, I want to thank you for your collaboration, advice, and support. Being part of this consortium, I have had the opportunity to meet experts from all over the world. I am delighted to have had the chance to learn from the bioinformatics professionals, Professor Elisa Ficarra, Ph.D. Marta Lovino, Elena Pianfetti, and Francesca Miccolis from the University of Modena and Reggio Emilia, Italy. I regret missing the opportunity to carry out the planned internship at your lab.

The experts from the Turku Proteomics Facility supported by Biocenter Finland are thanked for conducting the mass spectrometry analyses at the University of Turku and Åbo Akademi University. I want to acknowledge Professor Eeva-Liisa Eskelinen and Ph.D. Markus Peurla, for their advice in correlative light-electron microscopy experiments performed in the Electron Microscopy Laboratory at the University of Turku. I am grateful for Ph.D. Noora Andersson from the University of Helsinki and HUS Diagnostics, for performing the RNA *in situ* hybridization.

I want to thank Professor Pekka Taimen, Ph.D. Gun West, MD Kimmo Kettunen, and Ph.D. Laura Virtanen, for their support and company over the past years. Gun, thank you for helping me with the confocal microscopy and generously sharing your expertise. I also want to thank all the lovely people in Medisiina D5. The superb senior laboratory technicians, Jukka Karhu and Minna Santanen, your help with many laboratory issues is greatly appreciated.

I warmly thank Docent Leena Latonen and Ph.D. Caroline Heckman, for reviewing and improving this thesis. I also thank Professor Johanna Schleutker for her advice in the Follow-up Committee meetings.

I want to thank my family and friends for being there. I have been fortunate to always have someone to share thoughts with. Miran, I want to thank you for your unconditional love, support, and encouragement during this project. I also appreciate your role as my IT support. Frida, my beloved bundle of joy, "värityskirja" is finally completed.

This work would have been impossible without the working and expenditure grants. I am grateful for receiving funding from the Finnish Cultural Foundation, the Instrumentarium Science Foundation and the Doctoral School of Drug Research Doctoral Program (DRDP) of University of Turku.

Kuopio, October 2023
Heidi Rausio

References

Abul-Husn, N. S., Soper, E. R., Odgis, J. A., Cullina, S., Bobo, D., Moscati, A., Rodriguez, J. E., Loos, R. J. F., Cho, J. H., Belbin, G. M., Suckiel, S. A., & Kenny, E. E. (2019). Exome sequencing reveals a high prevalence of BRCA1 and BRCA2 founder variants in a diverse population-based biobank. *Genome Medicine*, *12*(1), 1–12. https://doi.org/10.1186/S13073-019-0691-1/TABLES/4

Alderden, R. A., Hall, M. D., Hambley, T. W., & Kauffman, G. B. (2006). Chemistry for Everyone The Discovery and Development of Cisplatin Products of Chemistry edited by. *Journal of Chemical Education*, *83*(5), 22. www.JCE.DivCHED.org

Amelio, I., & Melino, G. (2020). Context is everything: extrinsic signalling and gain-of-function p53 mutants. *Cell Death Discovery 2020 6:1*, *6*(1), 1–7. https://doi.org/10.1038/s41420-020-0251-x

Anastasiadou, E., Jacob, L. S., & Slack, F. J. (2017). Non-coding RNA networks in cancer. *Nature Reviews Cancer 2017 18:1*, *18*(1), 5–18. https://doi.org/10.1038/nrc.2017.99

Anduril. (2021). https://www.anduril.org

AOCS. (2017). http://www.aocstudy.org/

Atkin, N. B., & Baker, M. C. (1987). Abnormal chromosomes including small metacentrics in 14 ovarian cancers. *Cancer Genetics and Cytogenetics*, *26*(2), 355–361. https://doi.org/10.1016/0165-4608(87)90070-7

Aubrey, B. J., Kelly, G. L., Janic, A., Herold, M. J., & Strasser, A. (2017). How does p53 induce apoptosis and how does this relate to p53-mediated tumour suppression? *Cell Death & Differentiation 2018 25:1*, *25*(1), 104–113. https://doi.org/10.1038/cdd.2017.169

Aydin, H. A., Pestereli, E., Ozcan, M., Bayramoglu, Z., Erdogan, G., & Simsek, T. (2018). A study detection of the ROS1 gene fusion by FISH and ROS1 protein expression by IHC methods in patients with ovarian malignant or borderline serous tumors. *Pathology Research and Practice*, *214*(11), 1868–1872. https://doi.org/10.1016/J.PRP.2018.09.016

Barresi, V., Cosentini, I., Scuderi, C., Napoli, S., Di Bella, V., Spampinato, G., & Condorelli, D. F. (2019). Fusion Transcripts of Adjacent Genes: New Insights into the World of Human Complex Transcripts in Cancer. *International Journal of Molecular Sciences*, *20*(21). https://doi.org/10.3390/IJMS20215252

Bashashati, A., Ha, G., Tone, A., Ding, J., Prentice, L. M., Roth, A., Rosner, J., Shumansky, K., Kalloger, S., Senz, J., Yang, W., McConechy, M., Melnyk, N., Anglesio, M., Luk, M. T. Y., Tse, K., Zeng, T., Moore, R., Zhao, Y., … Shah, S. P. (2013). Distinct evolutionary trajectories of primary high-grade serous ovarian cancers revealed through spatial mutational profiling. *The Journal of Pathology*, *231*(1), 21. https://doi.org/10.1002/PATH.4230

Bell, D., Berchuck, A., Birrer, M., Chien, J., Cramer, D. W., Dao, F., Dhir, R., Disaia, P., Gabra, H., Glenn, P., Godwin, A. K., Gross, J., Hartmann, L., Huang, M., Huntsman, D. G., Iacocca, M., Imielinski, M., Kalloger, S., Karlan, B. Y., … Thomson, E. (2011). The Cancer Genome Atlas Research Network. Integrated genomic analyses of ovarian carcinoma. *Nature 2011 474:7353*, *474*(7353), 609–615. https://doi.org/10.1038/nature10166

Bell, Daphne. (2012). *PIK3R1 (phosphoinositide-3-kinase, regulatory subunit 1 (alpha))*. Atlas Genet Cytogenet Oncol Haematol. https://atlasgeneticsoncology.org/gene/41717/pik3r1-(phosphoinositide-3-kinase-regulatory-subunit-1-(alpha))

Bello, M. J., & Rey, J. A. (1990). CHROMOSOME ABERRATIONS IN METASTATIC OVARIAN CANCER: RELATIONSHIP WITH ABNORMALITIES IN PRIMARY TUMORS. *Int. J. Cancer*, *45*, 50–54. https://doi.org/10.1002/ijc.2910450111

Benedet, J. L., Bender, H., Jones, H., Ngan, H. Y., & Pecorelli, S. (2000). FIGO staging classifications and clinical practice guidelines in the management of gynecologic cancers. FIGO Committee on Gynecologic Oncology. *International Journal of Gynaecology and Obstetrics: The Official Organ of the International Federation of Gynaecology and Obstetrics*, *70*(2), 209–262. https://doi.org/10.1016/S0020-7292(00)90001-8

Bhat, K. P., & Cortez, D. (2018). RPA and RAD51: fork reversal, fork protection, and genome stability. *Nature Structural & Molecular Biology 2018 25:6*, *25*(6), 446–453. https://doi.org/10.1038/s41594-018-0075-z

Bijron, J. G., Seldenrijk, C. A., Zweemer, R. P., Lange, J. G., Verheijen, R. H. M., & Van Diest, P. J. (2013). Fallopian tube intraluminal tumor spread from noninvasive precursor lesions: A novel metastatic route in early pelvic carcinogenesis. *American Journal of Surgical Pathology*, *37*(8), 1123–1130. https://doi.org/10.1097/PAS.0B013E318282DA7F

Bitbucket. (2021). https://bitbucket.org/alejandra_cervera/fungi

Bourdon, J. C. (2007). p53 and its isoforms in cancer. *British Journal of Cancer 2007 97:3*, *97*(3), 277–282. https://doi.org/10.1038/sj.bjc.6603886

Bowtell, D. D. (2010). The genesis and evolution of high-grade serous ovarian cancer. *Nature Reviews Cancer 2010 10:11*, *10*(11), 803–808. https://doi.org/10.1038/nrc2946

Brachova, P., Thiel, K. W., & Leslie, K. K. (2013). The Consequence of Oncomorphic TP53 Mutations in Ovarian Cancer. *International Journal of Molecular Sciences 2013, Vol. 14, Pages 19257-19275*, *14*(9), 19257–19275. https://doi.org/10.3390/IJMS140919257

Brien, G. L., Stegmaier, K., & Armstrong, S. A. (2019). Targeting chromatin complexes in fusion protein-driven malignancies. *Nature Reviews Cancer 2019 19:5*, *19*(5), 255–269. https://doi.org/10.1038/s41568-019-0132-x

Brozovic, A., & Osmak, M. (2007). Activation of mitogen-activated protein kinases by cisplatin and their role in cisplatin-resistance. *Cancer Letters*, *251*(1), 1–16. https://doi.org/10.1016/J.CANLET.2006.10.007

Burotto, M., Chiou, V. L., Lee, J. M., & Kohn, E. C. (2014). The MAPK pathway across different malignancies: A new perspective. *Cancer*, *120*(22), 3446. https://doi.org/10.1002/CNCR.28864

Caetano-Anollés, D. (2013). Polymerase Chain Reaction. *Brenner's Encyclopedia of Genetics: Second Edition*, 392–395. https://doi.org/10.1016/B978-0-12-374984-0.01186-4

Calabrese, C., Davidson, N. R., Demircioamp, D., Fonseca, N. A., He, Y., Lehmann, K.-V., Liu, F., Shiraishi, Y., Soulette, C. M., Urban, L., Greger, L., Li, S., Liu, D., Perry, M. D., Xiang, Q., Zhang, F., Zhang, J., Bailey, P., Erkek, S., … von Mering, C. (2020). Genomic basis for RNA alterations in cancer. *Nature 2020 578:7793*, *578*(7793), 129–136. https://doi.org/10.1038/s41586-020-1970-0

Calise, S. J., Abboud, G., Kasahara, H., Morel, L., & Chan, E. K. L. (2018). Immune response-dependent assembly of IMP dehydrogenase filaments. *Frontiers in Immunology*, *9*(NOV). https://doi.org/10.3389/FIMMU.2018.02789

Calise, S. J., & Chan, E. K. L. (2020). Anti-rods/rings autoantibody and IMPDH filaments: an update after fifteen years of discovery. *Autoimmunity Reviews*, *19*(10). https://doi.org/10.1016/J.AUTREV.2020.102643

Calise, S. J., Purich, D. L., Nguyen, T., Saleem, D. A., Krueger, C., Yin, J. D., & Chan, E. K. L. (2016). "Rod and ring" formation from imp dehydrogenase is regulated through the one-carbon metabolic pathway. *Journal of Cell Science*, *129*(15), 3042–3052. https://doi.org/10.1242/JCS.183400

Carcamo, W. C., Satoh, M., Kasahara, H., Terada, N., Hamazaki, T., Chan, J. Y. F., Yao, B., Tamayo, S., Covini, G., von Mühlen, C. A., & Chan, E. K. L. (2011). Induction of Cytoplasmic Rods and Rings Structures by Inhibition of the CTP and GTP Synthetic Pathway in Mammalian Cells. *PLoS ONE*, *6*(12). https://doi.org/10.1371/JOURNAL.PONE.0029690

Cardillo, N., Devor, E. J., Pedra Nobre, S., Newtson, A., Leslie, K., Bender, D. P., Smith, B. J., Goodheart, M. J., & Gonzalez-Bosquet, J. (2022). Integrated Clinical and Genomic Models to Predict Optimal Cytoreduction in High-Grade Serous Ovarian Cancer. *Cancers*, *14*(14). https://doi.org/10.3390/CANCERS14143554/S1

Carrara, M., Beccuti, M., Lazzarato, F., Cavallo, F., Cordero, F., Donatelli, S., & Calogero, R. A. (2013). State-of-the-Art Fusion-Finder Algorithms Sensitivity and Specificity. *BioMed Research International*, *2013*. https://doi.org/10.1155/2013/340620

Cellosaurus OVCAR-8. (2023). https://www.cellosaurus.org/CVCL_1629

Cervera, A., Rausio, H., Kähkönen, T., Andersson, N., Partel, G., Rantanen, V., Paciello, G., Ficarra, E., Hynninen, J., Hietanen, S., Carpén, O., Lehtonen, R., Hautaniemi, S., & Huhtinen, K. (2021). FUNGI: FUsioN Gene Integration toolset. *Bioinformatics*, *37*(19), 3353. https://doi.org/10.1093/BIOINFORMATICS/BTAB206

Chen, B., Garmire, L., Calvisi, D. F., Chua, M. S., Kelley, R. K., & Chen, X. (2020). Harnessing big 'omics' data and AI for drug discovery in hepatocellular carcinoma. *Nature Reviews Gastroenterology & Hepatology 2019 17:4*, *17*(4), 238–251. https://doi.org/10.1038/s41575-019-0240-9

Chen, Z. H., Yu, Y. P., Tao, J., Liu, S., Tseng, G., Nalesnik, M., Hamilton, R., Bhargava, R., Nelson, J. B., Pennathur, A., Monga, S. P., Luketich, J. D., Michalopoulos, G. K., & Luo, J. H. (2017). MAN2A1–FER Fusion Gene is Expressed by Human Liver and Other Tumor Types and has Oncogenic Activity in Mice. *Gastroenterology*, *153*(4), 1120. https://doi.org/10.1053/J.GASTRO.2016.12.036

Chesnokov, M. S., Khan, I., Park, Y., Ezell, J., Mehta, G., Yousif, A., Hong, L. J., Buckanovich, R. J., Takahashi, A., & Chefetz, I. (2021). The MEK1/2 Pathway as a Therapeutic Target in High-Grade Serous Ovarian Carcinoma. *Cancers*, *13*(6), 1–20. https://doi.org/10.3390/cancers13061369

Cheung, L. W. T., Yu, S., Zhang, D., Li, J., Ng, P. K. S., Panupinthu, N., Mitra, S., Ju, Z., Yu, Q., Liang, H., Hawke, D. H., Lu, Y., Broaddus, R. R., & Mills, G. B. (2014). Naturally occurring neomorphic PIK3R1 mutations activate the MAPK pathway dictating therapeutic response to MAPK pathway inhibitors. *Cancer Cell*, *26*(4), 479. https://doi.org/10.1016/J.CCELL.2014.08.017

Christie, E. L., Pattnaik, S., Beach, J., Copeland, A., Rashoo, N., Fereday, S., Hendley, J., Alsop, K., Brady, S. L., Lamb, G., Pandey, A., DeFazio, A., Thorne, H., Bild, A., & Bowtell, D. D. L. (2019). Multiple ABCB1 transcriptional fusions in drug resistant high-grade serous ovarian and breast cancer. *Nature Communications*, *10*(1). https://doi.org/10.1038/s41467-019-09312-9

Chui, M. H., Chang, J. C., Zhang, Y., Zehir, A., Schram, A. M., Konner, J., Drilon, A. E., Paula, A. D. C., Weigelt, B., & Grisham, R. N. (2021). Spectrum of BRAF Mutations and Gene Rearrangements in Ovarian Serous Carcinoma. *JCO Precision Oncology*, *5*(5), 1480–1492. https://doi.org/10.1200/PO.21.00055

Chui, M. H., Momeni Boroujeni, A., Mandelker, D., Ladanyi, M., & Soslow, R. A. (2020). Characterization of TP53-wildtype tubo-ovarian high-grade serous carcinomas: rare exceptions to the binary classification of ovarian serous carcinoma. *Modern Pathology 2020 34:2*, *34*(2), 490–501. https://doi.org/10.1038/s41379-020-00648-y

Chwalenia, K., Facemire, L., & Li, H. (2017). Chimeric RNAs in cancer and normal physiology. *WIREs RNA*, *8*, 1427. https://doi.org/10.1002/wrna.1427

Coleman, R. L., Oza, A. M., Lorusso, D., Aghajanian, C., Oaknin, A., Dean, A., Colombo, N., Weberpals, J. I., Clamp, A., Scambia, G., Leary, A., Holloway, R. W., Gancedo, M. A., Fong, P. C., Goh, J. C., O'Malley, D. M., Armstrong, D. K., Garcia-Donas, J., Swisher, E. M., … Vulfovich, M. (2017). Rucaparib maintenance treatment for recurrent ovarian carcinoma after response to platinum therapy (ARIEL3): a randomised, double-blind, placebo-controlled, phase 3 trial. *Lancet (London, England)*, *390*(10106), 1949. https://doi.org/10.1016/S0140-6736(17)32440-6

Coltri, P. P., dos Santos, M. G. P., & da Silva, G. H. G. (2019). Splicing and cancer: Challenges and opportunities. *Wiley Interdisciplinary Reviews: RNA*, *10*(3), e1527. https://doi.org/10.1002/WRNA.1527

Cooke, S. L., & Brenton, J. D. (2011). Evolution of platinum resistance in high-grade serous ovarian cancer. *The Lancet Oncology*, *12*(12), 1169–1174. https://doi.org/10.1016/S1470-2045(11)70123-1

Covini, G., Carcamo, W. C., Bredi, E., Von Mühlen, C. A., Colombo, M., & Chan, E. K. L. (2012). Cytoplasmic rods and rings autoantibodies developed during pegylated interferon and ribavirin therapy in patients with chronic hepatitis C. *Antiviral Therapy*, *17*(5), 805–811. https://doi.org/10.3851/IMP1993

Craig, M. E., Sudanagunta, S., & Billow, M. (2023, July 24). *Anatomy, Abdomen and Pelvis: Broad Ligaments*. StatPearls; StatPearls Publishing. https://www.ncbi.nlm.nih.gov/books/NBK499943/

Dasari, S., & Bernard Tchounwou, P. (2014). Cisplatin in cancer therapy: molecular mechanisms of action. *European Journal of Pharmacology*, *740*, 364. https://doi.org/10.1016/J.EJPHAR.2014.07.025

De Bont, R., & van Larebeke, N. (2004). Endogenous DNA damage in humans: a review of quantitative data. *Mutagenesis*, *19*(3), 169–185. https://doi.org/10.1093/MUTAGE/GEH025

Decider Project. (2021). https://www.deciderproject.eu/

Deepak, S., Kottapalli, K., Rakwal, R., Oros, G., Rangappa, K., Iwahashi, H., Masuo, Y., & Agrawal, G. (2007). Real-Time PCR: Revolutionizing Detection and Expression Analysis of Genes. *Current Genomics*, *8*(4), 234. https://doi.org/10.2174/138920207781386960

Dorney, R., Dhungel, B. P., Rasko, J. E., Hebbard, L., & Schmitz Corresponding author Ulf Schmitz, U. (2023). Recent advances in cancer fusion transcript detection. *Briefings in Bioinformatics*, *24*(1), 1–12. https://doi.org/10.1093/bib/bbac519

Downward, J. (2008). Targeting RAS and PI3K in lung cancer. *Nature Medicine 2008 14:12*, *14*(12), 1315–1316. https://doi.org/10.1038/nm1208-1315

Du Bois, A., Neijt, J. P., & Thigpen, J. T. (1999). First line chemotherapy with carboplatin plus paclitaxel in advanced ovarian cancer - a new standard of care? *Annals of Oncology*, *10*(SUPPL. 1), S35–S41. https://doi.org/10.1016/S0923-7534(20)31482-4

Du Bois, Andreas, Lück, H. J., Meier, W., Adams, H. P., Möbus, V., Costa, S., Bauknecht, T., Richter, B., Warm, M., Schröder, W., Olbricht, S., Nitz, U., Jackisch, C., Emons, G., Wagner, U., Kuhn, W., Pfisterer, J., von Maillot, K., Lange, W., … Flachsenberg, S. (2003). A Randomized Clinical Trial of Cisplatin/Paclitaxel Versus Carboplatin/Paclitaxel as First-Line Treatment of Ovarian Cancer. *JNCI: Journal of the National Cancer Institute*, *95*(17), 1320–1329. https://doi.org/10.1093/JNCI/DJG036

Erkko, H., Xia, B., Nikkilä, J., Schleutker, J., Syrjäkoski, K., Mannermaa, A., Kallioniemi, A., Pylkäs, K., Karppinen, S. M., Rapakko, K., Miron, A., Sheng, Q., Li, G., Mattila, H., Bell, D. W., Haber, D. A., Grip, M., Reiman, M., Jukkola-Vuorinen, A., … Winqvist, R. (2007). A recurrent mutation in PALB2 in Finnish cancer families. *Nature 2006 446:7133*, *446*(7133), 316–319. https://doi.org/10.1038/nature05609

Evans, T., & Matulonis, U. (2017). PARP inhibitors in ovarian cancer: Evidence, experience and clinical potential. *Therapeutic Advances in Medical Oncology*, *9*(4), 253–267. https://doi.org/10.1177/1758834016687254

Ewels, P. A., Peltzer, A., Fillinger, S., Patel, H., Alneberg, J., Wilm, A., Garcia, M. U., Di Tommaso, P., & Nahnsen, S. (2020). The nf-core framework for community-curated bioinformatics pipelines. *Nature Biotechnology 2020 38:3*, *38*(3), 276–278. https://doi.org/10.1038/s41587-020-0439-x

Färkkilä, A., Rodríguez, A., Oikkonen, J., Gulhan, D. C., Nguyen, H., Domínguez, J., Ramos, S., Mills, C. E., Perez-Villatoro, F., Lazaro, J. B., Zhou, J., Clairmont, C. S., Moreau, L. A., Park, P. J., Sorger, P. K., Hautaniemi, S., Frias, S., & D'Andrea, A. D. (2021). Heterogeneity and clonal evolution of acquired PARP inhibitor resistance in TP53- And BRCA1-deficient cells. *Cancer Research*, *81*(10), 2774–2787. https://doi.org/10.1158/0008-5472.CAN-20-2912/654402/AM/HETEROGENEITY-AND-CLONAL-EVOLUTION-OF-ACQUIRED

Farmer, H., McCabe, H., Lord, C. J., Tutt, A. H. J., Johnson, D. A., Richardson, T. B., Santarosa, M., Dillon, K. J., Hickson, I., Knights, C., Martin, N. M. B., Jackson, S. P., Smith, G. C. M., &

Ashworth, A. (2005). Targeting the DNA repair defect in BRCA mutant cells as a therapeutic strategy. *Nature 2005 434:7035*, *434*(7035), 917–921. https://doi.org/10.1038/nature03445

Feng, Z., Shao, D., Cai, Y., Bi, R., Ju, X., Chen, D., Song, C., Chen, X., Li, J., An, N., Li, Y., Zhou, Q., Xiu, Z., Zhu, S., Wu, X., & Wen, H. (2023). Homologous recombination deficiency status predicts response to platinum-based chemotherapy in Chinese patients with high-grade serous ovarian carcinoma. *Journal of Ovarian Research*, *16*(1), 53. https://doi.org/10.1186/S13048-023-01129-X

Fernandez-Banet, J., Esposito, A., Coffin, S., Horvath, I. B., Estrella, H., Schefzick, S., Deng, S., Wang, K., Aching, K., Ding, Y., Roberts, P., Rejto, P. A., & Kan, Z. (2015). OASIS: web-based platform for exploring cancer multi-omics data. *Nature Methods 2016 13:1*, *13*(1), 9–10. https://doi.org/10.1038/nmeth.3692

Finnish Cancer Registry. (2020). https://syoparekisteri.fi/

Freed-Pastor, W. A., & Prives, C. (2012). Mutant p53: one name, many proteins. *Genes & Development*, *26*(12), 1268–1286. https://doi.org/10.1101/GAD.190678.112

Friedman, L. S., Ostermeyer, E. A., Szabo, C. I., Dowd, P., Lynch, E. D., Rowell, S. E., & King, M. C. (1994). Confirmation of BRCA1 by analysis of germline mutations linked to breast and ovarian cancer in ten families. *Nature Genetics 1994 8:4*, *8*(4), 399–404. https://doi.org/10.1038/ng1294-399

Garsed, D. W., Pandey, A., Fereday, S., Kennedy, C. J., Takahashi, K., Alsop, K., Hamilton, P. T., Hendley, J., Chiew, Y. E., Traficante, N., Provan, P., Ariyaratne, D., Au-Yeung, G., Bateman, N. W., Bowes, L., Brand, A., Christie, E. L., Cunningham, J. M., Friedlander, M., … Bowtell, D. D. L. (2022). The genomic and immune landscape of long-term survivors of high-grade serous ovarian cancer. *Nature Genetics 2022 54:12*, *54*(12), 1853–1864. https://doi.org/10.1038/s41588-022-01230-9

Ghosh, S. (2019). Cisplatin: The first metal based anticancer drug. *Bioorganic Chemistry*, *88*, 102925. https://doi.org/10.1016/J.BIOORG.2019.102925

Goodwin, S., McPherson, J. D., & McCombie, W. R. (2016). Coming of age: ten years of next-generation sequencing technologies. *Nature Reviews Genetics 2016 17:6*, *17*(6), 333–351. https://doi.org/10.1038/nrg.2016.49

Guile, S. L., & Mathai, J. K. (2023). Ovarian Torsion. *Pediatric Surgery: Diagnosis and Treatment*, 773–788. https://doi.org/10.1007/978-3-030-96542-6_68

Gurney, H., Crowther, D., Anderson, H., Murphy, D., Prendiville, J., Ranson, M., Mayor, P., Swindell, R., Buckley, C. H., & Tindall, V. R. (1990). Original article: Five year follow-up and dose delivery analysis of cisplatin, iproplatin or carboplatin in combination with cyclophosphamide in advanced ovarian carcinoma. *Annals of Oncology*, *1*(6), 427–433. https://doi.org/10.1093/OXFORDJOURNALS.ANNONC.A057796

Hanahan, D. (2022). Hallmarks of Cancer: New Dimensions. *Cancer Discovery*, *12*(1), 31–46. https://doi.org/10.1158/2159-8290.CD-21-1059

Haupt, Y., Maya, R., & Kazaz, A. (1997). Mdm2 promotes the rapid degradation of p53. *Nature*, *387*, 296–299. https://doi.org/https://doi.org/10.1038/387296a0

Heisterkamp·, N., Stephenson·, J. R., Groffen·, J., Hansent, P. F., De Klein, A., Bartram, C. R., & Grosveld, G. (1983). Localization of the c-abl oncogene adjacent to a translocation break point in chronic myelocytic leukaemia. *NATURE*, *306*, 239–242.

Helleday, T., Petermann, E., Lundin, C., Hodgson, B., & Sharma, R. A. (2008). DNA repair pathways as targets for cancer therapy. *Nature Reviews Cancer 2008 8:3*, *8*(3), 193–204. https://doi.org/10.1038/nrc2342

Hendrikse, C. S. E., Theelen, P. M. M., van der Ploeg, P., Westgeest, H. M., Boere, I. A., Thijs, A. M. J., Ottevanger, P. B., van de Stolpe, A., Lambrechts, S., Bekkers, R. L. M., & Piek, J. M. J. (2023). The potential of RAS/RAF/MEK/ERK (MAPK) signaling pathway inhibitors in ovarian cancer: A systematic review and meta-analysis. *Gynecologic Oncology*, *171*, 83–94. https://doi.org/10.1016/j.ygyno.2023.01.038

Ho, G. Y., Woodward, N., & Coward, J. I. G. (2016). Cisplatin versus carboplatin: comparative review of therapeutic management in solid malignancies. *Critical Reviews in Oncology/Hematology*, *102*, 37–46. https://doi.org/10.1016/J.CRITREVONC.2016.03.014

Holland, A. J., & Cleveland, D. W. (2012). Chromoanagenesis and cancer: mechanisms and consequences of localized, complex chromosomal rearrangements. *Nature Medicine 2012 18:11*, *18*(11), 1630–1638. https://doi.org/10.1038/nm.2988

Hou, S. Q., Ouyang, M., Brandmaier, A., Hao, H., & Shen, W. H. (2017). PTEN in the maintenance of genome integrity: From DNA replication to chromosome segregation. *BioEssays : News and Reviews in Molecular, Cellular and Developmental Biology*, *39*(10). https://doi.org/10.1002/BIES.201700082

Houseley, J., & Tollervey, D. (2010). Apparent Non-Canonical Trans-Splicing Is Generated by Reverse Transcriptase In Vitro. *PLOS ONE*, *5*(8), e12271. https://doi.org/10.1371/JOURNAL.PONE.0012271

Huang, H., & Chen, J. (2017). Chromosome bandings. *Methods in Molecular Biology*, *1541*, 59–66. https://doi.org/10.1007/978-1-4939-6703-2_6/FIGURES/3

Jalali, M., Zaborowska, J., & Jalali, M. (2017). The Polymerase Chain Reaction: PCR, qPCR, and RT-PCR. *Basic Science Methods for Clinical Researchers*, 1–18. https://doi.org/10.1016/B978-0-12-803077-6.00001-1

Jazaeri, A. A., Bryant, J. L., Park, H., Li, H., Dahiya, N., Stoler, M. H., Ferriss, J. S., & Dutta, A. (2011). Molecular Requirements for Transformation of Fallopian Tube Epithelial Cells into Serous Carcinoma. *Neoplasia (New York, N.Y.)*, *13*(10), 899–911. https://doi.org/10.1593/NEO.11138

Jia, Y., Xie, Z., & Li, H. (2016). Intergenically Spliced Chimeric RNAs in Cancer. *Trends in Cancer*, *2*(9), 475–484. https://doi.org/10.1016/j.trecan.2016.07.006

Johnson, M. C., & Kollman, J. M. (2020). Cryo-EM structures demonstrate human IMPDH2 filament assembly tunes allosteric regulation. *ELife*, *9*. https://doi.org/10.7554/ELIFE.53243

Kang, M., Chong, K. Y., Hartwich, T. M. P., Bi, F., Witham, A. K., Patrick, D., Morrisson, M. J., Cady, S. L., Cerchia, A. P., Kelk, D., Liu, Y., Nucci, J., Madarikan, O., Ueno, D., Shuch, B. M., & Yang-Hartwich, Y. (2020). Ovarian BDNF promotes survival, migration, and attachment of tumor precursors originated from p53 mutant fallopian tube epithelial cells. *Oncogenesis 2020 9:5*, *9*(5), 1–15. https://doi.org/10.1038/s41389-020-0243-y

Kannan, K., Coarfa, C., Chao, P. W., Luo, L., Wang, Y., Brinegar, A. E., Hawkins, S. M., Milosavljevic, A., Matzuk, M. M., & Yen, L. (2015). Recurrent BCAM-AKT2 fusion gene leads to a constitutively activated AKT2 fusion kinase in high-grade serous ovarian carcinoma. *Proceedings of the National Academy of Sciences of the United States of America*, *112*(11), E1272–E1277. https://doi.org/10.1073/PNAS.1501735112/-/DCSUPPLEMENTAL

Kannan, K., Coarfa, C., Rajapakshe, K., Hawkins, S. M., Matzuk, M. M., Milosavljevic, A., & Yen, L. (2014). CDKN2D-WDFY2 Is a Cancer-Specific Fusion Gene Recurrent in High-Grade Serous Ovarian Carcinoma. *PLoS Genetics*, *10*(3). https://doi.org/10.1371/journal.pgen.1004216

Kannan, K., Kordestani, G. K., Galagoda, A., Coarfa, C., & Yen, L. (2015). Aberrant MUC1-TRIM46-KRTCAP2 Chimeric RNAs in High-Grade Serous Ovarian Carcinoma. *Cancers*, *7*(4), 2083. https://doi.org/10.3390/CANCERS7040878

Karst, A. M., & Drapkin, R. (2010). Ovarian Cancer Pathogenesis: A Model in Evolution. *Journal of Oncology*, *2010*, 1–13. https://doi.org/10.1155/2010/932371

Kelland, L. (2007). The resurgence of platinum-based cancer chemotherapy. *Nature Reviews Cancer 2007 7:8*, *7*(8), 573–584. https://doi.org/10.1038/nrc2167

Kielbik, M., Krzyzanowski, D., Pawlik, B., Klink, M., Kielbik, M., Krzyzanowski, D., Pawlik, B., & Klink, M. (2018). Cisplatin-induced ERK1/2 activity promotes G1 to S phase progression which leads to chemoresistance of ovarian cancer cells. *Oncotarget*, *9*(28), 19847–19860. https://doi.org/10.18632/ONCOTARGET.24884

Kim, J., Park, E. Y., Kim, O., Schilder, J. M., Coffey, D. M., Cho, C. H., & Bast, R. C. (2018). Cell Origins of High-Grade Serous Ovarian Cancer. *Cancers*, *10*(11), 433. https://doi.org/10.3390/CANCERS10110433

Kindelberger, D. W., Lee, Y., Miron, A., Hirsch, M. S., Feltmate, C., Medeiros, F., Callahan, M. J., Garner, E. O., Gordon, R. W., Birch, C., Berkowitz, R. S., Muto, M. G., & Crum, C. P. (2007). Intraepithelial carcinoma of the fimbria and pelvic serous carcinoma: Evidence for a causal relationship. *American Journal of Surgical Pathology*, *31*(2), 161–169. https://doi.org/10.1097/01.PAS.0000213335.40358.47

Krejci, L., Altmannova, V., Spirek, M., & Zhao, X. (2012). Homologous recombination and its regulation. *Nucleic Acids Research*, *40*(13), 5795–5818. https://doi.org/10.1093/NAR/GKS270

Kubbutat, M., Jones, S., & Vousden, K. (1997). Regulation of p53 stability by Mdm2. *Nature*, *387*, 299–303. https://doi.org/https://doi.org/10.1038/387299a0

Kurman, R. J., & Shih, I. M. (2016). The dualistic model of ovarian carcinogenesis revisited, revised, and expanded. *American Journal of Pathology*, *186*(4), 733–747. https://doi.org/10.1016/J.AJPATH.2015.11.011

Kusyk, C. J., Turpening, E. L., Edwards, C. L., Taylor Wharton, J., & Copeland, L. J. (1982). Karyotype Analysis of Four Solid Gynecologic Tumors'. *GYNECOLOGIC ONCOLOGY*, *14*, 324–338.

Kuusisto, K. M., Bebel, A., Vihinen, M., Schleutker, J., & Sallinen, S. L. (2011). Screening for BRCA1, BRCA2, CHEK2, PALB2, BRIP1, RAD50, and CDH1 mutations in high-risk Finnish BRCA1/2-founder mutation-negative breast and/or ovarian cancer individuals. *Breast Cancer Research : BCR*, *13*(1), R20. https://doi.org/10.1186/BCR2832

Lastair, A., Ood, J. J. W., Owinsky, R. K. R., Oss, R., & Onehower, C. D. (1995). Paclitaxel (Taxol). *Https://Doi.Org/10.1056/NEJM199504133321507*, *135*(12), 393–396. https://doi.org/10.1056/NEJM199504133321507

Latysheva, N. S., & Babu, M. M. (2016). Discovering and understanding oncogenic gene fusions through data intensive computational approaches. *Nucleic Acids Research*, *44*(10), 4487. https://doi.org/10.1093/NAR/GKW282

Lei, Q., Li, C., Zuo, Z., Huang, C., Cheng, H., & Zhou, R. (2016). Evolutionary Insights into RNA trans-Splicing in Vertebrates. *Genome Biology and Evolution*, *8*(3), 562. https://doi.org/10.1093/GBE/EVW025

Li, H., Wang, J., Mor, G., & Sklar, J. (2008). A neoplastic gene fusion mimics trans-splicing of RNAs in normal human cells. *Science*, *321*(5894), 1357–1361. https://doi.org/10.1126/SCIENCE.1156725/SUPPL_FILE/LI.SOM.PDF

Li, Z., Zhou, W., Zhang, Y., Sun, W., Yung, M. M. H., Sun, J., Li, J., Chen, C. W., Li, Z., Meng, Y., Chai, J., Zhou, Y., Liu, S. S., Cheung, A. N. Y., Ngan, H. Y. S., Chan, D. W., Zheng, W., & Zhu, W. (2019). ERK regulates HIF-1α-mediated platinum resistance by directly targeting PHD2 in ovarian cancer. *Clinical Cancer Research : An Official Journal of the American Association for Cancer Research*, *25*(19), 5947. https://doi.org/10.1158/1078-0432.CCR-18-4145

Lisio, M. A., Fu, L., Goyeneche, A., Gao, Z. H., & Telleria, C. (2019). High-Grade Serous Ovarian Cancer: Basic Sciences, Clinical and Therapeutic Standpoints. *International Journal of Molecular Sciences 2019, Vol. 20, Page 952*, *20*(4), 952. https://doi.org/10.3390/IJMS20040952

Liu, H., Jia, S., Guo, K., & Li, R. (2022). INK4 cyclin-dependent kinase inhibitors as potential prognostic biomarkers and therapeutic targets in hepatocellular carcinoma. *Bioscience Reports*, *42*(7), 20221082. https://doi.org/10.1042/BSR20221082

Liu, P., Cheng, H., Roberts, T. M., & Zhao, J. J. (2009). Targeting the phosphoinositide 3-kinase pathway in cancer. *Nature Publishing Group*, *8*(8), 627–644. https://doi.org/10.1038/nrd2926

Liu, T., & Huang, J. (2016). DNA End Resection: Facts and Mechanisms. *Genomics, Proteomics & Bioinformatics*, *14*(3), 126. https://doi.org/10.1016/J.GPB.2016.05.002

Lou, D. I., McBee, R. M., Sawyer, S. L., Hussmann, J. A., Press, W. H., Acevedo, A., & Andino, R. (2013). High-Throughput dna sequencing errors are reduced by orders of magnitude using circle sequencing. *Proceedings of the National Academy of Sciences of the United States of America*, *110*(49), 19872–19877. https://doi.org/10.1073/PNAS.1319590110/SUPPL_FILE/PNAS.201319590SI.PDF

Lovatt, D., & Eberwine, J. (2013). Northern Blotting. *Brenner's Encyclopedia of Genetics: Second Edition*, 105–107. https://doi.org/10.1016/B978-0-12-374984-0.01065-2

Lu, B., Jiang, R., Xie, B., Wu, W., & Zhao, Y. (2021). Fusion genes in gynecologic tumors: the occurrence, molecular mechanism and prospect for therapy. *Cell Death & Disease 2021 12:8*, *12*(8), 1–11. https://doi.org/10.1038/s41419-021-04065-0

Maki, C. G., & Howley, P. M. (1997). Ubiquitination of p53 and p21 is differentially affected by ionizing and UV radiation. *Molecular and Cellular Biology*, *17*(1), 355–363. https://doi.org/10.1128/MCB.17.1.355

Maltzman, W., & Czyzyk, L. (1984). UV irradiation stimulates levels of p53 cellular tumor antigen in nontransformed mouse cells. *Molecular and Cellular Biology*, *4*(9), 1689–1694. https://doi.org/10.1128/MCB.4.9.1689-1694.1984

Mark, J., Dahlenfors, R., Ekedahl, C., & Stenman, G. (1980). The mixed salivary gland tumor — A normally benign human neoplasm frequently showing specific chromosomal abnormalities. *Cancer Genetics and Cytogenetics*, *2*(3), 231–241. https://doi.org/10.1016/0165-4608(80)90030-8

Markman, M. (2003). Optimizing primary chemotherapy in ovarian cancer. *Hematology/Oncology Clinics of North America*, *17*(4), 957–968. https://doi.org/10.1016/S0889-8588(03)00058-3

McGuire, W. P., Hoskins, W. J., Brady, M. F., Kucera, P. R., Partridge, E. E., Look, K. Y., Clarke-Pearson, D. L., & Davidson, M. (1996). Cyclophosphamide and Cisplatin Compared with Paclitaxel and Cisplatin in Patients with Stage III and Stage IV Ovarian Cancer. *Https://Doi.Org/10.1056/NEJM199601043340101*, *334*(1), 1–6. https://doi.org/10.1056/NEJM199601043340101

McPherson, A., Hormozdiari, F., Zayed, A., Giuliany, R., Ha, G., Sun, M. G. F., Griffith, M., Moussavi, A., Senz, J., Melnyk, N., Pacheco, M., Marra, M. A., Hirst, M., Nielsen, T. O., Sahinalp, S. C., Huntsman, D., & Shah, S. P. (2011). deFuse: An Algorithm for Gene Fusion Discovery in Tumor RNA-Seq Data. *PLoS Computational Biology*, *7*(5), 1001138. https://doi.org/10.1371/JOURNAL.PCBI.1001138

Mertens, F., Johansson, B., Fioretos, T., & Mitelman, F. (2015). The emerging complexity of gene fusions in cancer. *Nature Reviews Cancer 2015 15:6*, *15*(6), 371–381. https://doi.org/10.1038/nrc3947

Meyerson, M., Gabriel, S., & Getz, G. (2010). Advances in understanding cancer genomes through second-generation sequencing. *Nature Reviews Genetics 2010 11:10*, *11*(10), 685–696. https://doi.org/10.1038/nrg2841

Mirza, M. R., Monk, B. J., Herrstedt, J., Oza, A. M., Mahner, S., Redondo, A., Fabbro, M., Ledermann, J. A., Lorusso, D., Vergote, I., Ben-Baruch, N. E., Marth, C., Mądry, R., Christensen, R. D., Berek, J. S., Dørum, A., Tinker, A. V., du Bois, A., González-Martín, A., … Matulonis, U. A. (2016). Niraparib Maintenance Therapy in Platinum-Sensitive, Recurrent Ovarian Cancer. *New England Journal of Medicine*, *375*(22), 2154–2164. https://doi.org/10.1056/NEJMOA1611310/SUPPL_FILE/NEJMOA1611310_DISCLOSURES.PDF

Mitelman, F., Johansson, B., & Mertens, F. (2007). The impact of translocations and gene fusions on cancer causation. *Nature Reviews Cancer 2007 7:4*, *7*(4), 233–245. https://doi.org/10.1038/nrc2091

Moriya, T. (2018). *Pathology of Female Cancers: Precursor and Early-Stage Breast, Ovarian and Uterine Carcinomas* [Book]. Springer Singapore Pte. Limited. https://doi.org/10.1007/978-981-10-8606-9

Mottini, C., Napolitano, F., Li, Z., Gao, X., & Cardone, L. (2021). Computer-aided drug repurposing for cancer therapy: Approaches and opportunities to challenge anticancer targets. *Seminars in Cancer Biology*, *68*, 59–74. https://doi.org/10.1016/J.SEMCANCER.2019.09.023

Mukherjee, S., Sunanda, |, Mukherjee, B., & Frenkel-Morgenstern, M. (2023). Functional and regulatory impact of chimeric RNAs in human normal and cancer cells cancer, chimeric RNA, drug-resistance, precision medicine, sense-antisense chimeric RNA. *WIREs RNA*. https://doi.org/10.1002/wrna.1777

Mutch, D. G., & Prat, J. (2014). 2014 FIGO staging for ovarian, fallopian tube and peritoneal cancer. *Gynecologic Oncology*, *133*(3), 401–404. https://doi.org/10.1016/J.YGYNO.2014.04.013

Na, K., Sung, J. Y., & Kim, H. S. (2017). TP53 Mutation Status of Tubo-ovarian and Peritoneal High-grade Serous Carcinoma with a Wild-type p53 Immunostaining Pattern. *Anticancer Research*, *37*(12), 6697–6703. https://doi.org/10.21873/ANTICANRES.12128

Nadhan, R., Isidoro, C., Song, Y. S., & Dhanasekaran, D. N. (2022). Signaling by LncRNAs: Structure, Cellular Homeostasis, and Disease Pathology. *Cells*, *11*(16). https://doi.org/10.3390/CELLS11162517

Nagasawa, S., Ikeda, K., Shintani, D., Yang, C., Takeda, S., Hasegawa, K., Horie, K., & Inoue, S. (2022). Identification of a Novel Oncogenic Fusion Gene SPON1-TRIM29 in Clinical Ovarian Cancer That Promotes Cell and Tumor Growth and Enhances Chemoresistance in A2780 Cells. *International Journal of Molecular Sciences*, *23*(2). https://doi.org/10.3390/IJMS23020689/S1

Namba, S., Ueno, T., Kojima, S., Kobayashi, K., Kawase, K., Tanaka, Y., Inoue, S., Kishigami, F., Kawashima, S., Maeda, N., Ogawa, T., Hazama, S., Togashi, Y., Ando, M., Shiraishi, Y., Mano, H., & Kawazu, M. (2021). Transcript-targeted analysis reveals isoform alterations and double-hop fusions in breast cancer. *Communications Biology 2021 4:1*, *4*(1), 1–16. https://doi.org/10.1038/s42003-021-02833-4

Nattestad, M., Goodwin, S., Ng, K., Baslan, T., Sedlazeck, F. J., Rescheneder, P., Garvin, T., Fang, H., Gurtowski, J., Hutton, E., Tseng, E., Chin, C. S., Beck, T., Sundaravadanam, Y., Kramer, M., Antoniou, E., McPherson, J. D., Hicks, J., Richard McCombie, W., & Schatz, M. C. (2018). Complex rearrangements and oncogene amplifications revealed by long-read DNA and RNA sequencing of a breast cancer cell line. *Genome Research*, *28*(8), 1126–1135. https://doi.org/10.1101/GR.231100.117/-/DC1

NCI. (2017). *Many Ovarian Cancers May Start in Fallopian Tubes - NCI*. National Cancer Institute. https://www.cancer.gov/news-events/cancer-currents-blog/2017/ovarian-cancer-fallopian-tube-origins

Nero, C., Vizzielli, G., Lorusso, D., Cesari, E., Daniele, G., Loverro, M., Scambia, G., & Sette, C. (2021). Patient-derived organoids and high grade serous ovarian cancer: from disease modeling to personalized medicine. *Journal of Experimental & Clinical Cancer Research*, *40*(116). https://doi.org/10.1186/s13046-021-01917-7

Nesic, K., Wakefield, M., Kondrashova, O., Scott, C. L., & McNeish, I. A. (2018). Targeting DNA repair: the genome as a potential biomarker. *The Journal of Pathology*, *244*(5), 586–597. https://doi.org/10.1002/PATH.5025

Ng, A., & Barker, N. (2015). Ovary and fimbrial stem cells: biology, niche and cancer origins. *Nature Reviews Molecular Cell Biology*, *16*(10), 625–638. https://doi.org/10.1038/nrm4056

Nowak-Sliwinska, P., Scapozza, L., & Altaba, A. R. i. (2019). Drug repurposing in oncology: Compounds, pathways, phenotypes and computational approaches for colorectal cancer. *Biochimica et Biophysica Acta. Reviews on Cancer*, *1871*(2), 434. https://doi.org/10.1016/J.BBCAN.2019.04.005

Nowell, P. C., & Hungerford, D. A. (1960). Chromosome Studies on Normal and Leukemic Human Leukocytes. *JNCI: Journal of the National Cancer Institute*, *25*(1), 85–109. https://doi.org/10.1093/JNCI/25.1.85

Nurmi, A., Muranen, T. A., Pelttari, L. M., Kiiski, J. I., Heikkinen, T., Lehto, S., Kallioniemi, A., Schleutker, J., Bützow, R., Blomqvist, C., Aittomäki, K., & Nevanlinna, H. (2019). Recurrent moderate-risk mutations in Finnish breast and ovarian cancer patients. *International Journal of Cancer*, *145*(10), 2692. https://doi.org/10.1002/ijc.32309

Ortega, S., Malumbres, M., & Barbacid, M. (2002). Cyclin D-dependent kinases, INK4 inhibitors and cancer. *Biochimica et Biophysica Acta (BBA) - Reviews on Cancer*, *1602*(1), 73–87. https://doi.org/10.1016/S0304-419X(02)00037-9

Panigrahi, P., Jere, A., & Anamika, K. (2018). FusionHub: A unified web platform for annotation and visualization of gene fusion events in human cancer. *PLoS ONE*, *13*(5). https://doi.org/10.1371/JOURNAL.PONE.0196588

Pareek, V., Pedley, A. M., & Benkovic, S. J. (2021). Human de novo Purine Biosynthesis. *Critical Reviews in Biochemistry and Molecular Biology*, *56*(1), 1. https://doi.org/10.1080/10409238.2020.1832438

Parker, B. C., & Zhang, W. (2013). Fusion genes in solid tumors: an emerging target for cancer diagnosis and treatment. *Chinese Journal of Cancer*, *32*(11), 594. https://doi.org/10.5732/CJC.013.10178

Parmar, M. K. B., Adams, M., Balestrino, M., Bertelsen, K., Bonazzi, C., Calvert, H., Colombo, N., Delaloye, J. F., Durando, A., Guthrie, D., Hagen, B., Harper, P., Mangioni, C., Perren, T., Poole, C., Qian, W., Rustin, G., Sandercock, J., Tumolo, S., … Grazia-Valsecchi, M. (2002). Paclitaxel plus carboplatin versus standard chemotherapy with either single-agent carboplatin or cyclophosphamide, doxorubicin, and cisplatin in women with ovarian cancer: The ICON3 randomised trial. *Lancet*, *360*(9332), 505–515. https://doi.org/10.1016/S0140-6736(02)09738-6

Patch, A. M., Christie, E. L., Etemadmoghadam, D., Garsed, D. W., George, J., Fereday, S., Nones, K., Cowin, P., Alsop, K., Bailey, P. J., Kassahn, K. S., Newell, F., Quinn, M. C. J., Kazakoff, S., Quek, K., Wilhelm-Benartzi, C., Curry, E., Leong, H. S., Hamilton, A., … Bowtell, D. D. L. (2015). Whole–genome characterization of chemoresistant ovarian cancer. *Nature 2015 521:7553*, *521*(7553), 489–494. https://doi.org/10.1038/nature14410

Pederzoli, F., Bandini, M., Marandino, L., Ali, S. M., Madison, R., Chung, J., Ross, J. S., & Necchi, A. (2020). Targetable gene fusions and aberrations in genitourinary oncology. *Nature Reviews Urology 2020 17:11*, *17*(11), 613–625. https://doi.org/10.1038/s41585-020-00379-4

Pennington, K. P., Walsh, T., Harrell, M. I., Lee, M. K., Pennil, C. C., Rendi, M. H., Thornton, A., Norquist, B. M., Casadei, S., Nord, A. S., Agnew, K. J., Pritchard, C. C., Scroggins, S., Garcia, R. L., King, M. C., & Swisher, E. M. (2014). Germline and somatic mutations in homologous recombination genes predict platinum response and survival in ovarian, fallopian tube, and peritoneal carcinomas. *Clinical Cancer Research*, *20*(3), 764–775. https://doi.org/10.1158/1078-0432.CCR-13-2287/85977/AM/GERMLINE-AND-SOMATIC-MUTATIONS-IN-HOMOLOGOUS

Permuth-Wey, J., Chen, Y. A., Tsai, Y. Y., Chen, Z., Qu, X., Lancaster, J. M., Stockwell, H., Dagne, G., Iversen, E., Risch, H., Barnholtz-Sloan, J., Cunningham, J. M., Vierkant, R. A., Fridley, B. L., Sutphen, R., McLaughlin, J., Narod, S. A., Goode, E. L., Schildkraut, J. M., … Sellers, T. A. (2011). Inherited Variants in Mitochondrial Biogenesis Genes May Influence Epithelial Ovarian Cancer Risk. *Cancer Epidemiology, Biomarkers & Prevention : A Publication of the American Association for Cancer Research, Cosponsored by the American Society of Preventive Oncology*, *20*(6), 1131. https://doi.org/10.1158/1055-9965.EPI-10-1224

Petrović, M., & Todorović, D. (2016). BIOCHEMICAL AND MOLECULAR MECHANISMS OF ACTION OF CISPLATIN IN CANCER CELLS. *Facta Universitatis, Series: Medicine and Biology*, *18*(1), 12–18. http://casopisi.junis.ni.ac.rs/index.php/FUMedBiol/article/view/1730

Piek, J. M. J., Van Diest, P. J., Zweemer, R. P., Jansen, J. W., Poort-Keesom, R. J. J., Menko, F. H., Gille, J. J. P., Jongsma, A. P. M., Pals, G., Kenemans, P., & Verheijen, R. H. M. (2001). Dysplastic changes in prophylactically removed Fallopian tubes of women predisposed to developing ovarian cancer. *The Journal of Pathology*, *195*(4), 451–456. https://doi.org/10.1002/PATH.1000

Pujade-Lauraine, E., Ledermann, J. A., Selle, F., Gebski, V., Penson, R. T., Oza, A. M., Korach, J., Huzarski, T., Poveda, A., Pignata, S., Friedlander, M., Colombo, N., Harter, P., Fujiwara, K., Ray-Coquard, I. L., Banerjee, S., Liu, J., Lowe, E. S., Bloomfield, R., … Vergote, I. (2017). Olaparib tablets as maintenance therapy in patients with platinum-sensitive, relapsed ovarian cancer and a BRCA1/2 mutation (SOLO2/ENGOT-Ov21): a double-blind, randomised, placebo-controlled, phase 3 trial. *The Lancet Oncology*, *18*(9), 1274–1284. https://doi.org/10.1016/S1470-2045(17)30469-2

Quartuccio, S. M., Karthikeyan, S., Eddie, S. L., Lantvit, D. D., Hainmhire, E. O., Modi, D. A., Wei, J. J., & Burdette, J. E. (2015). Mutant p53 expression in fallopian tube epithelium drives cell migration. *International Journal of Cancer*, *137*(7), 1528–1538. https://doi.org/10.1002/IJC.29528

Ren, R. (2005). Mechanisms of BCR–ABL in the pathogenesis of chronic myelogenous leukaemia. *Nature Reviews Cancer 2005 5:3*, *5*(3), 172–183. https://doi.org/10.1038/nrc1567

Rigby, C. H., Aljassim, F., Powell, S. G., Wyatt, J. N. R., Hill, C. J., & Hapangama, D. K. (2022). The immune cell profile of human fallopian tubes in health and benign pathology: a systematic review. *Journal of Reproductive Immunology*, *152*, 103646. https://doi.org/10.1016/J.JRI.2022.103646

Rinne, N., Christie, E. L., Ardasheva, A., Kwok, C. H., Demchenko, N., Low, C., Tralau-Stewart, C., Fotopoulou, C., & Cunnea, P. (2021). Targeting the PI3K/AKT/mTOR pathway in epithelial ovarian cancer, therapeutic treatment options for platinum-resistant ovarian cancer. *Cancer Drug Resistance*, *4*(3), 573. https://doi.org/10.20517/CDR.2021.05

Rosner, J., Samardzic, T., & Sarao, M. S. (2022). Physiology, Female Reproduction. *StatPearls*. https://www.ncbi.nlm.nih.gov/books/NBK537132/

Rowley, J. D. (1973). A New Consistent Chromosomal Abnormality in Chronic Myelogenous Leukaemia identified by Quinacrine Fluorescence and Giemsa Staining. *Nature 1973 243:5405*, *243*(5405), 290–293. https://doi.org/10.1038/243290a0

Saleh, A., & Perets, R. (2021). Mutated p53 in HGSC—From a Common Mutation to a Target for Therapy. *Cancers 2021, Vol. 13, Page 3465*, *13*(14), 3465. https://doi.org/10.3390/CANCERS13143465

Salzman, J., Marinelli, R. J., Wang, P. L., Green, A. E., Nielsen, J. S., Nelson, B. H., Drescher, C. W., & Brown, P. O. (2011). ESRRA-C11orf20 Is a Recurrent Gene Fusion in Serous Ovarian Carcinoma. *PLoS Biology*, *9*(9). https://doi.org/10.1371/JOURNAL.PBIO.1001156

Schmid, B. C., & Oehler, M. K. (2015). Improvements in Progression-Free and Overall Survival Due to the Use of Anti-Angiogenic Agents in Gynecologic Cancers. *Current Treatment Options in Oncology*, *16*(1), 1–14. https://doi.org/10.1007/S11864-014-0318-0/TABLES/1

Schram, A. M., Chang, M. T., Jonsson, P., & Drilon, A. (2017). Fusions in solid tumours: diagnostic strategies, targeted therapy, and acquired resistance. *Nature Reviews Clinical Oncology 2017 14:12*, *14*(12), 735–748. https://doi.org/10.1038/nrclinonc.2017.127

Schuster, S. C. (2007). Next-generation sequencing transforms today's biology. *Nature Methods 2008 5:1*, *5*(1), 16–18. https://doi.org/10.1038/nmeth1156

Shakoori, A. R. (2017). Fluorescence In Situ Hybridization (FISH) and Its Applications. *Chromosome Structure and Aberrations*, 343–367. https://doi.org/10.1007/978-81-322-3673-3_16

Shih, I.-M., Wang, Y., Wang, T.-L., & Shih, M. (2021). The Origin of Ovarian Cancer Species and Precancerous Landscape. *The American Journal of Pathology*, *191*(1), 26–39. https://doi.org/10.1016/j.ajpath.2020.09.006

Shiroguchi, K., Jia, T. Z., Sims, P. A., & Xie, X. S. (2012). Digital RNA sequencing minimizes sequence-dependent bias and amplification noise with optimized single-molecule barcodes. *Proceedings of the National Academy of Sciences of the United States of America*, *109*(4), 1347–1352. https://doi.org/10.1073/PNAS.1118018109/-/DCSUPPLEMENTAL

Shiyu, D., Wenqing, H., Xiaoting, L., Xuming, L., Nana, C., Qiong, X., Yukun, H., Wen, S., & Jun, Z. (2018). IMPDH2 promotes colorectal cancer progression through activation of the PI3K/AKT/mTOR and PI3K/AKT/FOXO1 signaling pathways. *Journal of Experimental & Clinical Cancer Research : CR*, *37*(1). https://doi.org/10.1186/S13046-018-0980-3

Shtivelman, E., Lifshitz, B., Gale, R. P., & Canaani, E. (1985). Fused transcript of abl and bcr genes in chronic myelogenous leukaemia. *Nature 1985 315:6020*, *315*(6020), 550–554. https://doi.org/10.1038/315550a0

Sibley, C. R., Blazquez, L., & Ule, J. (2016). Splice sites Lessons from non-canonical splicing. *NATURE REVIEWS | GENETICS*, *17*, 407. https://doi.org/10.1038/nrg.2016.46

Siddiqui, A., & Ceppi, P. (2020). A non-proliferative role of pyrimidine metabolism in cancer. *Molecular Metabolism*, *35*, 100962. https://doi.org/10.1016/J.MOLMET.2020.02.005

Singh, N., McCluggage, W. G., & Gilks, C. B. (2017). High-grade serous carcinoma of tubo-ovarian origin: recent developments. *Histopathology*, *71*(3), 339–356. https://doi.org/10.1111/HIS.13248

Skorda, A., Bay, M. L., Hautaniemi, S., Lahtinen, A., & Kallunki, T. (2022). Kinase Inhibitors in the Treatment of Ovarian Cancer: Current State and Future Promises. *Cancers*, *14*(24). https://doi.org/10.3390/CANCERS14246257

Sleep, J. A., Schreiber, A. W., & Baumann, U. (2013). Sequencing error correction without a reference genome. *BMC Bioinformatics*, *14*(1), 1–9. https://doi.org/10.1186/1471-2105-14-367/TABLES/4

Smebye, M. L., Agostini, A., Johannessen, B., Thorsen, J., Davidson, B., Tropé, C. G., Heim, S., Skotheim, R. I., & Micci, F. (2017). Involvement of DPP9 in gene fusions in serous ovarian carcinoma. *BMC Cancer*, *17*(1), 642. https://doi.org/10.1186/s12885-017-3625-6

Soslow, R. A., Han, G., Park, K. J., Garg, K., Olvera, N., Spriggs, D. R., Kauff, N. D., & Levine, D. A. (2012). Morphologic patterns associated with BRCA1 and BRCA2 genotype in ovarian carcinoma. *Modern Pathology*, *25*(4), 625–636. https://doi.org/10.1038/MODPATHOL.2011.183

Southern, E. (2006). Southern blotting. *NATURE PROTOCOLS*, *518*(2). https://doi.org/10.1038/nprot.2006.73

Stewart, M. D., Vega, D. M., Arend, R. C., Baden, J. F., Barbash, O., Beaubier, N., Collins, G., French, T., Ghahramani, N., Hinson, P., Jelinic, P., Marton, M. J., McGregor, K., Parsons, J., Ramamurthy, L., Sausen, M., Sokol, E. S., Stenzinger, A., Stires, H., … Allen, J. (2022). Homologous Recombination Deficiency: Concepts, Definitions, and Assays. *The Oncologist*, *27*(3), 167. https://doi.org/10.1093/ONCOLO/OYAB053

Sullivan, K. D., Galbraith, M. D., Andrysik, Z., & Espinosa, J. M. (2017). Mechanisms of transcriptional regulation by p53. *Nature Publishing Group*, *25*, 133–143. https://doi.org/10.1038/cdd.2017.174

Sun, P., Sehouli, J., Denkert, C., Mustea, A., Könsgen, D., Koch, I., Wei, L., & Lichtenegger, W. (2005). Expression of estrogen receptor-related receptors, a subfamily of orphan nuclear receptors, as new tumor biomarkers in ovarian cancer cells. *Journal of Molecular Medicine*, *83*(6), 457–467. https://doi.org/10.1007/S00109-005-0639-3/TABLES/4

Sung, H., Ferlay, J., Siegel, R. L., Laversanne, M., Soerjomataram, I., Jemal, A., & Bray, F. (2021). Global Cancer Statistics 2020: GLOBOCAN Estimates of Incidence and Mortality Worldwide for 36 Cancers in 185 Countries. *CA: A Cancer Journal for Clinicians*, *71*(3), 209–249. https://doi.org/10.3322/CAAC.21660

Taniue, K., & Akimitsu, N. (2021). Fusion Genes and RNAs in Cancer Development. *Non-Coding RNA*, *7*(1), 1–14. https://doi.org/10.3390/NCRNA7010010

TP53 gene. (2023). https://www.ensembl.org/Homo_sapiens/Gene/Summary?db=core;g=ENSG00000141510;r=17:7661779-7687538

Tuna, M., Amos, C. I., & Mills, G. B. (2019). Molecular mechanisms and pathobiology of oncogenic fusion transcripts in epithelial tumors. Oncotarget, 10(21), 2095–2111. www.oncotarget.com

van Belzen, I. A. E. M., Schönhuth, A., Kemmeren, P., & Hehir-Kwa, J. Y. (2021). Structural variant detection in cancer genomes: computational challenges and perspectives for precision oncology. Npj Precision Oncology 2021 5:1, 5(1), 1–11. https://doi.org/10.1038/s41698-021-00155-6

Van Der Riet-Fo, M. F., Retief, A. E., & Niekerk, Van, W. A. (1979). Chromosome changes in 17 human neoplasms studied with banding. Chromosome Changes in 17 Human Neoplasms Studied with Banding, 44(6), 2108–2119. https://acsjournals.onlinelibrary.wiley.com/doi/epdf/10.1002/1097-0142%28197912%2944%3A6%3C2108%3A%3AAID-CNCR2820440622%3E3.0.CO%3B2-O

Vang, R., Jeffrey D. Seidman, & Anna. Yemelyanov. (2017). Gynecologic tract (J. D. Seidman & A. Yemelyanova (Eds.)) [Book]. Wolters Kluwer.

Vang, R., Shih, I. M., & Kurman, R. J. (2013). Fallopian tube precursors of ovarian low- and high-grade serous neoplasms. Histopathology, 62(1), 44–58. https://doi.org/10.1111/HIS.12046

Vaughan, S., Coward, J. I., Bast, R. C., Berchuck, A., Berek, J. S., Brenton, J. D., Coukos, G., Crum, C. C., Drapkin, R., Etemadmoghadam, D., Friedlander, M., Gabra, H., Kaye, S. B., Lord, C. J., Lengyel, E., Levine, D. A., McNeish, I. A., Menon, U., Mills, G. B., … Balkwill, F. R. (2011). Rethinking Ovarian Cancer: Recommendations for Improving Outcomes. Nature Reviews. Cancer, 11(10), 719. https://doi.org/10.1038/NRC3144

Villa, E., Ali, E. S., Sahu, U., & Ben-Sahra, I. (2019). Cancer Cells Tune the Signaling Pathways to Empower de Novo Synthesis of Nucleotides. Cancers, 11(5). https://doi.org/10.3390/CANCERS11050688

Vogelstein, B., Papadopoulos, N., Velculescu, V. E., Zhou, S., Diaz, L. A., & Kinzler, K. W. (2013). Cancer genome landscapes. Science, 340(6127), 1546–1558. https://doi.org/10.1126/SCIENCE.1235122/SUPPL_FILE/VOGELSTEIN.SM.COVER.PAGE.PDF

Walsh, C. S. (2015). Two decades beyond BRCA1/2: Homologous recombination, hereditary cancer risk and a target for ovarian cancer therapy. Gynecologic Oncology, 137(2), 343–350. https://doi.org/10.1016/J.YGYNO.2015.02.017

Walsh, T., Casadei, S., Lee, M. K., Pennil, C. C., Nord, A. S., Thornton, A. M., Roeb, W., Agnew, K. J., Stray, S. M., Wickramanayake, A., Norquist, B., Pennington, K. P., Garcia, R. L., King, M. C., & Swisher, E. M. (2011). Mutations in 12 genes for inherited ovarian, fallopian tube, and peritoneal carcinoma identified by massively parallel sequencing. Proceedings of the National Academy of Sciences of the United States of America, 108(44), 18032–18037. https://doi.org/10.1073/PNAS.1115052108/-/DCSUPPLEMENTAL

Wang, Y., Zou, Q., Li, F., Zhao, W., Xu, H., Zhang, W., Deng, H., & Yang, X. (2021). Identification of the cross-strand chimeric RNAs generated by fusions of bi-directional transcripts. Nature Communications 2021 12:1, 12(1), 1–14. https://doi.org/10.1038/s41467-021-24910-2

Weckselblatt, B., & Rudd, M. K. (2015). Human Structural Variation: Mechanisms of Chromosome Rearrangements. Trends in Genetics : TIG, 31(10), 587–599. https://doi.org/10.1016/J.TIG.2015.05.010

Weiss, M. M., Hermsen, M. A. J. A., Meijer, G. A., Van Grieken, N. C. T., Baak, J. P. A., Kuipers, E. J., & Van Diest, P. J. (1999). Comparative genomic hybridisation. Molecular Pathology, 52(5), 243–251. https://doi.org/10.1136/MP.52.5.243

Williams, C. J., & Erickson, G. F. (2012). Morphology and Physiology of the Ovary - Endotext - NCBI Bookshelf. Endotext. https://www.ncbi.nlm.nih.gov/sites/books/NBK278951/

Winuthayanon, W., & Li, S. (2018). Fallopian Tube/Oviduct: Structure and Cell Biology. Encyclopedia of Reproduction, 2, 282–290. https://doi.org/10.1016/B978-0-12-801238-3.64401-X

Wooster, R., Neuhausen, S. L., Mangion, J., Quirk, Y., Ford, D., Collins, N., Nguyen, K., Seal, S., Tran, T., Averill, D., Fields, P., Marshall, G., Narod, S., Lenoir, G. M., Lynch, H., Feunteun, J., Devilee, P., Cornelisse, C. J., Menko, F. H., … Stratton, M. R. (1994). Localization of a breast cancer susceptibility gene, BRCA2, to chromosome 13q12-13. *Science*, *265*(5181), 2088–2090. https://doi.org/10.1126/SCIENCE.8091231

Wu, H., Singh, S., Xie, Z., Li, X., & Li, H. (2020). Landscape characterization of chimeric RNAs in colorectal cancer. *Cancer Letters*, *489*, 56–65. https://doi.org/10.1016/J.CANLET.2020.05.037

Zhang, Y., Gong, M., Yuan, H., Park, H. G., Frierson, H. F., & Li, H. (2012). Chimeric transcript generated by cis- splicing of adjacent genes regulates prostate cancer cell proliferation. Cancer Discovery, 2(7), 598–607. https://doi.org/10.1158/2159-8290.CD-12-0042/42981/P/CHIMERIC-TRANSCRIPT-GENERATED-BY-CIS-SPLICING-OF

Zhao, S., Agafonov, O., Azab, A., Stokowy, T., & Hovig, E. (2020). Accuracy and efficiency of germline variant calling pipelines for human genome data. *Scientific Reports 2020 10:1*, *10*(1), 1–12. https://doi.org/10.1038/s41598-020-77218-4

TURUN
YLIOPISTO
UNIVERSITY
OF TURKU

Painosalama, Turku, Finland 2023

ISBN 978-951-29-9521-9 (PRINT)
ISBN 978-951-29-9522-6 (PDF)
ISSN 0355-9483 (Print)
ISSN 2343-3213 (Online)